MAPPING HUMAN VISUAL CORTEX WITH POPULATION RECEPTIVE FIELD MODEL: TUNING FMRI AND STIMULUS PARAMETERS, AND EXPLORING RECEPTIVE FIELD SIZES

A THESIS SUBMITTED TO

THE GRADUATE SCHOOL OF ENGINEERING AND SCIENCE

OF BILKENT UNIVERSITY

IN PARTIAL FULFILLMENT OF THE REQUIREMENTS FOR

THE DEGREE OF

MASTER OF SCIENCE

IN

NEUROSCIENCE

By

O. Batuhan Erkat

July 2019

MAPPING HUMAN VISUAL CORTEX WITH POPULATION
RECEPTIVE FIELD MODEL: TUNING FMRI AND STIMULUS
PARAMETERS, AND EXPLORING RECEPTIVE FIELD SIZES

By O. Batuhan Erkat

July 2019

We certify that we have read this thesis and that in our opinion it is fully adequate, in scope and in quality, as a thesis for the degree of Master of Science.

———————————————————
Hüseyin Boyacı(Advisor)

———————————————————
Hacı Hulusi Kafalıgönül

———————————————————
Funda Yıldırım

Approved for the Graduate School of Engineering and Science:

———————————————————
Ezhan Karaşan
Director of the Graduate School

ABSTRACT

MAPPING HUMAN VISUAL CORTEX WITH POPULATION RECEPTIVE FIELD MODEL: TUNING FMRI AND STIMULUS PARAMETERS, AND EXPLORING RECEPTIVE FIELD SIZES

O. Batuhan Erkat

M.S. in Neuroscience

Advisor: Hüseyin Boyacı

July 2019

Human visual cortex has been studied extensively since blood oxygen-level dependent (BOLD) signal was discovered by magnetic resonance imaging (MRI) researchers in 1990's [1]. It was not long after that, the researchers achieved to map human visual cortex with functional MRI [2, 3, 4]. In recent past, population receptive field (pRF) method was proposed by Dumoulin and Wandell for receptive field mapping [5]. Compared to phase-encoded methods, their model added a size parameter to receptive fields, referring to the extent of visual field region processed by neuronal populations. fMRI sequences from Human Connectome Project [6] that used accelerated imaging to scan the whole brain of subjects at ultra-high resolutions were adapted to conduct retinotopy experiments in our institute, National Magnetic Resonance Center, Ankara. pRF maps estimated with three types of stimuli were compared. A local pRF estimation method was tested for a specific region on visual field to achieve greater detail in pRF maps. Subject specific hemodynamic response function (HRF) was estimated in a separate experiment to enhance the pRF estimation analysis. Moreover, pRF size differences were compared between stimuli, hemispheres, and visual processing streams. The results implied that stimulation by natural images yields reliable maps in higher level visual regions, and therefore was selected as the best stimulation protocol. pRF sizes were higher in right hemisphere, and in dorsal processing stream. In addition, a guideline has been prepared for vision researchers to conduct pRF analysis.

Keywords: pRF Method, Optimization, Receptive Fields.

ÖZET

POPÜLASYON ALICI BÖLGELER MODELİ İLE GÖRSEL KORTEKS HARİTALANDIRILMASI: İMRG VE UYARAN PARAMETRELERİNİN AYARLANMASI VE ALICI BÖLGE BÜYÜKLÜĞÜ İNCELEMELERİ

O. Batuhan Erkat

Nörobilim, Yüksek Lisans

Tez Danışmanı: Hüseyin Boyacı

Temmuz 2019

Manyetik rezonans görüntüleme (MRG) araştırmacıları tarafından 1990'lı yıllarda [1] BOLD sinyali keşfedildiğinden beri insan görsel korteksi geniş ölçüde çalışılmıştır. BOLD keşfinden sonra, birçok laboratuvar işlevsel MRG deneyleri ile insan görsel korteksini haritalandırmayı başarmıştır [2, 3, 4]. Yakın geçmişte, popülasyon alıcı alan (pAB) metodu, görsel korteksin haritalandırılmasında kullanılmak üzere Dumoulin ve Wandell tarafından ortaya atıldı [5]. Diğer haritalama yöntemleriyle karşılaştırıldığında bu model, araştırmacıların görsel alıcı bölgelerin büyüklüğünü de ortaya koymalarını sağlamaktadır. Human Connectome Project'ten [6] uyarlanan hızlandırılmış çok bantlı iMRG sekansları, pAB deneylerinde kullanılmak için optimize edildi. pRF haritaları üç farklı uyaranla tahminlenmiş ve sonuçlar karşılaştırılmıştır. Görsel alandaki belirli bir bölgeyi daha ayrıntılı olarak incelemek için yerel bir pAB tahmin yöntemi test edildi. pAB tahmin protokolünü geliştirmek için hemodinamik tepki fonksiyonu ayrı bir deney çekiminde tahmin edilmiştir. Bunların yanı sıra, uyarım protokolleri, hemisferler ve görsel işlem akışları arasında ortaya çıkan pAB boyut farklarını araştırıldı. Doğal sahne görüntülerinin kullanımı ile pAB haritalarında yüksek mertebeli görsel korteks bölgeleri güvenilir bir şekilde haritalandırılmıştır, bu nedenle en iyi uyarım yöntemi olarak doğal sahne görüntüleri seçilmiştir. pAB boyutlarının sağ hemisferde vedorsal yolakta daha büyük olduğu gösterilmiştir. Ayrıca, araştırmacıların pAB analizi yapmalarını kolaylaştıracak talimatlar içeren bir kılavuz hazırladık.

Anahtar sözcükler: pAB Metodu, Optimizasyon, Alıcı Bölgeler.

Acknowledgement

First of all, I would like to thank Hüseyin Boyacı, who accepted me into his Computational and Biological Vision Group, guided me to conduct this research and supported me tremendously throughout my time in Bilkent. His door was always open whenever I had a question, and his invaluable feedback coupled with intellectual insights allowed me to advance further in my studies. He allowed me to take such courses that led me to build a substantial knowledge in different subfields of neuroscience.

I would like to thank Hulusi Kafalıgönül for his lectures on systems neuroscience that truly widened my horizon, and his support and encouragement throughout my studies. His academic guidance helped me in many ways, and I am truly indebted to him. His insights about vision science and feedback to this study contributed immeasurably.

I would like to thank Funda Yıldırım for being on my committee, and accepting to visit Ankara for the occasion. Her invaluable comments and suggestions improved this thesis substantially.

I am very thankful to Erhan Genc and Benjamin de Haas for sharing their insights, resources and codes that significantly accelerated my speed of establishing the analysis protocols used in this study.

I am truly thankful to my partner Sercan, who encouraged me to take a step into the field of neuroscience. Without his love and support I may not have been pursuing my dream today. I am grateful to my family who never stopped supporting me from the day I was born. I feel very lucky to have met the members of Computational and Biological Vision Group, Cortical Dynamics and Perception Laboratory and Twin Laboratory. Without their friendship, I would feel terribly alone in Ankara. I would like to give my thanks to Beyza, Dilara, Cemre, Rabia, Buse, Ecem, Cem, Sibel, Seda, and all the other office buddies for their friendship, kindness and scientific contributions. It was a pleasure to work with

Cemre on pRF methods, our discussions led to substantial contributions on this study, and with Dilara and Beyza on the perceptual learning study, with whom we wrote a proposal for funding, hope you get rich this summer!

Contents

List of Figures

List of Tables

Chapter 1

Introduction

Animals need to perpetually interact with the external world to survive in their environment. This crucial interaction is only possible through specialized structures dedicated to process the information coming from the environment. Visual system is an example for such a complex system which consists of multiple special structures that act in harmony to process the information of light and allows us to understand shape, motion and depth to build a continuous internal representation of the world around us.

In the following sections, the visual system will be explained briefly to establish background information for the readers and will be followed by retinotopy imaging and analysis methods. This thesis is dedicated to apply and optimize human retinotopy on three points of investigation. First of all, fMRI sequences retrieved from Human Connectome Project [6] will be adapted to the scanner in our institute, National Magnetic Resonance Research Center, Bilkent University, Ankara, and the scanning parameters will be optimized for retinotopy imaging. Secondly

different stimulus configurations will be tested to estimate receptive field maps including higher level visual regions. Finally, additions to and improvements on pRF imaging and its analysis will be explained.

1.1 The Visual System

Visual system is devoted to process the information of light from the external physical world. The process of phototransduction is the initial step for constructing an internal visual representation of our external world. Briefly, as light falls on the retina, photoreceptors undergo a cascade of events which results in hyperpolarization of the cell, leading to decreased excitatory neurotransmitter release from photoreceptor cells to the synaptic cleft. With the hyperpolarization event, physical energy is converted into chemical energy, exchanged into retinal circuirty currency. The retinal circuitry consists of many cell types, such as photoreceptors (i.e. rods and S, M, and L-cones), interneurons and horizontally connected cells.

The photoreceptor density on retina differs for fovea and peripheral areas. At the fovea, cone receptor density is very high, and convergence in circuitry is very low, referring to a one-to-one relationship of photoreceptors and retinal ganglion cells. On the contrary, peripheral regions are dense with rods and circuitry follows a convergent and interconnected information flow from rods to ganglion cells, resulting in a ganglion cell receiving input from more than one photoreceptor. Foveal cone density leads to higher input specificity and acuity (e.g. visual stimulus discrimination capability) on central visual field. On the contrary, peripheral regions are highly excitable due to neural summation of inputs, yet lower in acuity due to convergence, referring to a many to one connection between rods to

ganglion cells. Based on these properties, it is possible to argue that amount of electrical signals projected from fovea to occipital cortex is higher than peripheral regions. This property is reflected in cortical maps of visual fields, where fovea is represented on a large area at the occipital pole. [7]

The retinal ganglion cells receive input from the interneurons and the horizontal cells, and project signals to the dorsal lateralgeniculate nucleus (dLGN) in thalamus through optic nerves. Optic fibers follow a labelled lines principle, meaning that information is not intermixed. The optic fibers carry projections from nasal and temporal retina down to optic chiasm, where the fibers descending from nasal retina cross over to the contralateral hemisphere and propagate to dLGN. The fibers descending from temporal retina continue their propagation ipsilaterally. As a result, left and right visual hemifields are processed in respectively right and left hemispheres, which is referred as the contralateral processing principle of visual system. In Figure 1.1 the contralateral processing of visual information is demonstrated.

There are three main types of retinal ganglion cells classified basen on their morphology and response properties, namely parvocellular (P), magnocellular (M) and koniocellular (K) ganglions. The regions of dLGN that receive input from M, P and K cells follow labelled lines principle. Layers of dLGN that receive input from corresponding type of retinal ganglion cells are referred as P, M and K layers. [8]

The retinogeniculostriate pathway follows a bottom up hierarchy in visual information processing. M-dominated pathway leads to dorsal pathway of visual processing by following a propagation from V1 to dorsal regions up to parietal
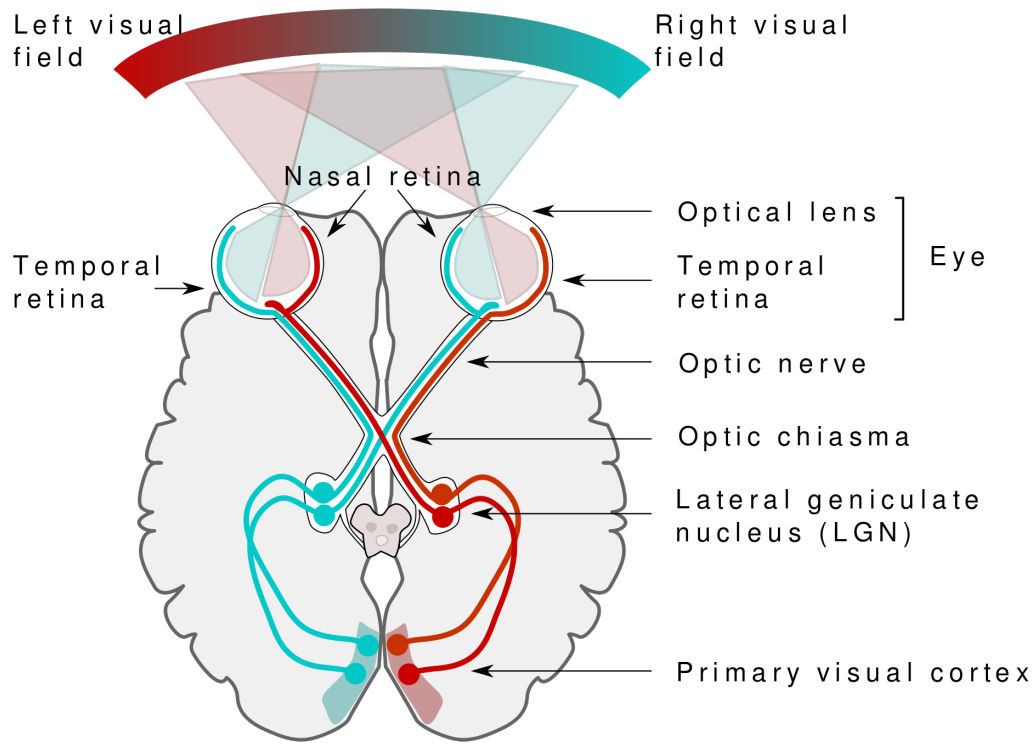
Figure 1.1: Contralateral processing in visual system. Drawn by Miquel Perello Nieto, under shareable license [CC BY-SA 4.0 (https://creativecommons.org/licenses/by-sa/4.0)]

cortex, and propagates further to anterior regions. Dorsal processing stream is also referred as the "where" pathway, as it has been demonstrated to process temporal information of visual input and spatial relationships [8]. This stream connects with sensory-motor cortex and plays an important role in visual decision making and visually guided actions. Main cortical regions involved in dorsal stream are visual region 1 (V1), visual region 2 dorsal (V2d), visual region 3 dorsal (V3d), visual region 3A and 3B (V3A/B), intraparietal sulcus (IPS), motion area (MT+). [7]

The parvo-dominated pathway has been shown to process color, contour, orientation, and non-cartesian patterns of the stimuli, and leads to the ventral processing stream [8]. The ventral processing stream is also referred as the "what" pathway which takes part in object and face recognition. Main cortical regions involved in ventral stream are visual region 1 (V1), visual region 2 ventral (V2v), visual region 3 ventral (V3v), human visual region 4, ventral occipital region (VO). Even though a hierarchy of information processing is prevalent in the visual system, feedback and feedforward relationships between visual areas is accepted and implying that it is a highly interconnected system. In Figure 1.2 the ventral and dorsal processing streams are shown on a template human brain including main visual regions. The arrows on Figure 1.2 shows the main pathways for information flow.

The ventral and dorsal processing pathways are the building blocks of the visual system in terms of localization of visual function. Normal functioning of these pathways lead to internal representations of our external environment with regard to stimulus features (i.e shape, color, motion), which will be investigated in the following sections by comparing receptive field profiles under different stimuli.

1.2 Receptive Fields

A receptive field refers to a region of input that our senses can be stimulated [10]. In the visual system, the location of light projected onto retina would define the receptive field if the stimulus leads to spiking activity for the neuron [11]. All ganglion cells at retina make up our visual field, that can be understood as a window to our environment, where visual sensation is evoked to form perception
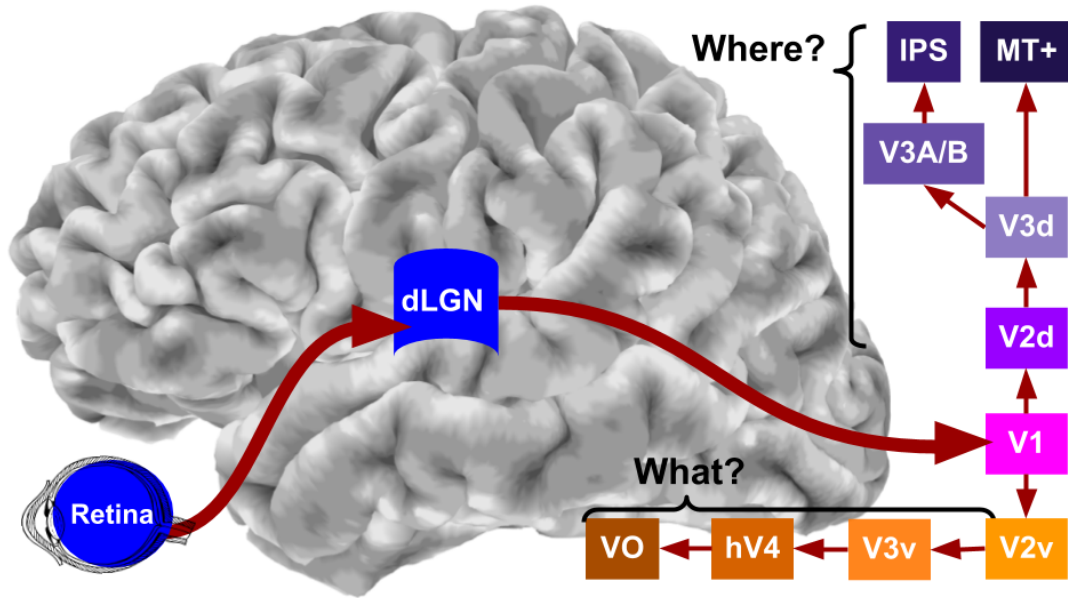
Figure 1.2: Dorsal and ventral processing streams of visual system. [9]

[11, 12]. As explained in Section 1.1, neurons in visual cortex receive information in terms of labelled lines in an organized and hierarchical manner. Thus visual field is represented topographically in the visual cortex. Early studies investigating the visual field representation in cortex demonstrated a retinotopic organization prevalent in visual cortex.

For the first time, Talbot and Marshal's investigation on visual cortex of macaque monkeys and cats with electrophysiological methods showed a functional organization in visual cortex [13]. The organization demonstrated contralateral processing of left and right visual hemifields and an upside down representation of upper and bottom visual hemifields around the calcarine sulcus of primary visual cortex. Zeki's lesion study on various areas in the visual cortex of macaque monkeys showed regional relationships within the visual cortex by tracing degenerated fibers [14]. Based on his tracing method, he provided a schematic representation of receptive fields in the visual cortex consistent with Talbot and

Marshal's findings [13]. Daniel and Whiteridge in 1961 replicated Talbot and Marshall's results, and mathematically described a cortical magnification factor by electrophysiological measurements [15]. Cortical magnification factor refers to the mechanism where projections from fovea occupy a greater extent of cortical space, and as distance to fovea increases in retina, the cortical surface that the retinal projections occupy decreases logaritmically. In this study cortical magnification factor, eccentricity and polar angle information was represented on visual cortex based on electrode recordings on monkeys. Later in 1985, Dow and his colleagues [16] reproduced a foveal retinotopic map on rhesus monkey's striate cortex with single electrode recordings too, and further modelled cortical magnification factor in primate visual cortex. Furthermore, in Hubel and Wiesel's studies [17] the authors showed that the response of cortical neurons upon stimulation by a light projected on cat retina was affected by the stimulus location and configuration. With detailed investigation they have revealed that some of the cortical cells produced spiking activity to a stimulus when its center is blank but edges are lighted up, which replicated and established previous findings about on and off properties of receptive fields [18, 11].

In the following section I will explain visual field mapping in depth with current developments and clinical applications.

1.3 Retinotopic Mapping in Humans

Visual field mapping in humans goes back as early as to Inouye's work on brain damaged veterans of Russo-Japanese war around 1905 [19]. Based on bullet damage trajectory in the occipital cortex of veterans, sight in a specific visual

field region was lost. A general map of visual field representation in human visual cortex could be derived by matching the damaged areas and lack of sight through postmortem investigations.

Positron emission tomography (PET) was used to record the activity of V1 of healthy humans for the first time in 1986. In the following year same group demonstrated a retinotopic organization in human visual cortex by showing subjects an expanding ring with high-contrast pattern [20, 21].

Improvements in magnetic resonance imaging (MRI) methods paved the way for anatomical investigations on patients with cortical damage in visual cortex, similar to Inouye's approach [19]. It became possible to detect the damaged visual regions with high spatial resolution and accuracy. Horton and Hoyt's study demonstrated the effects of damage beyond V1, and based on their findings they argued that V2 and V3 surrounds human V1 regions, and homologous to other primates [22].

Ogawa and his colleagues' discovery of blood oxygen level dependent (BOLD) signal opened a new window to human brain. Functional magnetic resonance imaging (fMRI) studies started to be conducted and scientific interest in functional studies of human brain grew as BOLD was proven to reflect neuronal activity, calculated based on the difference between oxygenated and deoxygenated hemoglobin's contrasting magnetic properties in brain tissue [1]. With BOLD discovered, investigations on human visual cortex proceeded in more depth. Engel and his colleagues mapped the human visual cortex based on BOLD data. In their experiments, subjects fixated at a point while an expanding ring stimulated the visual field with high-contrast patterns. The expansion of the ring induces

travelling waves in the visual cortex. This pattern of neural activity leads to oxygen consumption and blood flow that is captured as BOLD signal. BOLD data retrieved for each position of the ring was analyzed to determine voxels responding to visual stimulus. After the analysis, the responses given to stimulation at different eccentricities and polar angles are color coded and superimposed on the subject's inflated cortex, representing the receptive fields in human visual cortex [4]. Sereno and his colleagues, and DeYoe and his colleagues mapped the receptive fields with a similar approach in past consecutive years [2, 3].

Anatomical landmarks and their argued functional properties in visual cortex [22, 19] were validated by retinotopic mapping researchers [3, 4, 2]. With a validated correspondence between anatomical and functional properties, researchers delineate visual regions. The findings implied that calcarine sulcus includes the V1 region folded, where it's dip represents the horizontal meridian of contralateral visual field. Then from the dip to the upper peak, lower visual hemifield is processed, whereas to lower peak the upper visual hemifield is processed. Thus the visual field is represented vertically flipped on visual cortex. Foveal input is processed at occipital pole, extends to the anteriors of calcarine sulcus, during the extension eccentricity increases.

Due to the folded structure of human cortex, using inflated versions of anatomical images, and registering anatomical and functional slices together is a common practice that allows researchers to conduct retinotopic analysis and visualize maps. This method is used in current analysis methods of retinotopic maps and prevalent most of the recent retinotopy literature. [23, 24, 25, 26, 27, 28].

The borders for visual fields V1, V2 and V3 are detected based on the polar angle

reversals. The dorsal and ventral borders between V1 and V2 is determined by the lower and upper vertical meridian, respectively. V2 and V3 borders are at the region corresponding to the horizontal meridian. V3 region starts with the horizontal meridian and ends with lower (for V3d) and upper (for V3v) vertical meridians. If we consider ourselves travelling from the dip of calcarine sulcus in the dorsal direction, we would start from contralateral horizontal meridian, reach the vertical meridian of lower visual hemifield, and then we would encounter contralateral horizontal meridian again at V2d/V3d border and as we continue, we would reach to vertical meridian of lower visual hemifield again at V3d/V3A-B border. The underlying reasons and possible benefits of functional reversals in primary visual cortex polar angle processing, and if it is a common property for other species is not well known. [29]

The intermediate and higher levels of processing in visual cortex are argued to propagate dorsally in V3A/B, LO, MT+, IPS and ventrally in V4 to VO. With improvements in MRI technology and enhanced SNR of fMRI sequences, the detection and functional mapping of these regions became more plausible. It is argued that in these regions neurons process higher level features, and therefore, high-contrast visual stimulus can fail to achieve strong BOLD signal in these regions. Therefore, researchers utilize a set of natural images instead of high-contrast patterns in their stimulation protocol to evoke BOLD signal in intermediate and higher visual regions. When a set of images consisting of natural scenery instead of high-contrast patterns are used, extrastriate cortex can be mapped. [24]

Dumoulin and Wandell's proposed model (can be seen on Figure 1.3) suggests that previous methods have shortcomings as they detect the location of visual

pRF Estimation Analysis Pipeline
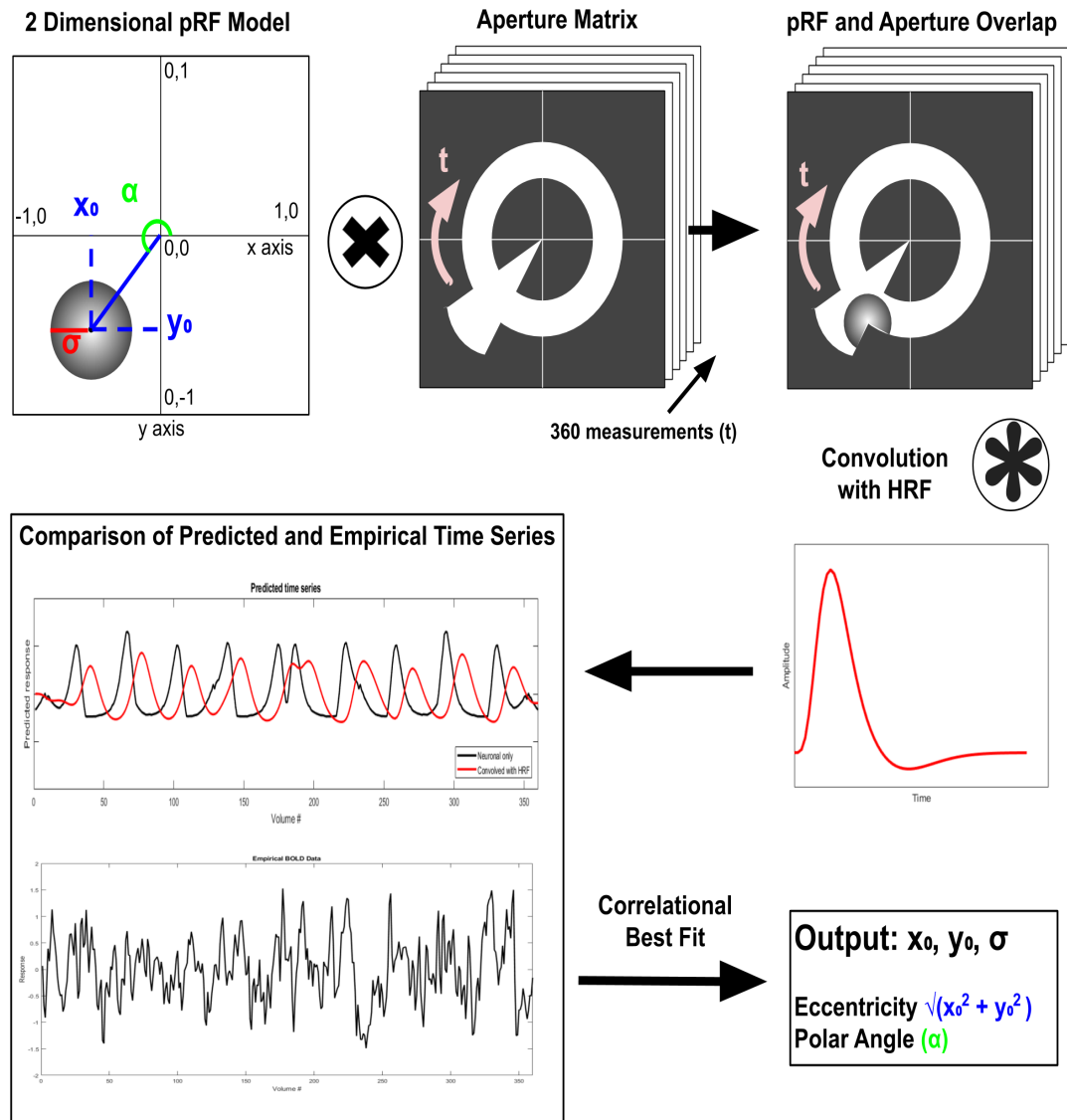
Figure 1.3: pRF Model

field based on the highest BOLD signal in response to a stimulus at the location [5]. As a voxel of human brain contains various neural populations that may be selective to different aspects of the stimulus, it should be considered as a population activity, and therefore, a representation of azimuth and elevation would refer to population receptive field parameters (pRF) at that voxel. Domoulin and Wandell's proposed retinotopy model and analysis pipeline allows researchers to unravel the size of the receptive fields in addition to eccentricity and polar angle maps. Their model suggests that receptive fields can be defined in terms of two dimensional Gaussian curves with parameters x, y, and σ

$$g(x,y) = \exp\left(-\frac{(x-x_0)^2 + (y-y_0)^2}{2\sigma^2}\right), \tag{1.1}$$

where x_0, y_0 refers to the center, σ is the standard deviation of Gaussian curve. In terms of visual field parameters, σ refers to pRF size, x and y refer to azimuth and elevation of receptive field. As can be seen on Figure 1.3, this method defines BOLD signal ($y(t)$) in terms of predicted BOLD signal ($p(t)$) multiplied by a factor (β) and addition of an error term (e)

$$y(t) = p(t)\beta + e. \tag{1.2}$$

The stimulus is defined in terms of $s(x, y, t)$, represents the azimuth (x) and elevation (y) parameters on the visual field at different time points (t). The stimulus in this method can be a moving bar, a combined wedge and ring with a high-contrast pattern, or anything researchers would like to investigate. The masks of the stimulus at each time point are transferred into a binary matrix that shows the stimulated regions of the visual field, termed as 'aperture matrix', representing the stimulated x, y locations in pixel units at the visual field. This

aperture file acts as a filter to produce predicted BOLD response for different population receptive fields on the visual field. The predicted BOLD signal $(r(t))$ is produced as Gaussian curve and the binary aperture matrix overlaps, as seen on Equation 1.3, followed by a convolution with hemodynamic response function (HRF) for the prediction of time series to be representative of BOLD response,

$$r(t) = \sum_{x,y} s(x, y, t)g(x, y) \tag{1.3}$$

$$p(t) = r(t) * h(t). \tag{1.4}$$

HRF refers to the response property of neurons during activity, related with central blood volume, blood flow and oxygenation [30]. HRF has been shown to change from subject to subject and between brain regions [31, 32]. Based on its contribution to the BOLD signal, it is an important aspect which can be modelled by finite impulse response (FIR) and other methods when applied to fMRI data derived from HRF estimation experiments [33].

As the last step, predicted BOLD response and empirical BOLD responses are compared with each other, whichever parameters of predicted BOLD correlates to empirical BOLD significantly are considered to represent the receptive field properties for the neural population at that voxel. Dumoulin and Wandell proposed to minimize the residual sum of squares (RSS) to find the best fitting parameters [5]:

$$RSS = \sum_{t} (y(t) - p(t)\beta)^2. \tag{1.5}$$

With the proposed model, the estimation of receptive field maps is argued to be more robust [5]. Therefore, this model has been applied to studies on diseases with or without visual symptoms [34, 35, 36, 37, 38, 39], on anatomy and development

[40, 41, 42, 43, 25] and visual perception [44, 45, 28, 46, 47, 48, 49].

1.3.1   Applications of pRF Imaging

Retinotopy experiments utilizing pRF model have been conducted to investigate various topics. Visual cortex development is one of the application areas. In the study by Dekker and his colleagues, they investigated the differences between children and adult pRFs by comparing the pRF size, eccentricity and polar angle maps [25]. Their results lead to the conclusion that there are no significant differences between late children and adult pRF maps. pRF experiments were conducted to investigate differences in visual cortex maps related with brain or vision related diseases as well. As pRF is a non-invasive method of investigation, it can provide insights on various diseases and could be utilized for diagnostic purposes to benefit human health. pRF differences in Alzheimer's patients were investigated and shown that surface size of V1, V2 and hV4 were decreased and pRF size in these regions were increased compared to healthy subjects [34]. FHONDA syndrome is an inherited disorder similar to albinism, occurring due to mutation in SLC38A8 gene, and leading to an abnormal contralateral cross over in optic chiasm. pRF maps of FHONDA patients were found to be abnormal, and showed higher pRF sizes [36]. pRF measurements on a patient who underwent brain damage at 4 months old showed no retinotopic organization in primary visual cortex, even though his acuity levels were normal [41]. In autism spectrum disorder patients, Schwarzkopf and his colleagues [35] found that pRF sizes were larger in extrastriate regions, but not in primary visual cortex, which may imply attention related differences but not sharper vision.

V1 lesions and optic radiation defects lead to visual field scotomas, occluding specific visual field regions. In a recent study, visual field defects corresponded well with retinotopic maps of patients [39] In another study [26], visual field defects were artificially simulated via masking pRF stimulus. The results showed that when there is no input from a specific visual field location, the pRF maps did not represent that location, referring to an immediate effect related with stimulus conditions.

pRF experiments were conducted to investigate various phenomenon related with visual perception. In relation with visual attention, researchers demonstrated cerebellar pRFs that argued to aid visual attention network [45]. In another study [48], researchers looked into the influence of spatial attention on pRFs, and demonstrated that attention fields attract pRFs in a cortical depth dependent manner. When attention is directed to a peripheral location the pRF sizes increased along the ventral processing stream compared to attending to fixation point at center [49].

To reveal temporal contrast sensitivity differences in visual cortex, Himmelberg and his colleagues [44] conducted an retinotopy experiment and demonstrated that contrast sensitivity differences between fovea and peripheral regions are corrected in visual cortex. In Yildirim's study [50], it has been demonstrated that targeting different neuronal populations is possible by tuning stimulus properties, and showed significant reductions in pRF sizes due to stimulus configurations. In relation with depth perception, in He's study [47] they have shown that the perceived size lead to position shifts of pRFs in visual cortex due to depth perception.

Today, pRF imaging continues to gain popularity as a visual cortex mapping

technique to investigate clinical, developmental and perceptual phenomena. We have estimated pRF maps that reliably estimated a high number of vertices and higher-level regions (VO, IPS, see Figure 1.2). We also paid attention to additional fMRI parameters that may be influential in other session, such as repetition time, referring to data acquisition period and the duration of visual stimulation.

In the following chapters I will elaborate on the optimization methods for sequence parameters, stimulus configurations and a recent pRF imaging method.

Chapter 2

pRF Estimation Method

2.1   pRF Imaging and Data Analysis Procedures

As briefly explained in Section 1.3, the pRF method employs a model for visual receptive fields and estimates the retinotopic organization by comparing predicted and empirical BOLD data. In this section, I will explain our pRF estimation protocol including each preprocessing step necessary for estimating pRFs successfully. The goal of this section is to explain our data analysis protocol used in optimization of fMRI parameters (Section 3.2) and optimization of stimulus configurations (Section 4.2).

We have used a wedge and ring filled with a high-contrast ripple pattern stimulus in pRF experiments for fMRI parameter tuning. The ripple stimulus is defined as follows

$$\delta = \frac{\sin\theta}{4} + \frac{1}{2}, \tag{2.1}$$

$$I(x,y) = \cos\frac{2\pi(\sin\frac{\delta\pi x}{180} + \cos\frac{\delta\pi y}{180})}{4}\sqrt{x^2 + y^2}, \tag{2.2}$$

where, I refers to pixel intensity at x and y coordinates, θ refers to phase, δ to spatial frequency [23]. A demonstration of stimulus can be inspected in Figure 4.1.A, which was used in sequence testing for fMRI parameter optimization explained in Section 3.2.

A pRF experiment session consisted of 12 fMRI runs with 185 measurements in each run, first 5 images were discarded from the analysis. In odd numbered runs wedge turned counter-clockwise and ring expanded; in even numbered runs wedge turned clockwise and ring contracted. Further details about the stimulation protocol will be explained in Section 4.2.

Data retrieved from pRF experiments consisted of a T1-weighted whole brain image, and 12 runs of T2*-weighted images that have been motion corrected by the scanner. An overlook of the preprocessing and pRF estimation steps can be seen on Figure 2.1.

T1-weighted images were analyzed using FreeSurfer v5.3 image analysis package [51]. The automatic reconstruction pipeline was used, which included motion correction, intensity normalization, skull and neck stripping, white matter segmentation, smoothing, inflation, spherical mapping and registration, cortical parcellation steps. Surface maps of participants brain were used during the estimation and visualization of pRF maps. After the reconstruction procedure, T2*-weighted images were preprocessed using Statistical Parametric Mapping Software 12 [52] on MATLAB 2017a [53]. T2*-weighted images were realigned to the first functional image and unwarped to correct for magnetic field distortions. Realignment step refers to estimating head motion on 3 parameters of translation and 3 parameters of rotation, followed by registration of the parameters to the first image
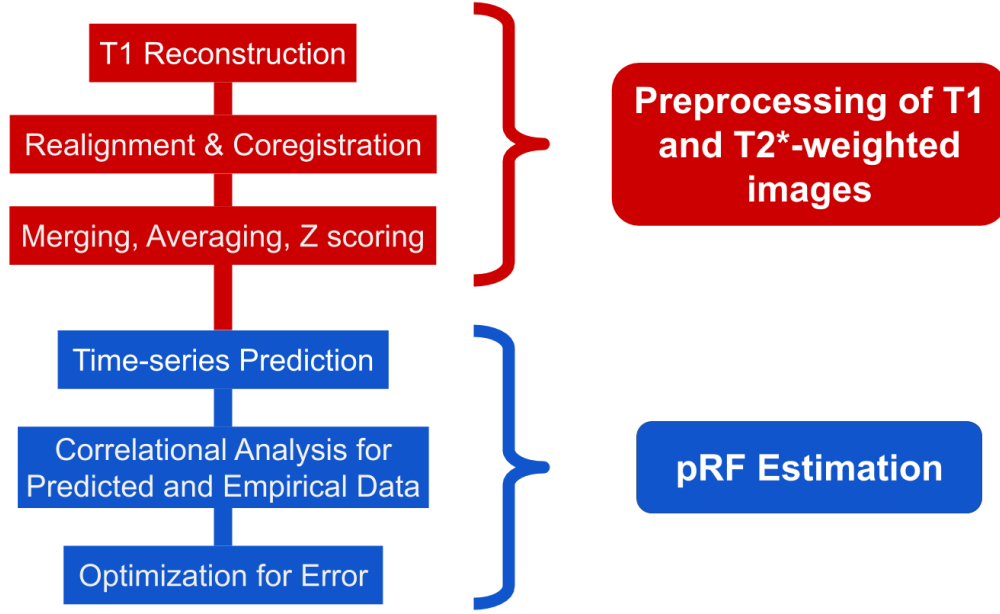
Figure 2.1: Preprocessing and pRF estimation steps

with an interpolation method. We have used second degree B-Spline interpolation method to register all T2*-weighted images to the first image with respect to esti- mated parameters. Unwarping refers to correcting functional images for magnetic field inhomogenities caused by head motion, brain tissue composition differences and air ducts. In the next step, we have coregistered functional images to the reconstructed structural image by estimating and minimizing the translation and rotation parameters between the structural and functional images. We have used normalized mutual information function for coregistration. Functional images were not resliced in structural image dimensions due to increased file size. The coregistration between structural and functional images was visually inspected for errors and there were no errors encountered.

Following the coregistration of T2* and T1-weighted images, we have conducted
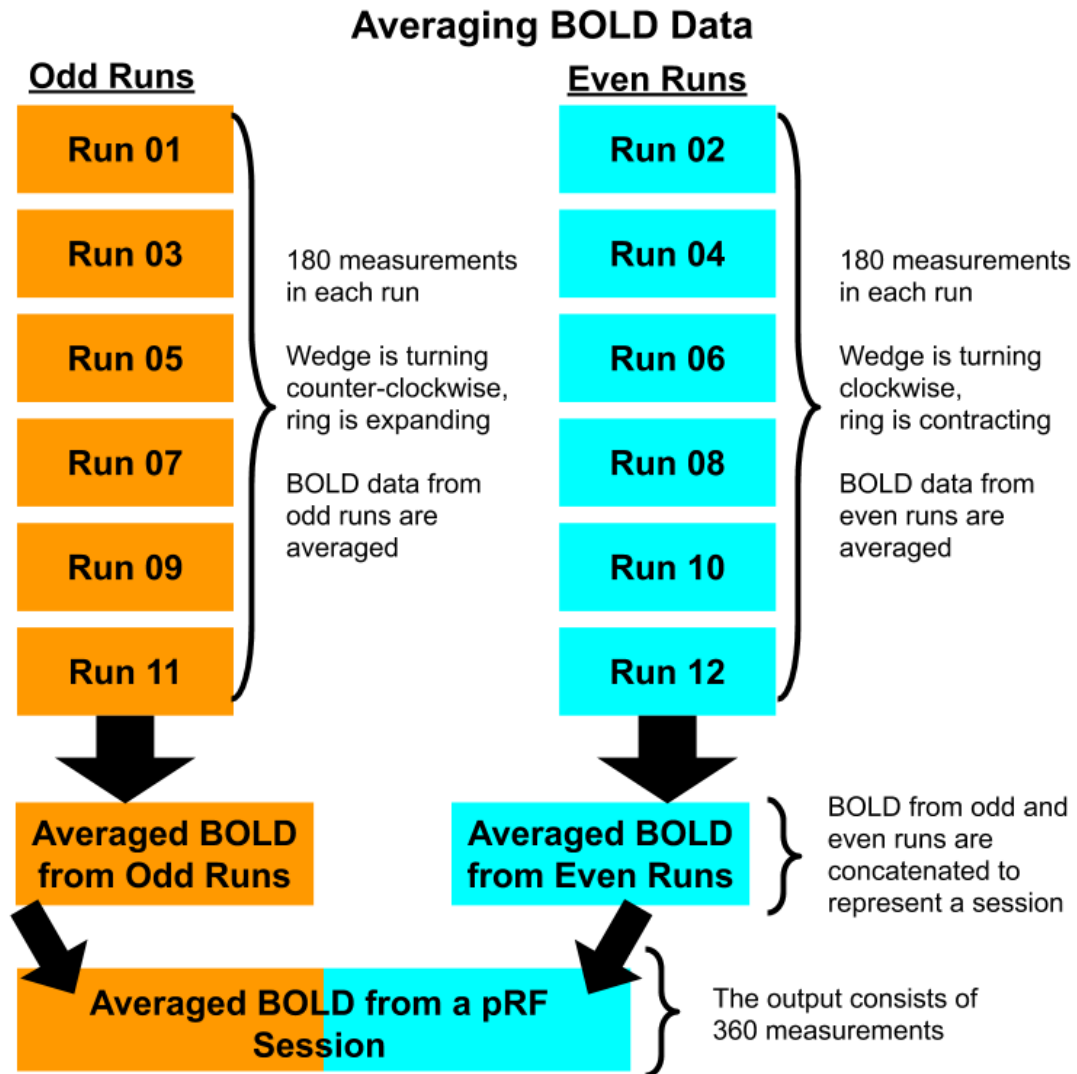
Figure 2.2: BOLD Averaging

merging, normalization and averaging on the data. Firstly, the T2*-weighted images from each run of a session were merged into a four dimensional (i.e. 4D NIFTI) file. Next, we have normalized the BOLD data (4D NIFTI files) by z-scoring and detrending for signal drift using MATLAB built-in functions. Following normalization, averaging of BOLD data was executed separately for odd and even numbered runs. The average BOLD from odd numbered runs and average BOLD from even numbered runs were concatenated to represent a single session of the experiment, with 360 measurements in total. An overlook on the averaging step of data analysis can be seen on Figure 2.2.

In next step, we projected the averaged BOLD data on the surface maps retrieved from reconstruction step. At this step, data from voxels are matched with vertices and attached to each vertex. After the attachment, pRF analysis pipeline is conducted. We estimated pRF maps using SamSrf 6.05 (https://osf.io/2rgsm/) on MATLAB 2017a [53]. After initialization of file structures, a search space is generated for x, y and σ parameters for the Gaussian model. A region of interest (ROI) file is created and loaded to restrict the analysis to occipital lobe of subject's brain. This is done for computational efficiency, since pRF estimation for whole brain can take a longer period of time. Next, predicted BOLD data is computed based on multiplication of receptive field profiles (i.e. 2D Gaussian curves centered on x and y values on a 2D coordinate space representing the visual field) with the aperture file (i.e. a binary matrix file representing stimulated areas in the visual field). The combination of all x, y and σ values from the generated search space array is used to generate time-series data. The predicted time-series are convolved with a canonical hemodynamic response function (HRF) of SPM12 [52] to represent properties of empirical BOLD data. The prediction and

convolution steps can be seen on Figure 1.3.

The empirical and predicted data are compared by correlating data from each vertex with each predicted BOLD data. The highest of significant correlations is retrieved and the predicted parameters (i.e. x_0, y_0 and σ) are assigned to the vertex. This correlational analysis and assignment is conducted to each vertex (around 55000 after restrictions to occipital lobe). After all of the vertices are assigned with best fitting parameter values, a "coarse fit map" is generated. A "fine fit map" is generated after the parameters are further tuned with an error minimization function. The fine fit map is smoothed during display of pRF maps for visualization purposes. An overall look on the pRF estimation analysis steps can be seen on Figure 2.1.

The optimized x_0, y_0 and σ values are used to create polar, eccentricity and pRF size maps. The polar map shows the cortical space that process information retrieved from specific polar angles of the visual field. Eccentricity map shows the receptive fields that process information retrieved from specific degree distances from the center of visual field. Sigma map is representative of the size of receptive fields. In other words, sigma values at a specific visual region represent a pool of information processing by the extent of circular radius centered on a specific x_0, y_0 location on visual field. The maps were delineated into visual areas manually following the retinotopy literature [54, 55, 56] and SamSrf Toolbox guidelines [29]. Further details, instructions and the code for the pRF estimation protocol steps can be found in Appendix B.2.

Chapter 3

fMRI Parameter Tuning and Results

3.1 Participants

A single participant (Subject 01) volunteered for the fMRI tuning experiments, named Test 1, 2 and 3. The participant had no history of any neurological or psychiatric disorder, were not using any drugs, both had corrected-to-normal vision. Participant gave his written informed consent before each pRF session. Experimental protocols and procedures were approved by the Human Ethics Committee.

3.2 Tuning fMRI for pRF Estimation

The first phase of our study was to optimize the MR scanning parameters for pRF experiments on MR scanner. We used multi-band echo planar imaging (EPI)

sequences adapted from Human Connectome Project [6]. As we tried to tune different parameters our aim was to attain a high spatial and temporal resolution. In a recent pRF study [57] conducted on 7T with multi-band protocols, the spatial resolution was 1.6 millimeters and the temporal resolution (repetition time) was 1000 milliseconds. We also arranged spatial resolution to be 1.6 mm (isotropic), and tested 1000 ms, 1500 ms and 2000 ms for repetition time (TR).

The pRF experiments were conducted on a 3-Tesla MRI Scanner (Siemens Magnetom Trio) at National Magnetic Resonance Research Center (UMRAM), Bilkent University, Ankara, Turkey. T1-weighted MPRAGE sequence was used to collect anatomical data (voxel dimensions, 1.0 mm^3 isotropic; repetition time (TR) = 2600 ms; echo Time (TE) = 3.02 ms). Detailed protocols were retrieved from the scanner and can be inspected in Appendix A.1.

We have named our test sequences as Test 1, 2 and 3 and provided a summary of MRI parameter values on Table 3.1. For the Test 1 sequence, repetition time (TR) was 1000 ms; echo time (TE) was 18 ms. A partial Fourier transformation was applied at scanner at 5/8 to retrieve BOLD signal from k-space. Bandwidth for the scan was 1666 Hz/px. Data was retrieved from 78 slices, with field of view (FoV) of 192 mm and base resolution of 120 mm, that makes up an image matrix of 192x120 mm with 1.60 mm spatial resolution in the transverse plane. To make it isotropic slice thickness was selected to be 1.60 mm. The multi-band acceleration factor was 6, meaning that data was retrieved from 6 slices simultaneously. Flip angle used for the scan was 22 degrees. Phase encoding direction was anterior to posterior.

For the Test 2 sequence, repetition time (TR) was 1500 ms; echo time (TE) was

Variables	Test 1	Test 2	Test 3
Number of Slices	78	84	84
TR (ms)	1000	1500	2000
TE (ms)	18	43	60
Partial Fourier	5/8	7/8	7/8
Bandwidth (Hz/px)	1666	1544	1042

Table 3.1: A Summary of Parameters for Test Sequences

43 ms. A partial Fourier transformation was applied at scanner at 7/8 to retrieve BOLD signal from k-space. Bandwidth for the scan was 1544 Hz/px. Data was retrieved from 84 slices. Image matrix, acceleration factor, flip angle and phase encoding direction were kept the same.

For the Test 3 sequence, repetition time (TR) was 2000 ms; echo time (TE) was selected to be 60 ms, since it was the lowest integer value allowed by the scanner. A partial Fourier transformation was applied at scanner at 7/8 to retrieve BOLD signal from k-space. Bandwidth for the scan was 1042 Hz/px. Data was retrieved from 84 slices. Image matrix, acceleration factor, flip angle and phase encoding direction were kept the same.

A pRF session consisted of 12 runs, and in each run 185 measurements were taken. Black and white ripple stimulus was used in each Test scan, as seen in Figure 4.1.A. The first 5 volumes of functional scans were discarded to allow gradient saturation. Whole brain of participants was imaged with a 32-channel head coil. Ear plugs were given to participants to avoid any adverse effects of high level of auditory noise from the scanner. Head stabilizers were used to prevent head motion during data collection. Visual stimulus was presented on 31.5"

MR compatible LCD screen (1920x1080, 60 Hz, TELEMED PMEco, İstanbul) through a mirror mounted on the head coil. The total length of the optical path between subject's eyes and the LCD screen was 165 centimeters. Therefore, we could measure on 13.5 visual degree of subject's central field of view. A fixation task was given during the stimulus presentation to control for and limit the eye movements of participants. The response to fixation task was collected with a fiber optic response box (fORP 904 fMRI trigger and response system, 4 Button Bimanual HHSC-2x2, Current Designs).

3.3 fMRI Parameter Optimization Results

For pRF estimation with Test 1, Test 2 and Test 3 sequences, we used SamSrf toolbox on MATLAB as explained briefly in Section 2.1 of Methods, and in detail in Appendix B.2. We have visually inspected the results and determined that Test 2 and Test 3 fMRI parameters yielded good results in terms of high number of vertices. In order to ensure a high level of SNR in pRF experiment scans, we have chosen fMRI parameters of Test 3 for further phases of the study. Except in Section 6.3, we achieved to further increase the SNR of Test 3 sequence, by further decreasing TE, and increasing the flip angle by calculating the Ernst angle.

The resulting pRF maps from Test 1, Test 2 and Test 3 are shown in Figure 3.1, 3.2 and 3.3, respectively. The Test 1 sequence did not yield a good pRF map. Upon visual inspection, it is possible to see that estimation resulted in a low number of significant vertices based on correlation between model prediction and empirical data ($R^2 >0.05$) leading to pRF maps within a very limited cortical area. The R^2 threshold is derived from the squared correlation coefficient (r), which refers to

the level of match between model predicted and empirical data, and signifies the extent of variance in empirical data that has been explained by the model for the vertices that were significantly correlated (p <0.05) to a pRF profile. Moreover, the polar angle and eccentricity maps were retinotopically unorganized, which refers that the data retrieved from pRF experiment with Test 1 sequence failed to estimate the x and y parameters correctly. It's worth noting that pRF maps of right hemisphere were slightly larger referring to a higher compliance between model prediction and empirical data at vertices.

The pRF size (i.e. σ) has been previously demonstrated to increase as eccentricity values increase within a visual region [50, 23, 24]. Since Test 1 did not yield accurate x and y parameters, we could not delineate the visual cortex into ROIs, and therefore, will not present the average pRF sizes at each eccentricity.

Test 2 sequence yielded good pRF maps, which can be inspected in Figure 3.2. Upon visual inspection, it is possible to see that estimation resulted in a higher number of significant vertices based on correlation between model prediction and empirical data ($R^2 > 0.087$, $p < 0.05$) then Test 1 sequence, and led to pRF maps in a larger cortical area. The polar angle and eccentricity maps were retinotopically organized, which shows that the data retrieved from pRF experiment with Test 2 sequence estimated the x and y parameters correctly.

The pRF size (i.e. σ) versus eccentricity plots were calculated by fitting a polynomial line to raw σ values at each eccentricity. In Figure 3.4, data from both hemispheres are combined in V1 region. The maximum stimulation eccentricity was 6.75 visual degrees.

Test 3 sequence yielded good pRF maps in terms of number of vertices, which
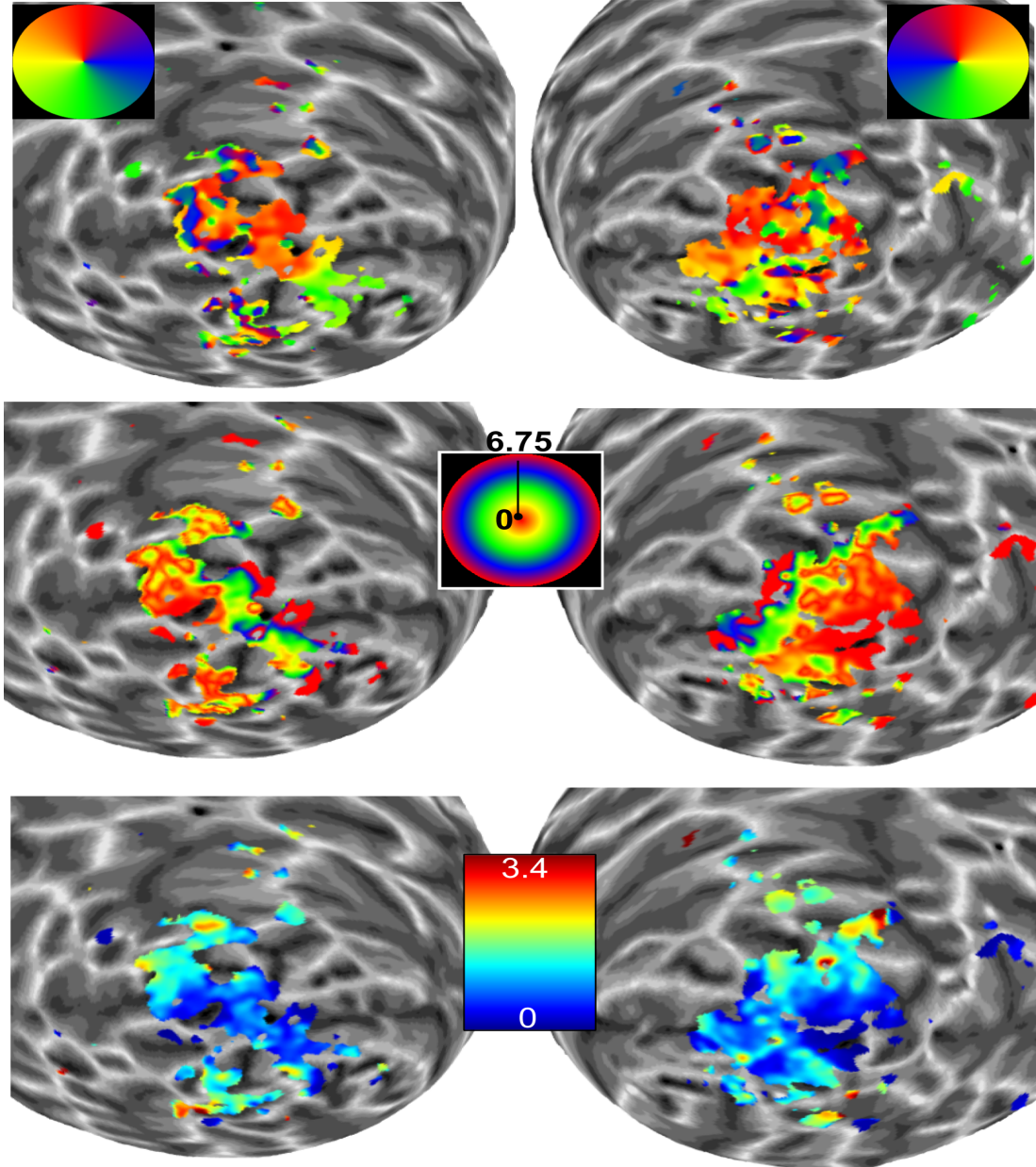
Figure 3.1: pRF estimation results of Test 1. The cortex is inflated in a sphere to allow ease in visual inspection of pRF maps. The first row represents the center of pRFs in terms of polar angle, where color represents an angle from 0 to 360 on Cartesian coordinates. The second row represents the center of pRFs in terms of distance from fovea, that is termed eccentricity, where color represents the visual degree from 0 to 6.75. The third row represents the width of Gaussian pRFs, termed as pRF size, color coded from 0 to 3.375.

Subject 01 Test 2 Full Field Retinotopy
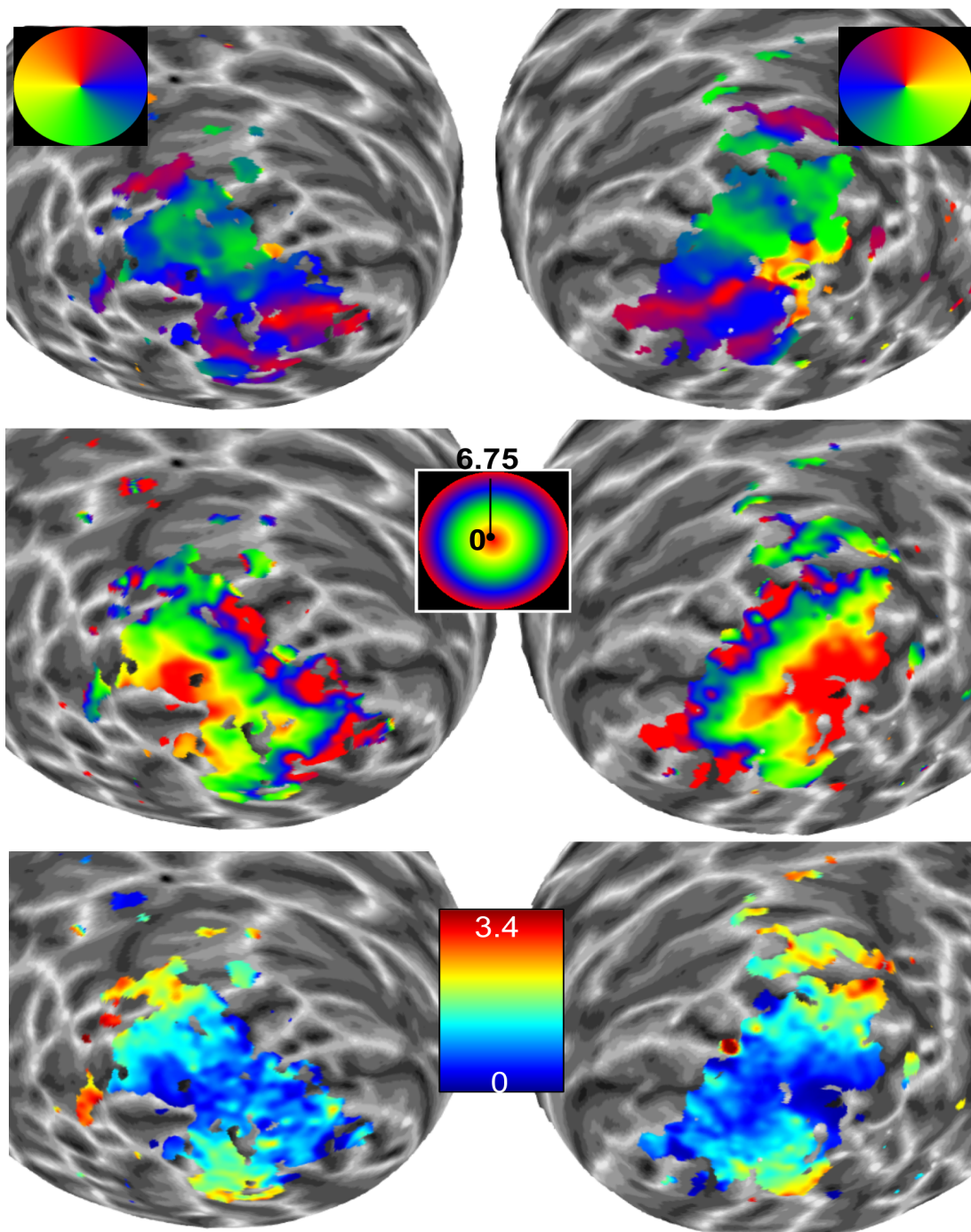
Figure 3.2: pRF estimation results of Test 2. The rows and colormaps correspond to same map type and values as in Figure 3.1.

Subject 01 Test 3 Full Field Retinotopy
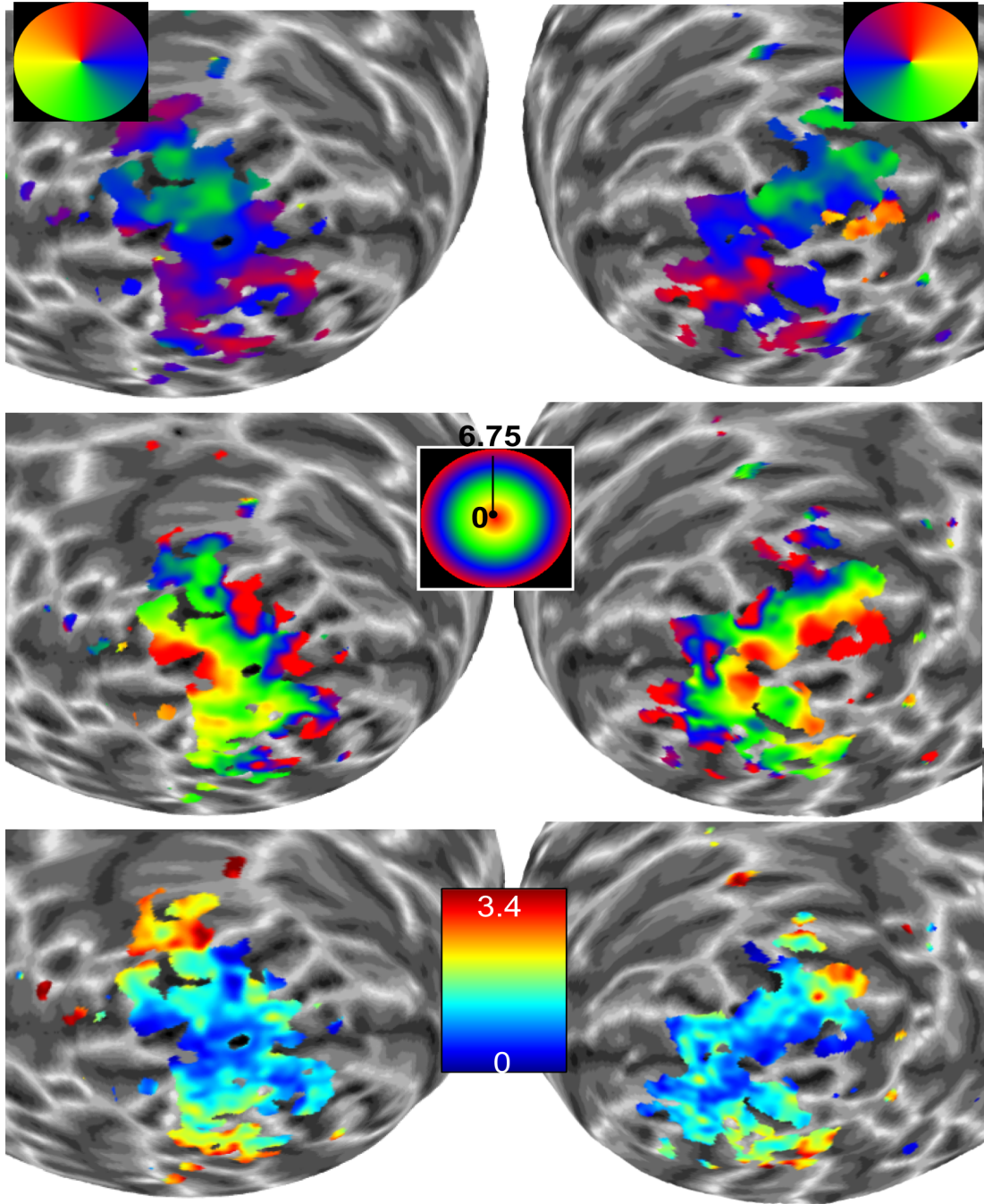
Figure 3.3: pRF estimation results of Test 3. The cortex is inflated in a sphere to allow ease in visual inspection of pRF maps. The rows and colormaps correspond to same map type and values as in Figure 3.1.
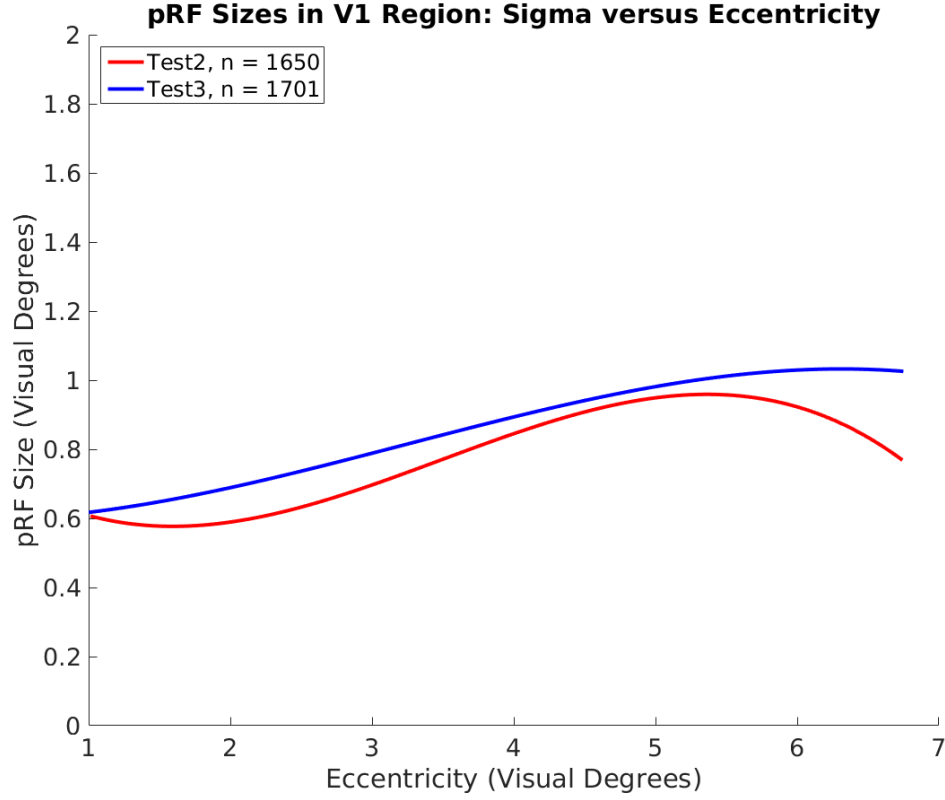
Figure 3.4: pRF sizes in V1 in both hemispheres estimated from Test 2 and 3 experiments.

can be inspected in Figure 3.3. Upon visual inspection, it is possible to see that estimation resulted around the same number of significant vertices based on correlation between model prediction and empirical data ($R^2 > 0.08$) than Test 2 sequence. The polar angle and eccentricity maps were retinotopically organized. The pRF size (i.e. σ) versus eccentricity plots were calculated with the same method applied for Test 2. In Figure 3.4, V1 data from both hemispheres are demonstrated. The pRF sizes increase as a function of eccentricity. At the corner of the stimulation area, around 6.75 visual degrees, the values start to decrease.

Unsmoothed pRF sizes at each eccentricity is fitted with a polynomial to eliminate the noise in raw pRF sizes, and the best fitting line to the data is demonstrated,
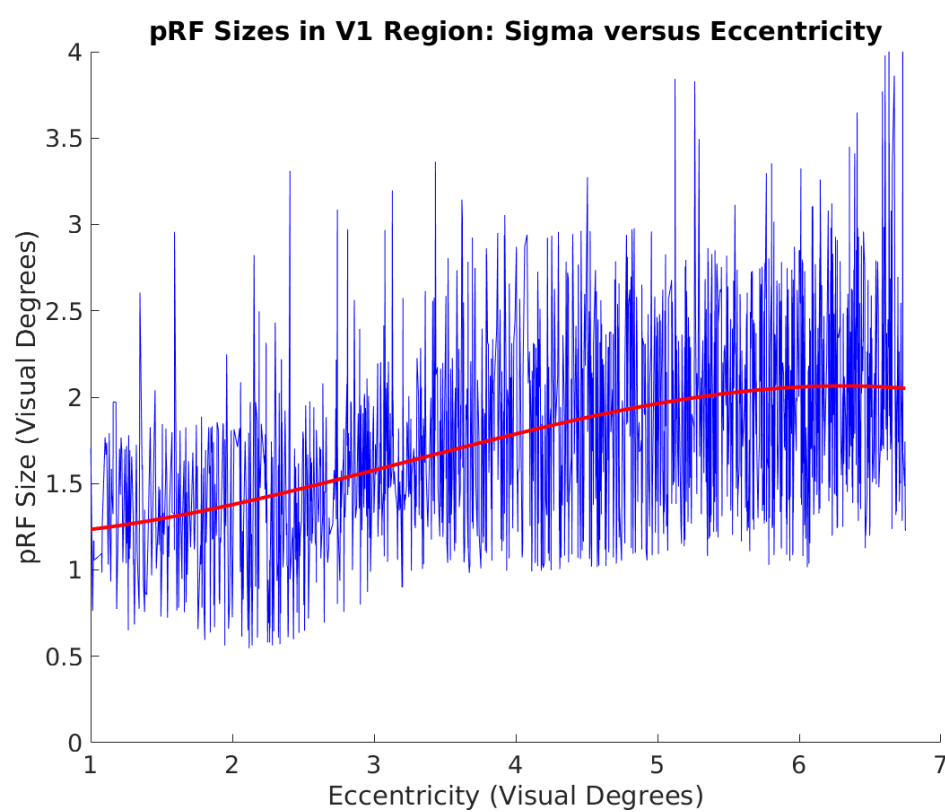
Figure 3.5: An example pRF size estimates in V1 cortex demonstrating the noise level and fitted polynomial curve in terms of visual degrees.

an example can be seen in Figure 3.5. It shows that pRF sizes increase in linear terms, but as we go to higher eccentricities the polynomials demonstrate some non-linearity.

Chapter 4

Stimulus Tuning and Results

4.1 Participants

For stimulus tuning experiments, named Stimulus 1, 2 and 3 and Local pRF experiments, named Local 1 and 2 a single participant (Subject 02) volunteered. Participant had no history of any neurological or psychiatric disorder, were not using any drugs, both had corrected-to-normal vision. Participant gave his written consent before each pRF session. Experimental protocols and procedures were approved by the Human Ethics Committee.

4.2 Optimization of Stimulus Configurations for pRF Estimation

For the second part of our study, we tested different stimulus configurations to achieve pRF estimation from a larger cortical area. The results from fMRI parameter tuning experiments undergone visual inspection and we have decided to continue our retinotopy experiments with Test 3 parameters (see Results 3.3).

The stimulus for pRF experiments were designed and presented with Psychtoolbox-3 [58] on MATLAB 2017a. The stimulus consisted of a wedge and a ring. In the odd numbered runs (i.e. 1, 3, 5, 7, 9 and 11) the wedge rotated counter-clockwise, and wedge contracted simultaneously in 180 time points. In the even numbered runs, the wedge rotated clockwise and the ring expanded simultaneously for 180 time points. In each run, the wedge completed the rotation cycle for 3 times in 60 steps, the ring completed the expansion or contraction cycle 5 times in 36 steps. The size of the wedge was kept constant at each step that corresponded to 15 polar degrees. The ring size was scaled logarithmically as follows

$$S = pix * e^{-4+x/9} \tag{4.1}$$

where, x refers to the number of step (1 to 36), pix refers to the number of pixels of the screen on the shorter axis, due to reducing oblong screen into a square, S refers to the size of the ring (i.e. its diameter) in pixel units at each step (the average diameter of 36 steps was 0.375 in visual degrees). The first step of expanding ring at the beginning of each cycle, and last step for contracting ring at the end of each cycle were manipulated to encircle the fixation point, to

overcome an unstimulated area between fixation point and the inner border of the ring.

We replicated the stimulation protocol of previous pRF studies [23, 24] aiming for pRF estimation from a larger cortical area. It was demonstrated that using a set of natural scene images lead to pRF maps covering extrastriate regions of visual cortex, more in comparison to high-contrast patterns and colorful versions of high-contrast patterns.

We have conducted three experiments, named Stimulus 1, Stimulus 2 and Stimulus 3. In Stimulus 1 experiment, we used black and white ripple stimulus as demonstrated in Figure 4.1.A. In Stimulus 2 experiment, we used colorful ripple stimulus as demonstrated in Figure 4.1.B. We used a natural image set in Stimulus 3 experiment retrieved from previous studies [23, 24] as demonstrated in Figure 4.1.C. The natural images were presented for 1000 ms, followed by another natural image from the set.

4.3   Stimulus Configuration Results

For pRF estimation with Stimulus 1, Stimulus 2 and Stimulus 3, we used SamSrf toolbox on MATLAB as explained in Section 2.1 of Methods, and in detail in Appendix B.2. We have visually inspected the results and determined that Stimulus 3 experiment yielded the best results in terms of a larger cortical area for maps, which was conducted with a natural image set. The pRF maps are shown in Figure 4.2, 4.3 and 4.4 respectively. The R^2 threshold to display the maps was at the significant level, 0.05.
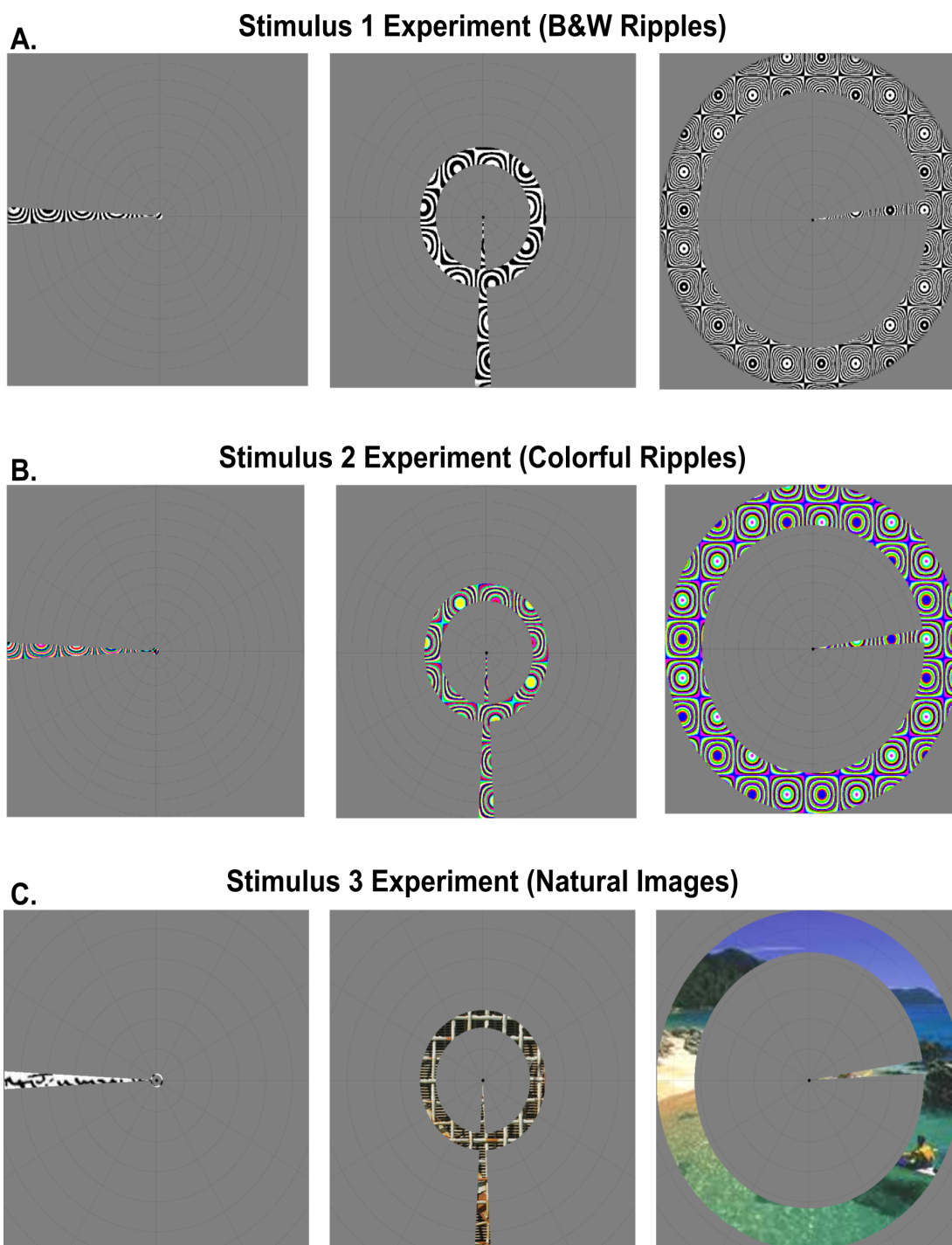
Figure 4.1: Example stimuli used in pRF experiments at three time points. A, black and white ripple stimulus; B, colorful ripple stimulus; C, natural image stimulus

Subject 02 Stimulus 1 Experiment
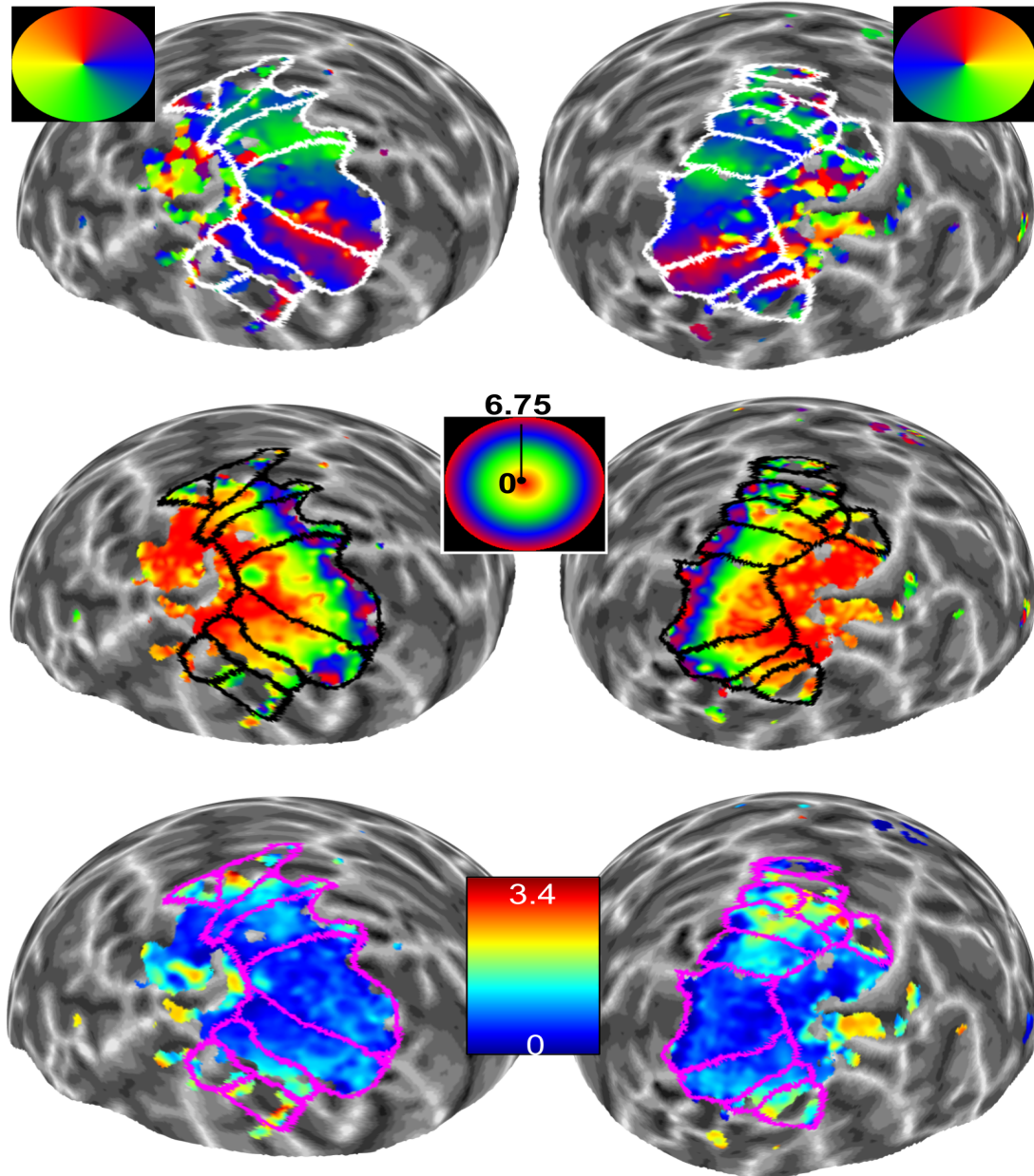
Figure 4.2: pRF estimation results of Stimulus 1 experiment. The cortex is inflated in a sphere to allow ease in visual inspection of pRF maps. The first row represents the center of pRFs in terms of polar angle, where color represents an angle from 0 to 360 on Cartesian coordinates. The second row represents the center of pRFs in terms of distance from fovea, that is termed eccentricity, where color represents the visual degree from 0 to 6.75.The third row represents the width of Gaussian pRFs, termed as pRF size, color coded from 0 to 3.375.
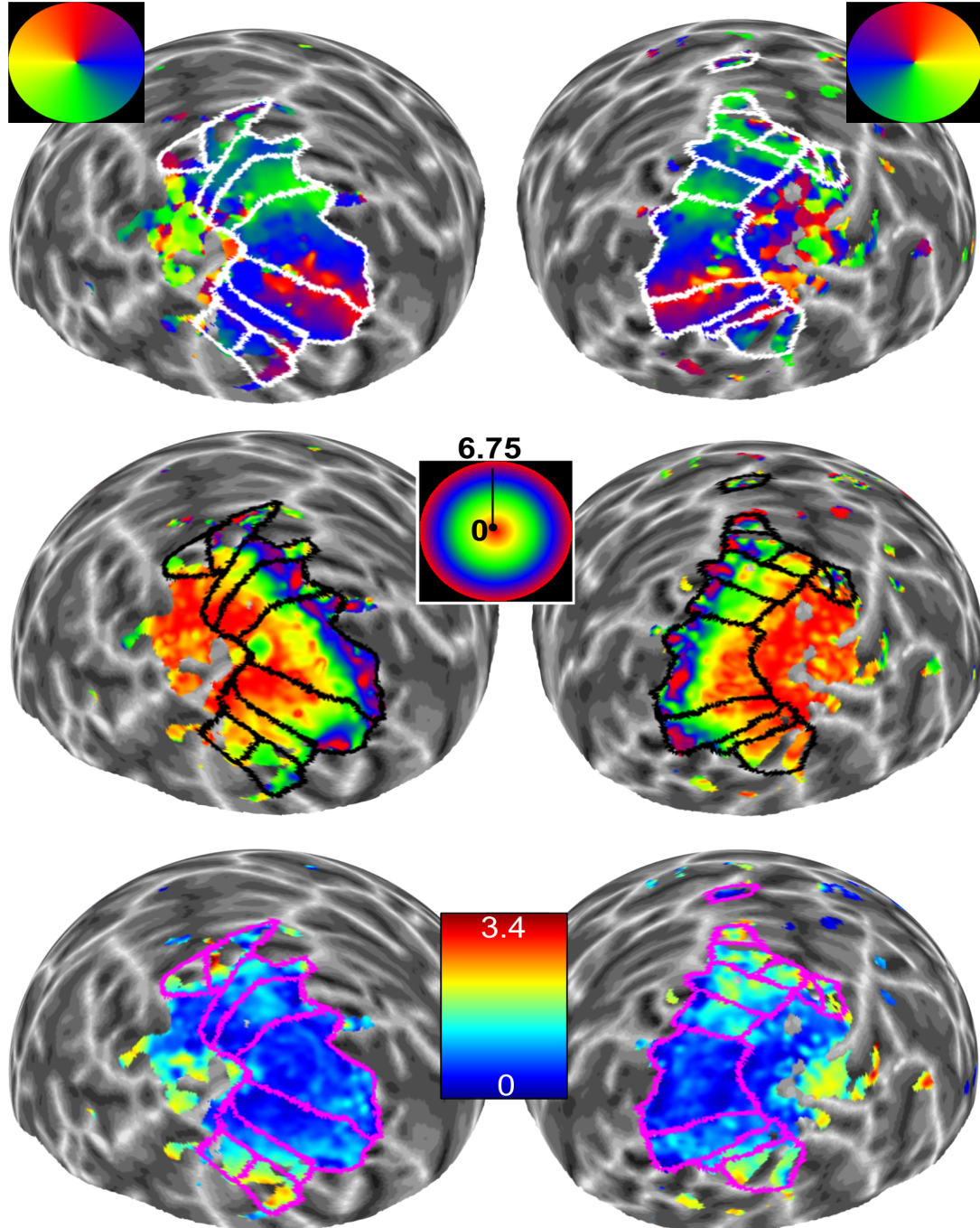
Figure 4.3: pRF estimation results of Stimulus 2 experiment. The rows and colormaps correspond to same map type and values as in Figure 4.2.

Subject 02 Stimulus 3 Experiment
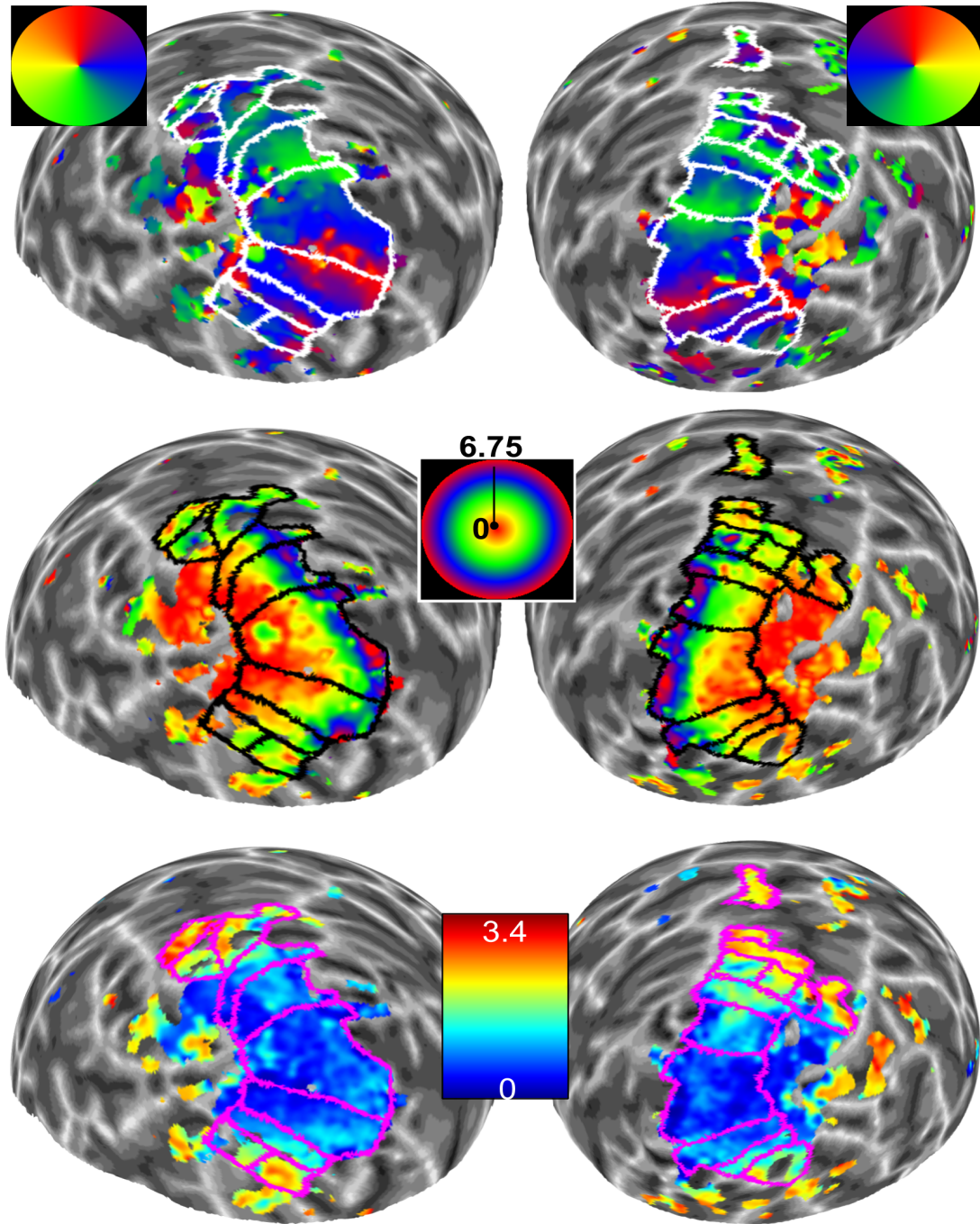
Figure 4.4: pRF estimation results of Stimulus 3 experiment. The rows and colormaps correspond to same map type and values as in Figure 4.2.

In Figure A.1 and A.2, the visual field of the subject is demonstrated as estimated from Stimulus 1, 2 and 3 experiments. The contralateral processing of the visual hemifields is demonstrated. The data demonstrated in both figures show that a limited ipsilateral processing is prevalent for foveal regions, at low eccentricities between 0 and 2. In Figure A.1 and A.2, it can be inspected that around 255 degrees, left hemisphere processes a mean eccentricity of 4 to 6 degrees.

In Figure 4.5 and 4.6, the mean pRF size in each ROI is shown that was estimated with Stimulus 1, Stimulus 2 and Stimulus 3 experiments. The results showed that pRF sizes increase in higher level regions such as V4, VO1, LO1 and LO2. IPS0 (V7) region can be delineated successfully in Stimulus 3 experiment in left hemisphere, and by all stimulus conditions in the right hemisphere. Therefore, our results indicate that Stimulus 3 experiment, that utilized natural images, yielded the best results in terms of higher number of visual region delineations. All ROI delineations were manually performed based on a previous study [54].

Based on the Table 4.1 and Figure 4.4 we claim that Stimulus 3 condition yielded the most robust maps to use in pRF estimation in further sections of this study. The robustness of the map was refers to the number of vertices being high and higher level visual areas being prevalent that can be delineated manually on the pRF maps.
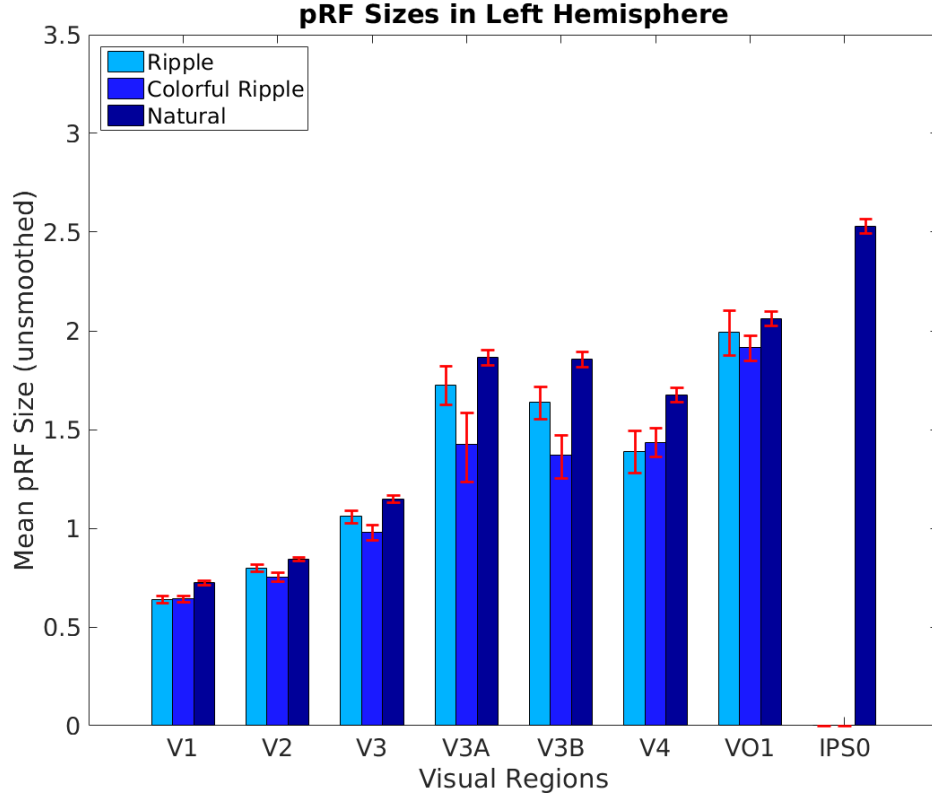
Figure 4.5: Mean pRF sizes in left hemisphere at each ROI in terms of visual degrees. The error bars refer to 95% confidence intervals of each mean value.

4.4 HRF Estimation Procedure for pRF Estimation

HRF is known to be influenced by subject specific parameters, such as central blood flow and differs between regions of the brain [30, 31, 32]. Therefore, we wanted to estimate subject-specific empirical HRF from visual ROIs determined by performing a general linear model (GLM) analysis. We replicated a stimulation protocol for HRF based on previous studies [23, 24]. Our HRF experiments consisted of 10 repetitions of 15 TR blocks. First TR of each block is termed as a "photic burst", when full field images encircled within 6.75 eccentricity to comply
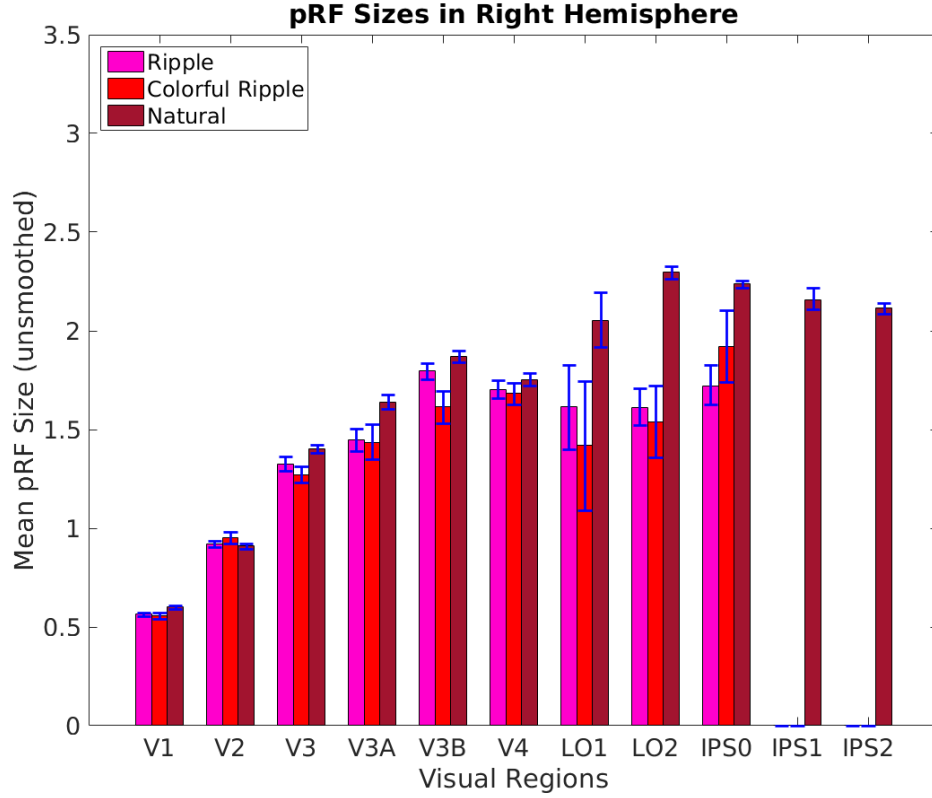
Figure 4.6: Mean pRF sizes in right hemisphere at each ROI in terms of visual degrees. The error bars refer to 95% confidence intervals of each mean value.

with pRF stimulation protocol were presented on the same MR compatible LCD screen (1920x1080, 60Hz). Each image was presented for 500 ms, and there were four images presented consecutively. The photic burst trial was followed by 14 TRs of resting period, where a blank screen was presented to the subject. The number of measurements was 155, of which first 5 were discarded from analysis. A fixation task was used to limit eye movements of the subject in both conditions.

We have conducted two HRF experiments with the same subject used in Stimulus 1, 2 and 3 experiments, and named them HRF 1 and HRF 2 experiments. In HRF 1, we utilized scrambled versions of the natural image set with an aim to prevent unforeseen effects of full field, unmasked images. In HRF 2, we used

Table 4.1: Total Number of Vertices from Two Hemispheres at each ROI

Conditions	Stimulus 1			Stimulus 2			Stimulus 3		
Region	LH	RH	Total	LH	RH	Total	LH	RH	Total
V1	1702	1183	2885	2274	1929	4203	1538	1464	3002
V2	1522	1110	2632	1903	1497	3400	1268	1190	2458
V3	798	856	1654	1115	985	2100	750	718	1468
V3A	194	93	287	188	237	425	273	111	384
V3B	87	190	277	155	162	317	191	218	409
LO1	0	108	108	0	61	61	0	155	155
LO2	0	112	112	0	63	63	0	330	330
IPS0	0	9	9	0	48	48	0	308	308
V4	99	343	442	280	434	714	226	449	675
VO1	112	0	112	374	0	374	220	0	220
Occ (Total)	6455	5574	12029	7784	7316	15100	6724	8302	15026

natural images without scrambling to investigate if there were differences in HRF curves. The images were presented for a duration of 500 ms on screen, therefore, at each photic burst trial there were 4 images interchanged within the trial. A sample protocol of the HRF experiments can be seen in Figure 4.7.

To estimate the HRF curves, we firstly conducted previously explained realignment and unwarping procedure, and then continued with coregistration. In the next step, GLM analysis was performed with a design and contrast matrix specifying and weighting the photic burst and the resting trials on SPM12 [52]. The stimulus train can be inspected in Figure 4.10. Based on the GLM results, we have determined visual ROIs with a significance level, $p = 0.001$. We set the minimum cluster size as 50 voxels to prevent single voxel activations on SPM12. We have found ROIs at both primary and extrastriate areas of the visual cortex, based on visual inspection of the activation clusters as seen in Figure 4.8.A and B. The region that ROI is extracted coarsely corresponds to region the pRFs were successfully estimated, as seen on the pRF map displayed on non-inflated brain in Figure 4.9.

Stimulation Protocol of HRF Experiments

1 TR Stimulation (Photic Burst)   **14 TRs Rest**

1 Block with 15 Trials

10 Repetitions of Blocks
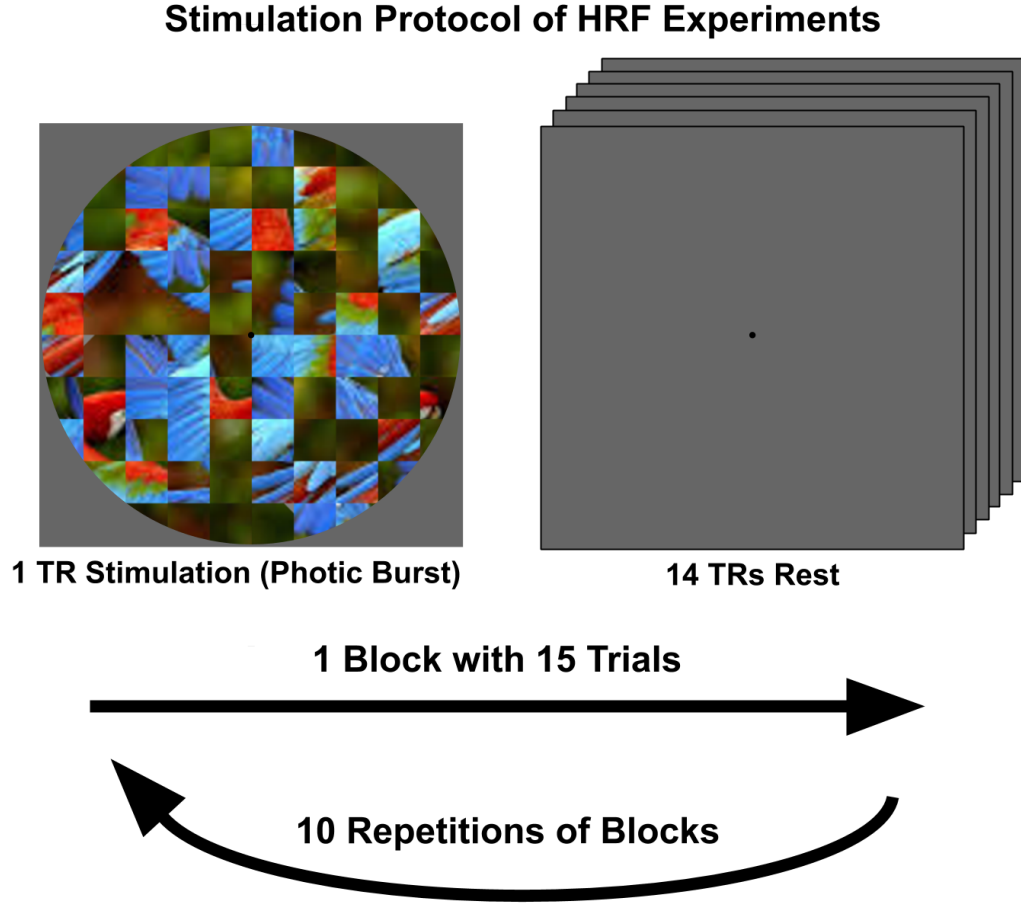
Figure 4.7: Sample demonstration of the stimulation protocol for HRF experiments.

We have estimated the HRF curve by utilizing finite impulse response (FIR) method on the raw data extracted from visual ROIs. We created our stimulus train and a corresponding FIR design matrix in line with our stimulation protocol. To estimate $\hat{\beta}$ for each TR of the HRF experiment, we used the equation for Ordinary Least Squares (OLS) solution

$$\hat{\beta}_{FIR} = y(X_{FIR}^T X_{FIR})^{-1} X_{FIR}, \tag{4.2}$$

where $\hat{\beta}$ refers to the β weights of HRF curve at each trial, y represents z-scored
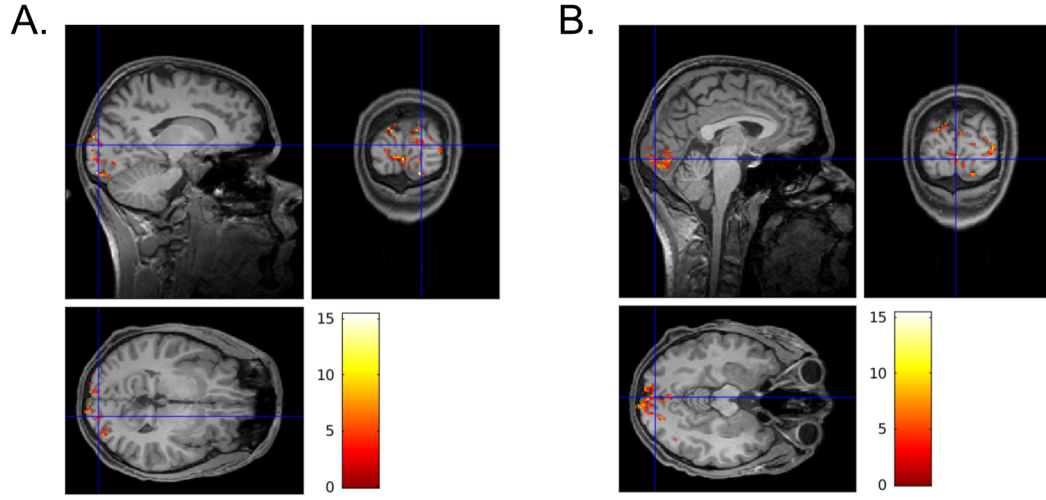
Figure 4.8: Voxels that responded to photic burst in, A., extrastriate areas within occipital lobe and B., primary areas near calcarine sulcus. The legend represents F values calculated by GLM analysis.

and detrended BOLD data from ROI voxels, and X_{FIR} is our FIR design matrix seen in Figure 4.10.

Following the $\hat{\beta}_{FIR}$ estimation for each block at each voxel, we calculated the mean HRF by averaging the results (i.e. $\bar{\hat{\beta}}_{FIR}$) and 95% confidence intervals of the mean. In the next step, we fitted our data with a double Γ function,

$$f_1(x_1|a_1 b_1) - f_2(x_2|a_2 b_2) = w_1 \frac{x_1^{a_1-1} e^{\frac{-x_1}{b_1}}}{b_1^{a_1}\Gamma(a_1)} - w_2 \frac{x_2^{a_2-1} e^{\frac{-x_2}{b_2}}}{b_2^{a_2}\Gamma(a_2)}, \qquad (4.3)$$

which was defined in terms of a and b parameters, where a is shape parameter, b is the scale parameter. x refers to a time variable, in our case the duration of a block in terms of TR, and w refers to function weights. With this equation we successfully found the best a and b parameters, and weights for both $f_1(x)$ and $f_2(x)$ to fit our empirical $\bar{\hat{\beta}}_{FIR}$ via optimizing the error with Sum of Squares

Polar Angle Map on Non-Inflated Brain
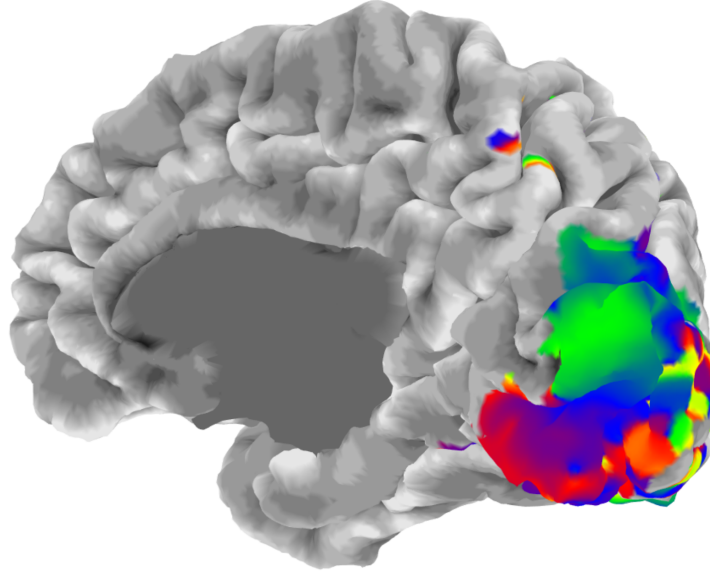
Figure 4.9: Polar Angle Map on Non-Inflated Brain

Error (SSE) equation

$$SSE = \sum(\bar{\hat{\beta}}_{FIR} - (f_1(x) - f_2(x))^2. \tag{4.4}$$

The results of HRF estimation from HRF 1 experiment will be explained in Section 4.5. The output of this estimation was used in pRF estimation analysis to convolve model-based time-series predictions with HRF from subject's visual cortex instead of a canonical HRF.

4.5   HRF Estimation Results

The GLM analysis resulted in a number of voxels in subject's visual cortex, as seen in Figure 4.8. In HRF 1, and the results consisted of 1248 voxels, and in
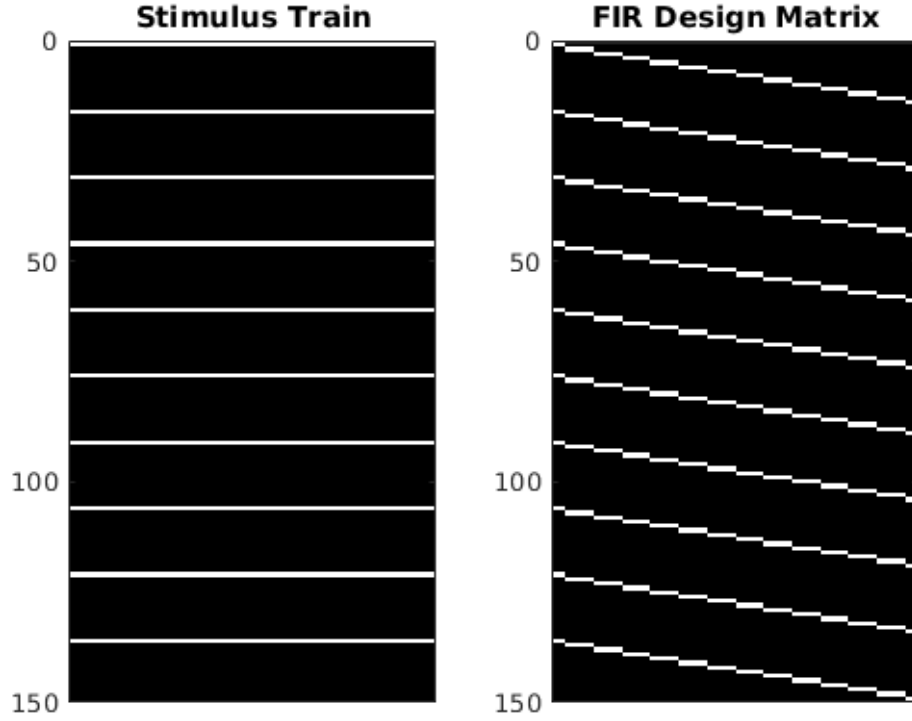
Figure 4.10: Stimulus train and FIR design matrix of the stimulation protocol in HRF experiment

HRF 2 it was 1220 voxels. Raw BOLD data from these voxels were extracted and processed as explained in Section 4.4. Our empirical HRF is referred as $\bar{\hat{\beta}}_{FIR}$, and its average values at each time point and the error bars representing 95% confidence interval of mean are shown in Figure 4.11.

We have fitted the previously demonstrated difference of two gamma probability distribution functions (Γ) in Equation 4.3 on data retrieved from each voxel by optimizing for parameters of the model by minimizing SSE in Equation 4.4. The code for FIR method and curve fitting can be inspected in Appendix B.1. The average of Γ functions from each voxel is shown in Figure 4.11, where we can argue that we have achieved to estimate a finely fitting function representative of

out empirical HRF.
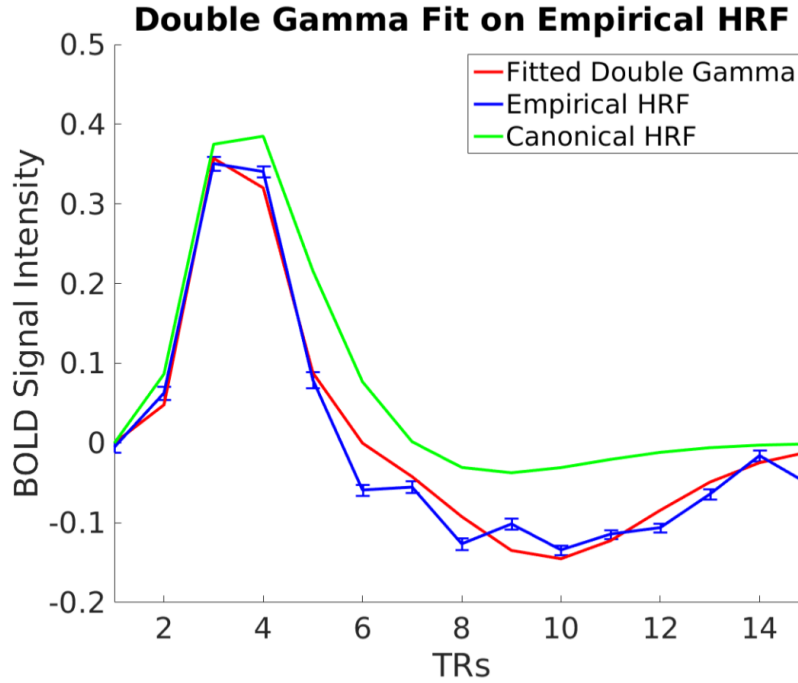
Figure 4.11: $\bar{\hat{\beta}}_{FIR}$ values at each TR. The function is not smooth since it consists of a single value at each TR.

As next, we have conducted the pRF analysis again on Stimulus 2 with subject specific HRF. The resulting pRF maps are can be inspected in Figure 4.12.

Following the inspections through plots, we performed Mann-Whitney U test on pRF sizes to compare the influence of canonical HRF and subject specific HRF over our estimation. pRF sizes did not differ when subject specific HRF was used in pRF estimation ($p > 0.05$).
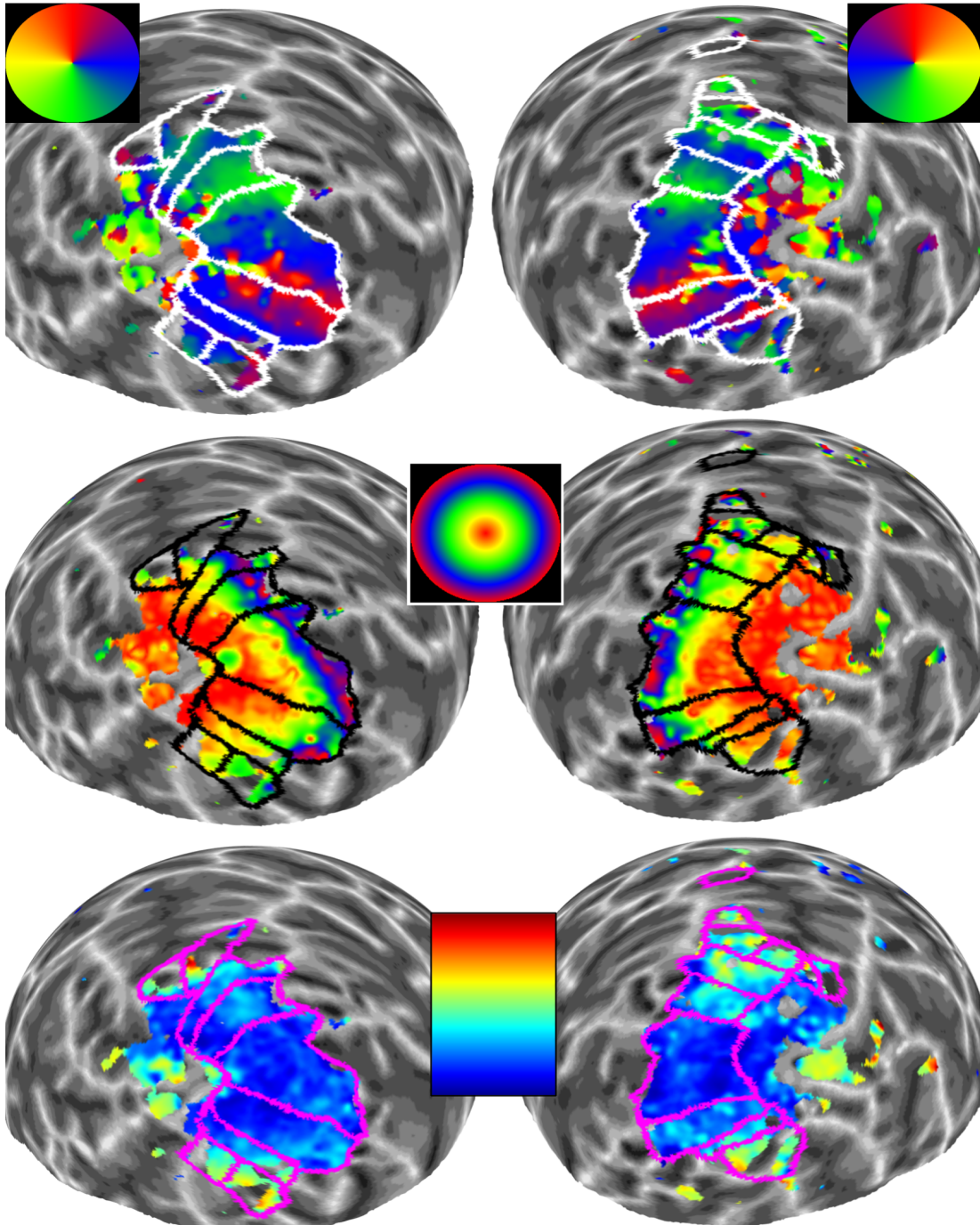
Figure 4.12: pRF Maps Estimated with Subject Specific HRF. The rows and colormaps correspond to same map type and values as in Figure 4.2.

Table 4.2: Number of vertices from two hemispheres at each ROI estimated with canonical and subject specific HRF

Conditions	Canonical HRF			Subject Specific HRF		
Region	LH	RH	Total	LH	RH	Total
V1	1827	1929	3756	2244	1828	4072
V2	1532	1497	3029	1923	1430	3353
V3	880	985	1865	1060	939	1999
V3A	124	237	361	168	216	384
V3B	95	162	257	109	159	268
V4	185	434	619	229	372	601
Occ (Total)	7201	7316	14517	7217	6635	13852

Chapter 5

Local pRF Estimation and Results

5.1 Local pRF Stimulus and Estimation Procedure

To further improve the location specificity of the pRF estimation method, we employed a new approach. We have restricted the visual stimulation to a specific location. A similar approach was employed in a study investigating influence of depth perception on receptive fields [47]. In this section, we have used a bar stimulus in order to cover receptive field at 240 polar angle and 4 degrees of eccentricity with a radius of 150 arcmin. We predicted that a wedge combined with ring stimulus could be insufficient due to low acuity levels in peripheral vision and thus would lead to a low level of variance explained in pRF estimation.

The bar stimulus rendered with a flickering checkerboard at 10 Hz was presented

Bar Stimulus for Local pRF Session
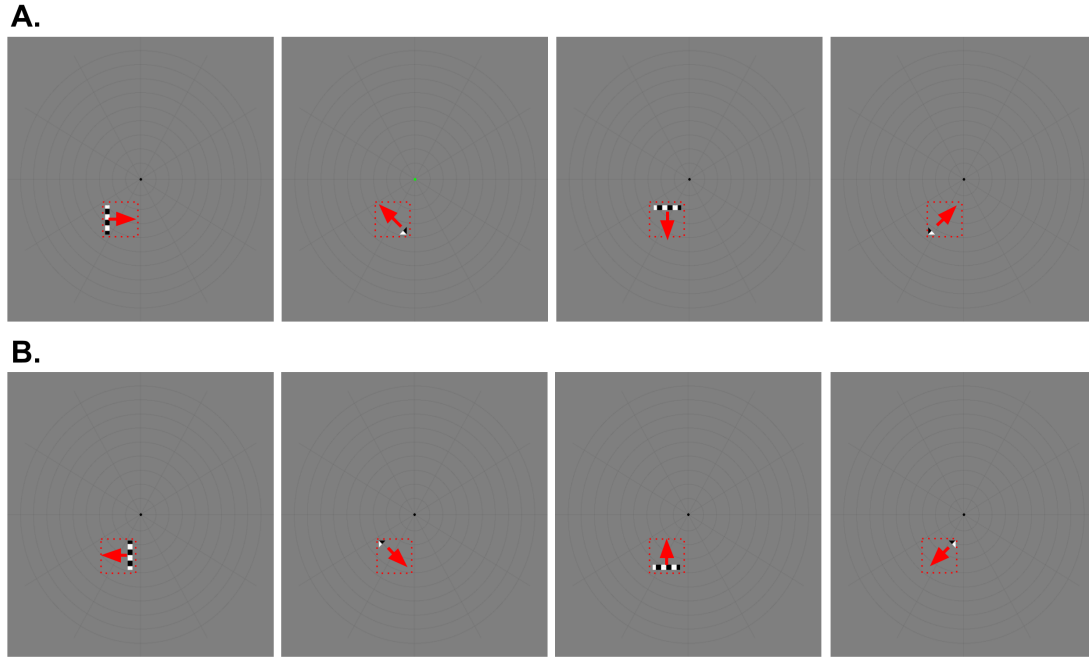
Figure 5.1: Bar stimulus for local pRF scanning. There were a total of eight directions, A. four forward directions and B. four reversed directions. Red square in dots represents 150 arcmin area on the visual field.

with Psychtoolbox-3 [58] on MATLAB 2017a [53]. The bar moved in eight directions to cover 150 arcmin field in six or eight steps in each direction. If the bar was in a horizontal or vertical position there were six steps to cover the area of 150 arcmin, if it was diagonal there were eight. The change in number of steps were planned to keep the bar size constant in each direction.

The first four directions of the bar were from left to right, from bottom right corner to top left corner, from top to bottom, and from bottom left corner to top right corner. After these directions were covered, they were reversed. Therefore, the bar scanned 150 arcmin field in eight directions. We have named these eight directions a block, which consisted of 56 measurements. 28 measurements were called forward motion, and the following 28 measurements were reversed motion

of the block. In a local pRF run, we have taken 224 measurements consisting of 4 blocks repeated after each other. There were no rest period between the blocks. In our local pRF experiment, we had 3 runs utilizing the high-contrast flickering checkerboard stimulus, and 3 runs with the same natural scene image set used in Section 4.2 made smaller to fit in 150 arcmin area. An example block of our stimulus with its directions can be seen on Figure 5.1.

We conducted two experiments, Local 1 and Local 2. In Local 1 experiment the flickering checkerboard stimulus was utilized; in Local 2 experiment we rendered the natural image set at the same specific location masked with travelling bars. During the analysis step we also combined the data from both sessions in order to control for and test if there is an effect of number of measurements in local pRF estimation on the resulting pRF map size.

5.2 Local pRF Estimation Results

Retinotopy experiment on a specific region at the visual field resulted in maps in Figure 5.2, 5.3 and 5.4 at R^2 threshold 0.3, displaying vertices that explained above 54% of variance. As in full field pRF scanning protocol, natural images yielded more vertices that complied with pRF model, meaning that the maps were spread on a larger cortical area. The results of local pRF maps corresponded well to the full field pRF maps. The location of the maps were on the V1-V2d border as we have expected. In addition to flickering checkerboard and natural image set local pRF estimation results, we have also combined all the data from both high-contrast and natural image runs. In full field pRF sessions we estimated pRF maps based on a total of 2160 measurements, whereas in a local pRF session we

only had 672 measurements. To control for number of measurements and any problems stemming with a low level of measurements, we combined the analysis with 1344 measurements, which resulted in larger maps at the same anatomical location, which can be inspected on Figure 5.4.

The correlation coefficient driven R^2 threshold estimates for Local 1 and Local 2 results were selected to be higher compared to the Stimulus 1, 2 and 3 experiments. Controlling for a number of measurements yielded larger pRF maps. We know that number of measurements is an influential parameter for full field pRF estimation protocol, as we have compared full field pRF maps estimated 8 and 12 runs before to shorten the duration of session regarding the subject, and found that 12 runs estimated larger pRF maps extending more to extrastriate areas.

We did not conduct further statistical tests to compare Local 1, 2 or combined data. We also did not plot pRF sizes against eccentricity values, as the eccentricity estimates did not match Stimulus 1, 2 and 3 experiment results at the V1/V2d border. This can be due to an attentional modulation towards periphery that may be inducing pRF location shifts. The map showed foveal eccentricity values at the regions with peripheral eccentricities are processed, based on pRF results of Stimulus experiments. The stimulation protocol may be influential on this problem, and we thought adding noise to the background can overcome this by evoking a baseline level of activity in visual cortex and allowing the detection of bar stimulus.
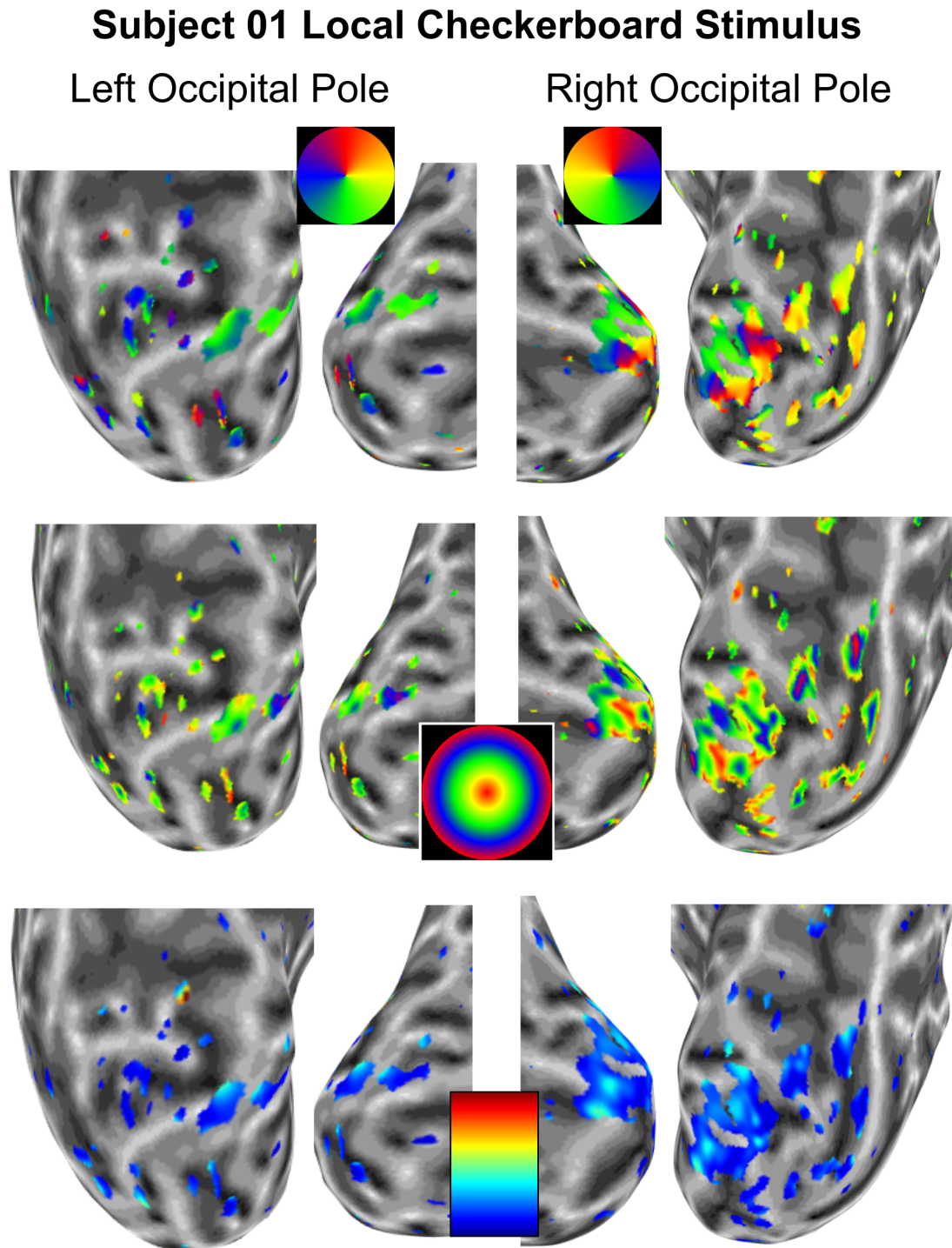
Figure 5.2: pRF estimation results of high-contrast checkerboard stimulation.
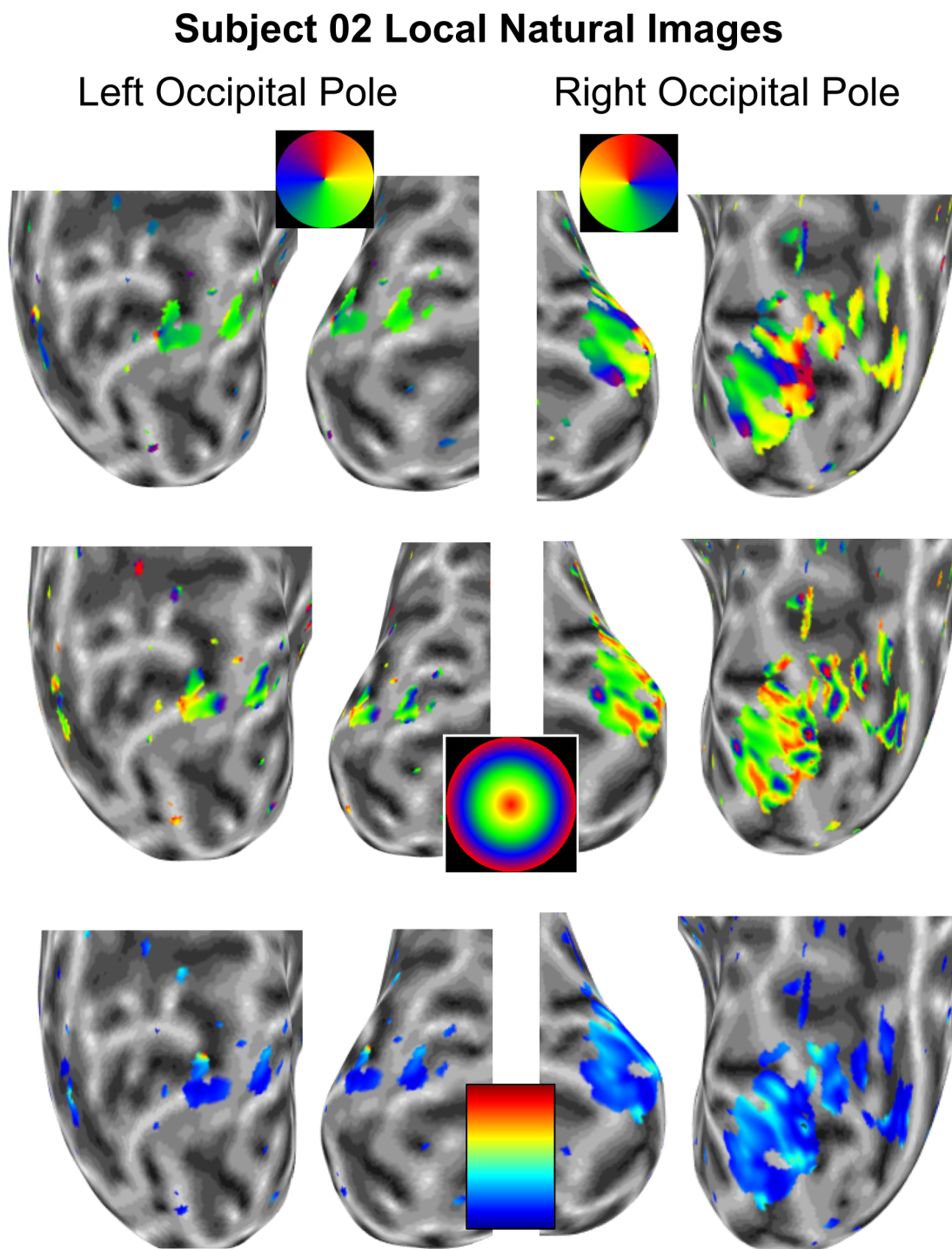
Figure 5.3: pRF estimation results of natural image stimulation stimulation
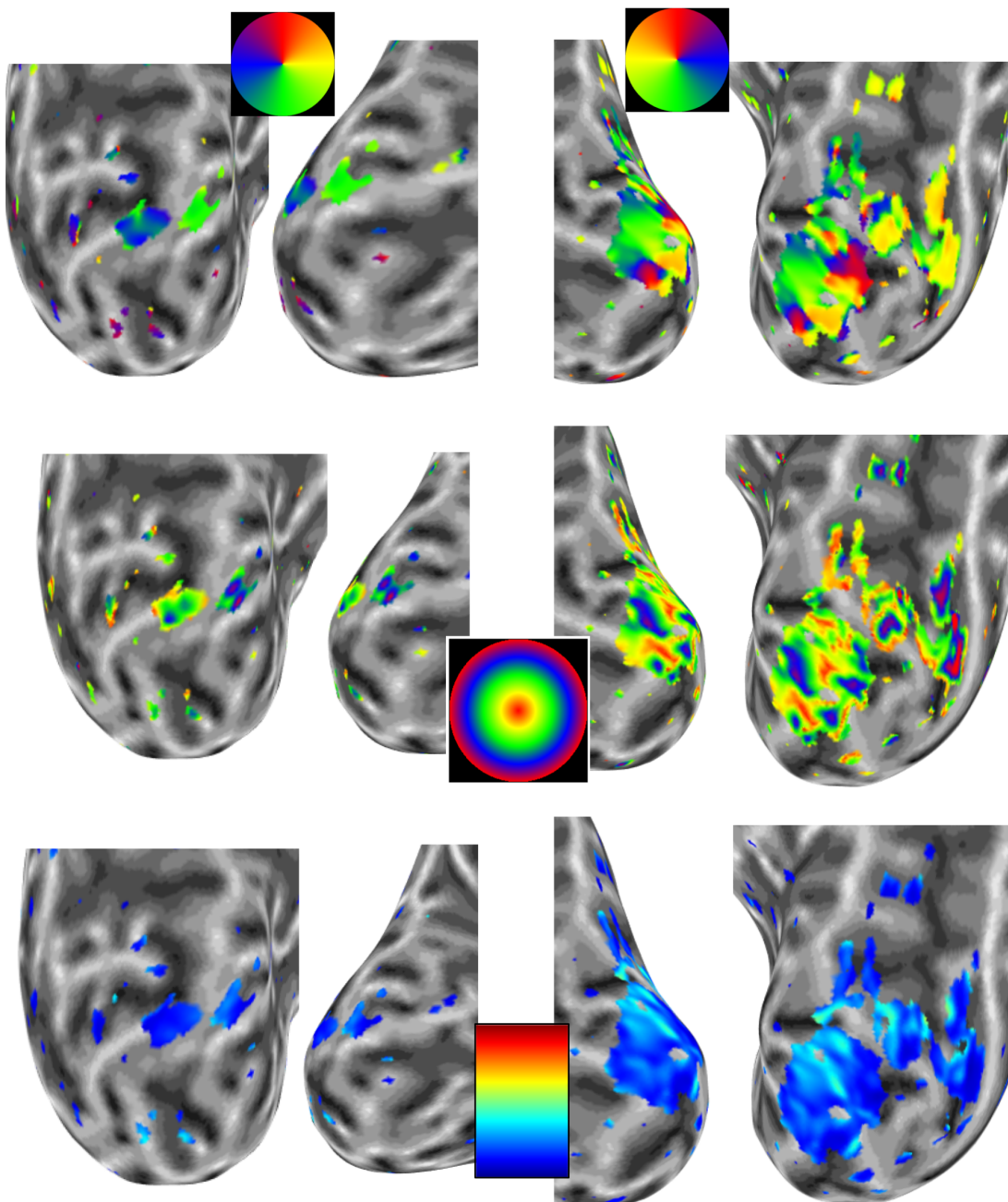
Figure 5.4: pRF estimation results of combined data

Chapter 6

Increasing the Sample Size

6.1 Participants

In this section, we increased our sample size in order to control for intersubject differences of pRF maps estimated with our protocol. Three participants volunteered for the study (Subject 03, 04 and 05). Participants had normal or corrected to normal vision, no history of any neurological condition and were not using any drugs. Participants gave their informed consent before each session. Experimental protocols and procedures were approved by the Human Ethics Committee.

In the first phase, the subjects participated to a full field pRF session with Stimulus 3 (i.e. with natural images) condition, on the next day, they participated to a local pRF session. The local pRF stimulus was manipulated by adding noise to the unstimulated areas on the presentation screen. The analysis procedures were kept the same as previously described.

6.2 Improving fMRI Parameters

The fMRI parameters of Test 3 sequence were further improved to ensure a higher level of SNR. The TE parameter was decreased to 43.8 ms, which is a recommended value for visual cortex mapping [59]. Flip angle was increased to 80 degrees by calculating the Ernst angle. Bandwidth was increased to 1544 Hz/px, excite pulse duration was increased to 6680 μs to attain lower TE and higher flip angle values. All other parameters were kept the same as Test 3 sequence.

6.3 Tuning Local pRF Stimulus

To improve the results of local pRF experiments, we added spatial noise to the background, where it was previously at mean luminance. The noise was defined by assigning each pixel randomly with values between 40% and 60% of the mean luminance. Randomly generated noise images (i.e salt and pepper noise) were presented with a speed of 10 Hz. By doing so, we expected to evoke a baseline BOLD response throughout the central visual field of 13.5 degrees. Furthermore, we expected that the estimation of the receptive fields at local field would be better (i.e. the polar and eccentricity values estimated with local and full field maps would match), because we could capture the correlation between predicted and empirical baseline signal, we can detect the bar stimulus response in more detail. In a local pRF session, there were 4 runs each containing 8 repetition of 56 measurements. The bar stimulus was rendered with a flickering checkerboard pattern at 10 Hz.

6.4 pRF Estimation Results and Statistics

The results of full field pRF experiment were similar to Stimulus 3 results in terms of dorsal stream regions on IPS being prevalent in each subject's retinotopic map. We have failed to estimate Subject 05's full field retinotopic map due to

coregistration mismatch between anatomical and functional slices, due to motion artifacts caused by participant.

The results of noise added local pRF experiments did not satisfy our expectations. Vertices on the border of dorsal V1/V2 near occipital pole was estimated similar to previous local pRF experiment results. All three subjects participated to the noise-added local pRF sessions self-reported adverse feelings due to rendered noise.

We conducted statistical tests to reveal if there are pRF size differences between dorsal and ventral streams and investigated intersubject variability in pRF sizes. The pRF size values were derived from vertices that had eccentricity values between 1 and 6 degrees, since foveal regions and the corners of stimulation area demonstrated a high level of variance. We have conducted tests on raw data (no smoothing was applied) that was above the threshold ($R^2 > 0.05$). We have tested the normality of data in both hemispheres by performing a Kruskall-Wallis Test and as none demonstrated a normal distribution, we have selected to perform Kolmogorov-Smirnov or Mann-Whitney U Test, based on the number of groups compared. Kolmogorov-Smirnov Test is a non-parametric test equivalent to one-way analysis of variance (ANOVA). Mann-Whitney U Test is another non-parametric test equivalent to T-Test.

To investigate intersubject variability, we combined raw data (i.e. unsmoothed) in ROIs (i.e. V1, V2 and V3) from both hemispheres and compared the pRF sizes within subjects. The results showed the pRF sizes of the subjects were different from each other in low level visual areas ($M_{s02} = 0.8865$, $M_{s03} = 0.8137$, $M_{s04} = 0.8889$, $N_{s02} = 8842$ $N_{s03} = 6055$ $N_{s04} = 5500$, $p < 0.001$). This result points out that receptvie field sizes are subject to individual differences. Therefore, researchers investigating systematic differences in pRF sizes of different groups of individuals must take intersubject variability into account.

To investigate differences between pRF sizes in early visual streams, we combined the vertices at dorsal half of V1, V2d and V3d from both hemispheres and compared with ventral half of V1, V2v and V3v from both hemispheres of

Subject 02, 03 and 04. The Mann-Whitney U test results showed that pRF sizes between early dorsal and ventral areas are not significantly different from each other ($M_{dorsal} = 0.8826$, $M_{ventral} = 0.8768$, $N_{dorsal} = 9722$ $N_{ventral} = 11465$, $p > 0.05$).

The pRF size differences between hemispheres were investigated. The data from V1, V2 and V3 regions of Subject 02, 03 and 04 were combined for left and right hemispheres separately. The results showed that, pRF sizes in right hemisphere were significantly larger than left hemisphere at low-level visual areas ($M_{left} = 0.8219$, $M_{right} = 0.9321$, $N_{left} = 10109$ $N_{right} = 11078$, $p < 0.001$).
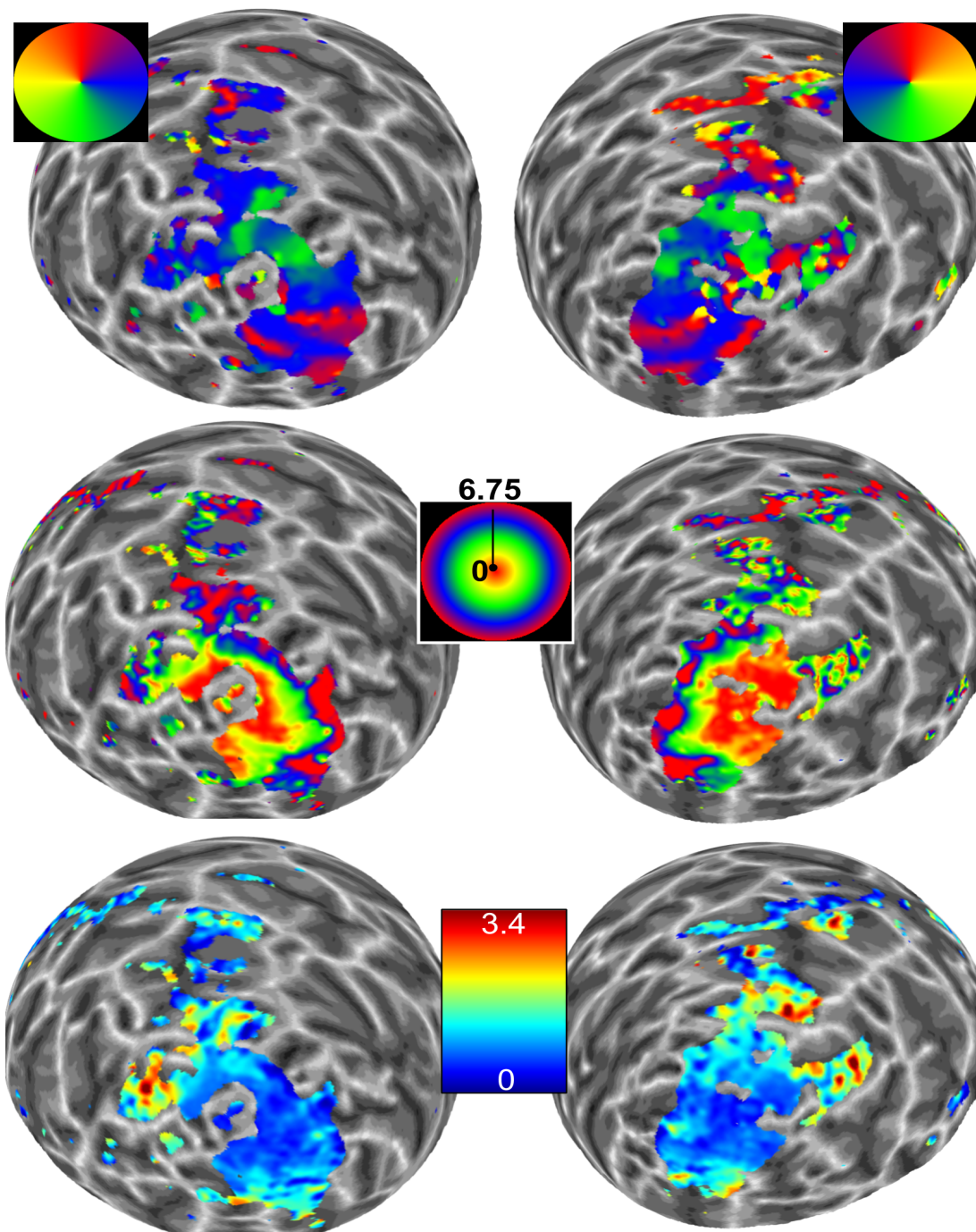
Figure 6.1: Full field pRF maps of Subject 03

Subject 04 Full Field Retinotopy
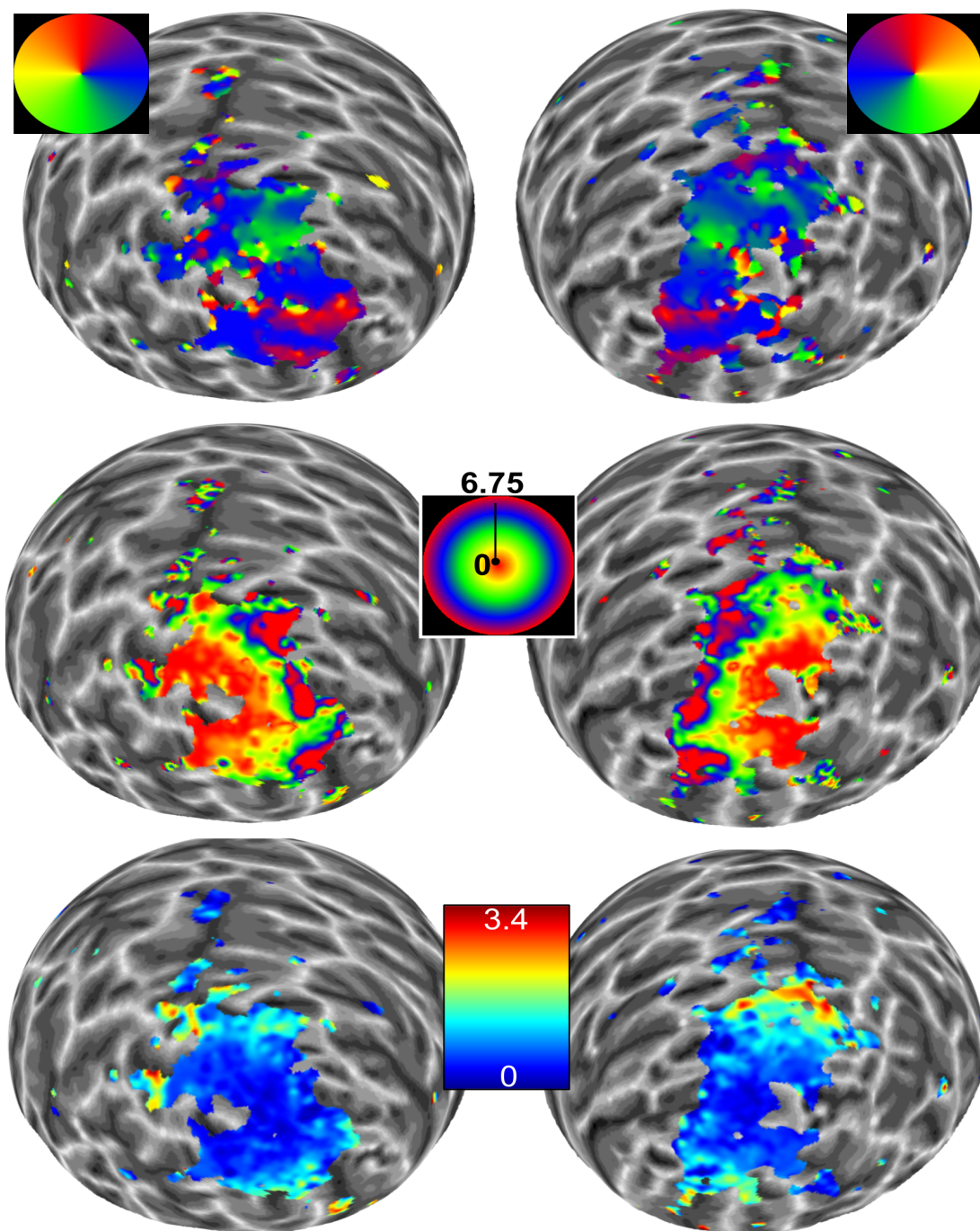
Figure 6.2: Full field pRF maps of Subject 04
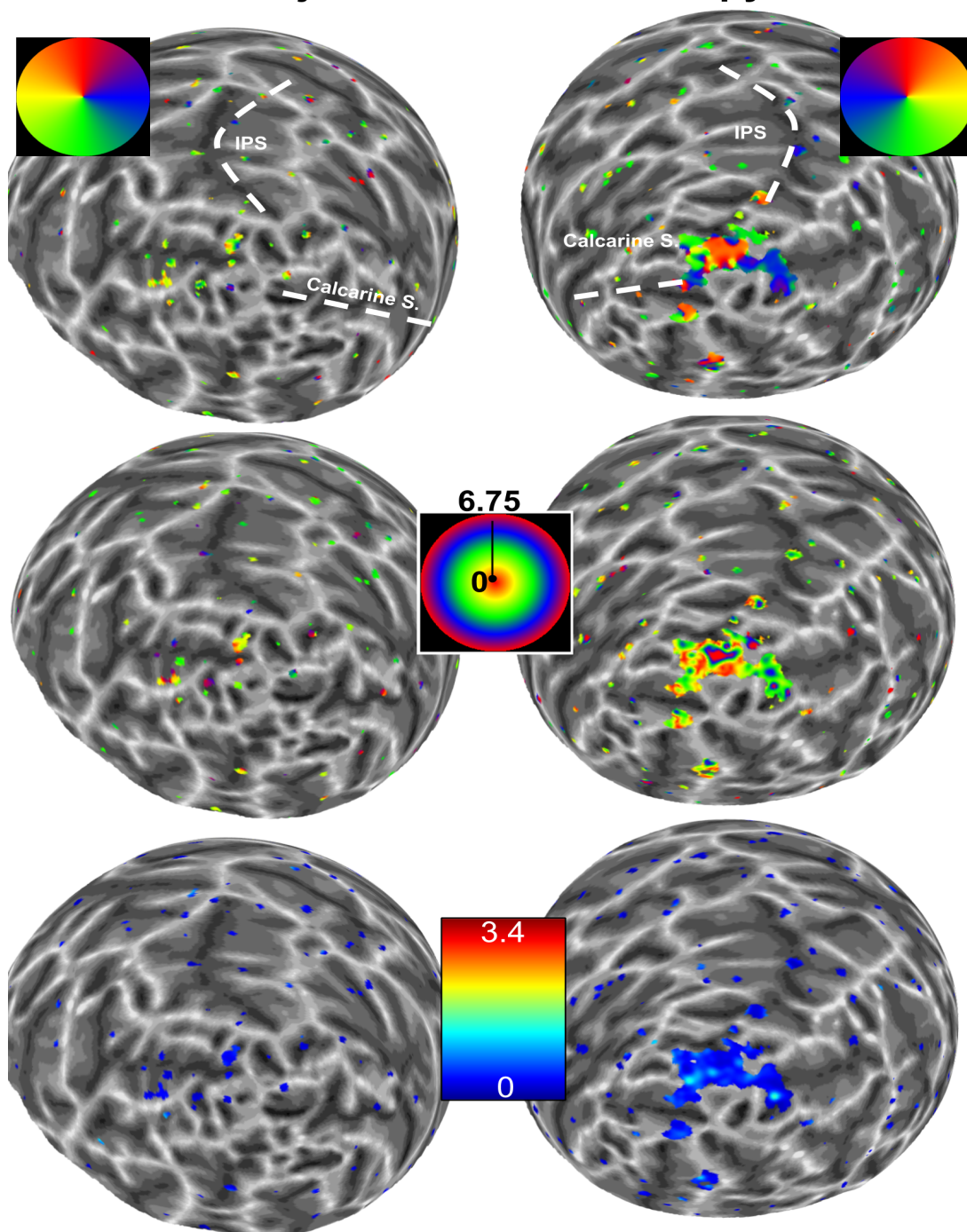
Figure 6.3: Full field pRF maps of Subject 03

Subject 04 Local Retinotopy
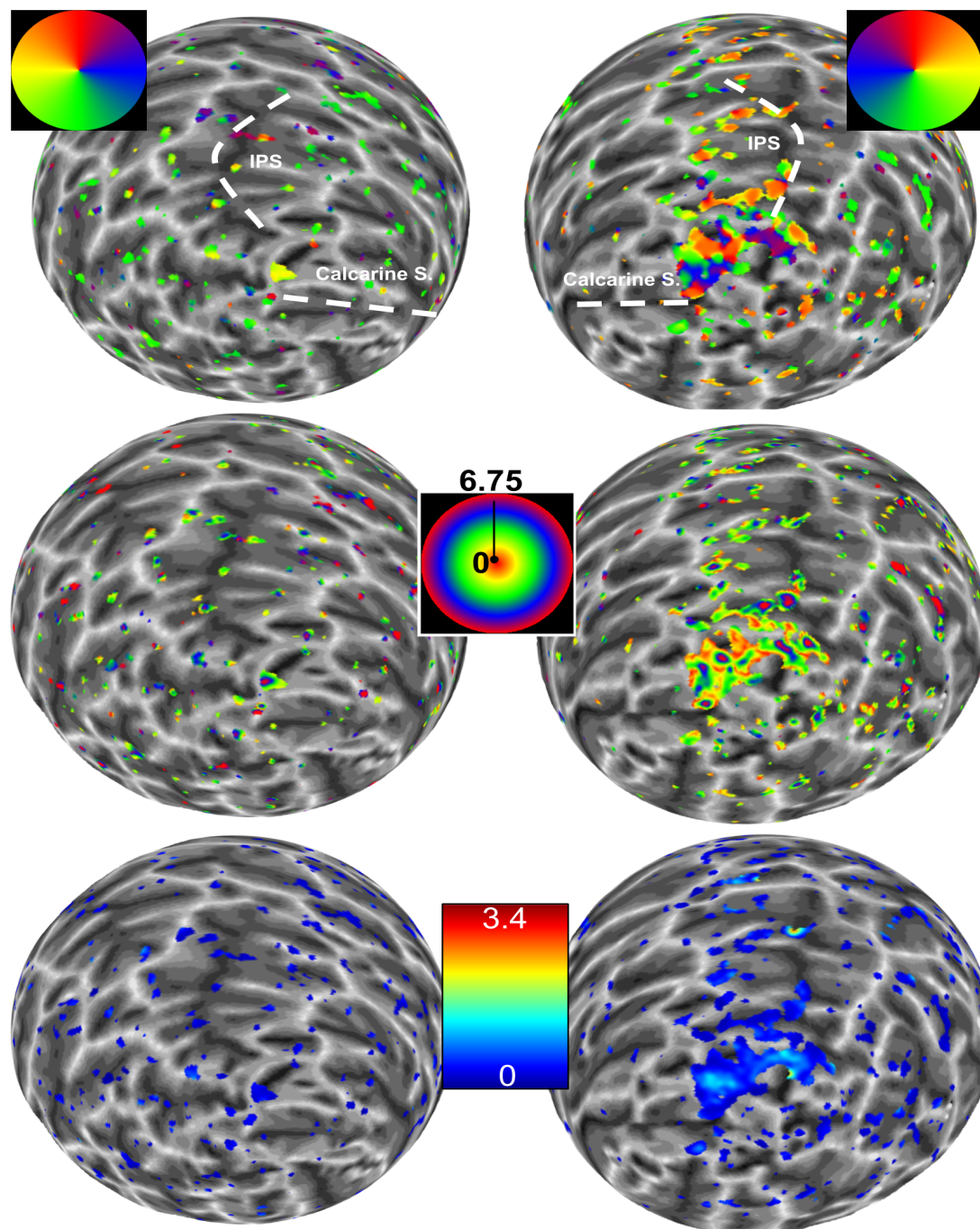
Figure 6.4: Full field pRF maps of Subject 04
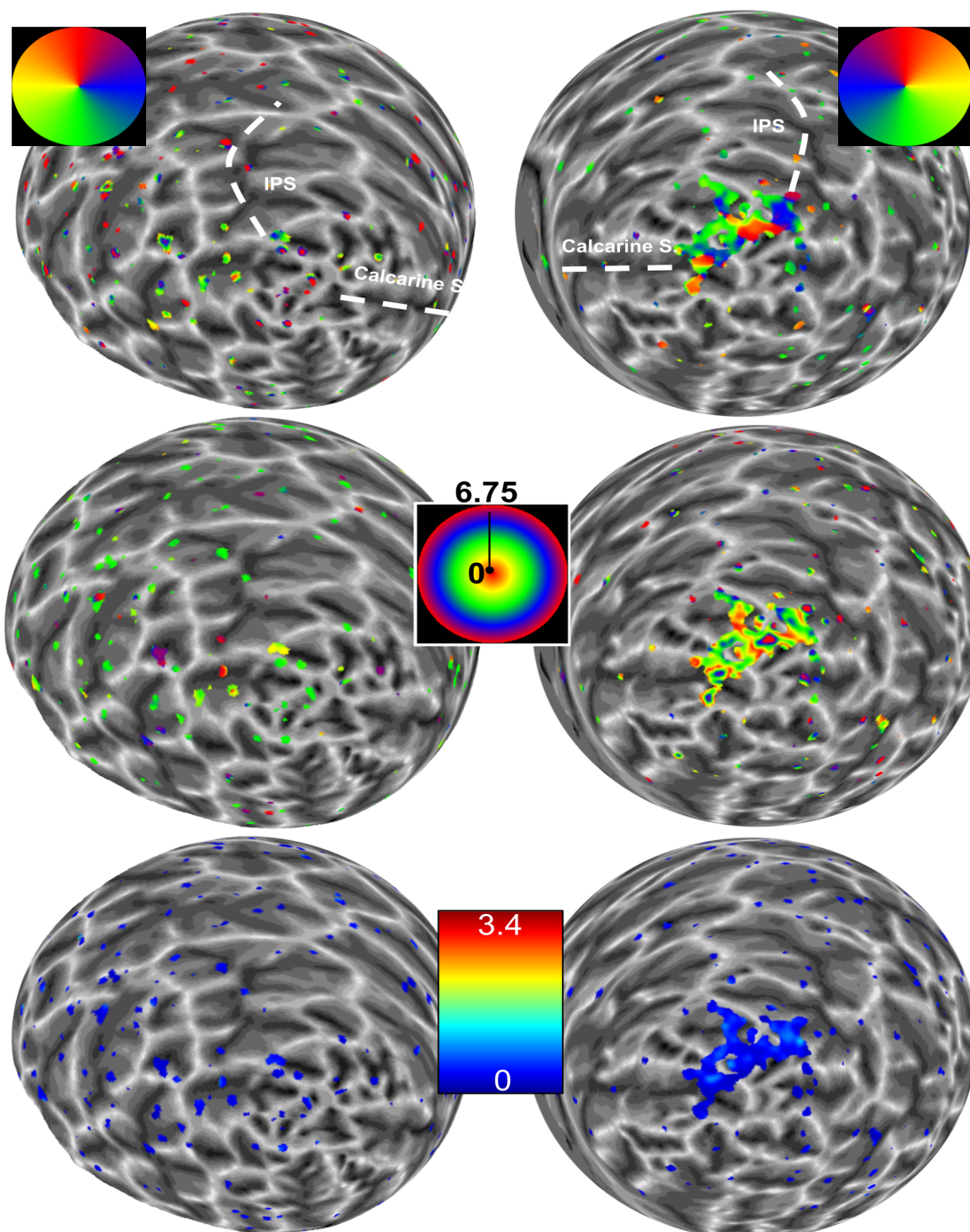
Figure 6.5: Full field pRF maps of Subject 05

Chapter 7

Discussion

7.1   fMRI Parameter Optimization

pRF experiments conducted with each testing sequence led to pRF maps of vary-
ing number of vertices and revealed different number of delineated visual regions.
For instance, Test 1 parameter did not yield large pRF maps, and the eccentricity
and polar angle values did not imply a robust retinotopic organization. Test 2
yielded robust maps, and was larger than maps estimated with Test 3 sequence.
We have chosen Test 3 sequence in our study to keep our stimulation period 2
seconds.

The optimal TE for visual cortex that leads to highest signal intensity was demon-
strated to be around 40 ms [59]. In our Test 3 sequence the TE was set to 60
ms, which was one of the lowest values we could go down to. This parameter was
further optimized by increasing the Bandwidth to 1544 Hz/px and excite pulse
duration to 6680 μs. The flip angle of the Test 3 sequence was increased from 22

to 80 degrees, by calculating Ernst angle based on TR and T1 parameters.

A limitation of the fMRI parameter optimization section in our study was the lack of objective measures for fMRI parameter estimation. We did not conduct tests on retrieved BOLD signal in order to investigate the SNR, tSNR and percent change measures, but we relied on pilot experiments and pRF maps to decide the most optimal parameters for retinotopic imaging.

7.2 Stimulus Optimization

The pRF map coverage of visual cortex differed under Stimulus 1, 2 and 3 conditions shown on Table 4.1. The Stimulus 2 and 3 experiments reliably estimated around the same number of vertices, however, Stimulus 3 experiment yielded more vertices in higher level regions (V4, V3A, V3B, LO1, LO2, IPS0); whereas Stimulus 2 experiment resulted in higher number of vertices in V2 and V3. To some extent, this was in line with our expectations. We did not foresee lower number of vertices in pRF estimations in low-level visual areas when natural images were utilized. It seems that as the complexity of stimulus features were increased (i.e. color, objects and faces), the mapping ability in high-level areas were increased too, on the other hand, a number of reliable vertices in early visual regions were decreased. Based on this finding, we claim that in cases where pRF estimation in V1 region is more important for the researchers than mapping the higher level regions, colorless high-contrast stimuli can be utilized. For low-level visual areas other than V1, color can be added to the high-contrast stimulus, and if mapping high-level visual areas is key to the study, they can utilize an image set containing natural scenes, faces, objects and patterned textures.

Delineation of ROIs was conducted manually by the author of this study. Although we delineated the regions based on previous studies in literature and guidelines [54, 55, 56, 29], and paid special attention and compared the ROI delineations back and forth between experiments to ensure their comparability, it is still subject to manual errors. To overcome this problem, we also tried to average T1-weighted images from stimulus optimization experiments in order to create a single anatomical image to conduct the analysis on, however this method did not work.

Although we have used non-parametric tests that are insensitive to the sample size differences between ROIs and hemispheres, it is possible that, unbalanced sample sizes may have decreased our statistical power. Moreover, we are confident in choosing non-parametric tests to investigate the differences. In cases the data do not pass normality tests, non-parametric tests are more powerful [60].

Repeating the experiments under the same stimulus conditions at different time periods could reveal the extent of stability or instability of pRF results. To control for additional variables, the hour of the day, hours of sleep, caffeine and nicotine intake information could have been asked to the participant while receiving the informed consent. Since it has been demonstrated that caffeine intake changes the cerebral blood flow (CBF) of subjects [61], and CBF underlies BOLD signal [31]. The other factors may be as well influencing the retrieved BOLD response of participants.

7.2.1 pRF Size Differences

The pRF size differences were explored in detail, on stimulus conditions, dorsal and ventral streams, hemispheres, and intersubject differences. The results showed that pRF size estimates differed due to stimulation protocol, between hemispheres and streams.

The right hemisphere had higher pRF sizes compared to the left, which may imply a functional hemispheric lateralization. Functional asymmetries in visual cortex has been previously studied on humans and other animals in terms of a local and global processing dominance between hemispheres [62, 63, 64, 65]. It has been demonstrated that the right hemisphere may be more dominant in processing global features and vice versa, related with a preferred spatial frequency. Our results are consistent with the local/global processing functional lateralization hypothesis, since pRF sizes were larger in the right hemisphere, which means that receptive fields are tuned to larger regions on the visual field, and therefore, right hemisphere may be more inclined for lower spatial frequency processing.

pRF sizes were influenced by stimulus configurations. The test results showed that Stimulus 1, Stimulus 2 and Stimulus 3 experiments elicited significantly different pRF sizes, and were highest in the Stimulus 3 condition. In connection with local/global processing hypothesis, natural image set including faces, objects, natural scenes and patterned textures, might have induced top-down modulatory effects that lead to an increase in pRF sizes. The modulation also may have been prevalent between hemispheres, such that object cues masked within the ring and wedge were processed simultaneously in both hemispheres, followed by feedforward projections to higher regions in both hemispheres, and feedback

within and between hemispheres, which has been shown to occur dominantly from right to left, since right hemisphere is suggested to attend to both visual fields [66, 67]. In order to investigate these relationships, effective connectivity measures must be conducted with masked natural image set to reveal the direction and extent of feedback and feedforward mechanisms, which could also lead to a standardization for the images used in pRF imaging experiments. The images we used was used in previous studies, therefore, we treated them as a standard protocol. Nevertheless, the features of the images when they are masked with ring and wedges can be subjected to further investigation. For instance presentation of masked natural images might have been grasping the attention of the subject more then a high-contrast stimulus, which would recall another network and contribute to modulatory mechanisms for BOLD response, which we may not be able dissociate without controlling for an effective connectivity design.

Higher pRF sizes in Stimulus 3 condition might be associated with a perceptual filling-in by the subject subconsciously, that may be inline with local/global processing dominance and bilateral processing hypothesis in attention of right visual cortex. As the images are masked with a ring and wedge that moves at each repetition time, the subject may be subconsciously predicting the image features in the next step by following the continuation of features from the information available in the ring and wedge, and creating a mental imagery of the whole picture. Such a mechanism may lead to a shift in the population activity towards a larger visual field compared with the pRF size it processes when a high-contrast pattern is presented. This can be considered as a top-down modulation that is initiated by the masked representation of natural scenes.

We compared pRF sizes on ventral and dorsal processing streams and found no

significant difference between streams. Our results were in contrast to a recent study [68], in which they have found the early ventral visual areas had higher receptive field sizes. However, our model was a circular Gaussian model, not an elliptical Gaussian model as it was utilized in their study [68]. As a further direction, the same data can be analyzed with an elliptical model and pRF sizes can be reevaluated. Also, we conducted our analysis on data retrieved from three participants (Subject 02, 03 and 04), which can be increased in future.

7.2.2 Local pRF Estimation

As our stimulus was in 240 polar angle degree with 4 degree eccentricity and covered 150 arc-minutes area on the visual field, we could only estimate a very limited area that fell on V1-V2d border. Interestingly, as can be seen on Figure A.1.A and B, and A.2, this region on the visual field is processed not only by the contralateral hemisphere, but as well by ipsilateral hemisphere to some extent. Therefore, we expected to see the polar angle estimates that corresponded to the stimulus location on the V1/V2d border of ipsilateral hemisphere. There was a small region corresponding to the stimulus in Subject 02 polar angle maps, but not in others, in hemisphere ipsilateral to the stimulus (at $R^2 = 0.3$). Upon visual inspection we have seen no retinotopic organization corresponding full field pRF maps in terms of eccentricity in Subject 02. We have further investigated model based bias in our results, when the R^2 threshold was set to 0, the polar plots that showed the eccentricity processing at each polar angle showed that estimates from whole occipital cortex were shifted towards the 240 polar angle covering around the stimulus area as can be seen on Figure A.3. Furthermore, we implemented a spatial noise to the local pRF stimulation to initiate a baseline level activity on

central 13.5 degree visual field of participants. The baseline activity was expected to yield better pRF maps, in terms of vertices and full field map correspondence. However, the results did not improve.

The pRF stimulation method relies on creating traveling waves on the cortical surface [12]. The local pRF estimation stimulus we used may have not achieved to initiate a travelling wave starting from the occipital pole to the anterior areas, nor within the calcarine sulcus. The eccentricity and polar angle estimations of the local pRF method may not be very accurate due to inefficiency in initiating such a travelling wave. However, pRF sizes may not be affected by this problem, since pRF size fitting is not a function of x and y coordinates in the model. Further investigation and optimization for local pRF imaging would be beneficial for future studies.

7.3 Subject Specific HRF

There were no meaningful differences between pRF maps upon visual inspection. pRF sizes differed for some ROIs, but the trends of pRF size values were similar, especially at early visual regions as seen on Table 4.2. When the same vertices which were reliably estimated in both subject-specific and canonical HRF conditions were compared, there were no significant differences in pRF size values. This showed that the HRF curve that is used in the analysis did not significantly influence the pRF estimation.

7.4 Summary

In this study, we optimized fMRI parameters and stimulus configurations for pRF experiments in our research center. We concluded that further optimized Test 3 sequence and using masked natural images yield the best results in terms of number of vertices and higher-level visual regions that could be delineated. Furthermore, we investigated pRF sizes under different stimulation conditions and shown that pRF sizes in natural images are estimated to be higher. We have compared the dorsal and ventral streams and found that receptive field sizes do not differ between streams. We also compared the right and left hemispheres and found that pRF sizes in right hemisphere were significantly higher than left hemisphere. The pRF sizes differed from subject to subject referring to individual differences in visual processing. We also estimated subject-specific HRF to predict BOLD time-series instead to a canonical HRf, the pRF estimates were not affected by using subject-specific HRF. We tried to estimate the local pRF at 240 polar angle with a coverage of 150 arcminutes centered at 4 visual degree eccentricity. To improve the results we added a spatial, salt and pepper type of noise to background, yet the results were similar.

Bibliography

[1] S. Ogawa, T. M. Lee, A. R. Kay, and D. W. Tank, "Brain magnetic resonance imaging with contrast dependent on blood oxygenation," *Proceedings of the National Academy of Sciences of the United States of America*, vol. 87(24), p. 9868–9872, 1991.

[2] M. I. Sereno, A. M. Dale, J. B. Reppas, K. K. Kwong, J. W. Belliveau, T. J. Brady, B. R. Rosen, and R. B. H. Tootell, "Borders of multiple visual areas in humans revealed by functional magnetic resonance imaging," *Science*, vol. 268, no. 5212, pp. 889–893, 1995.

[3] E. A. DeYoe, G. J. Carmani, P. Bendettini, S. Glickman, J. Wieser, R. Cox, D. Miller, and J. Neitz, "Mapping striate and extrastriate visual areas in human cerebral cortex," *Proceedings of the National Academy of Sciences of the United States of America*, vol. 93, pp. 2382–2386, 1996.

[4] S. A. Engel, G. H. Glover, and B. A. Wandell, "Retinotopic organization in human visual cortex and the spatial precision of functional MRI," *Cerebral Cortex*, vol. 7, pp. 181–192, 1997.

[5] S. O. Dumoulin and B. A. Wandell, "Population receptive field estimates in human visual cortex.," *NeuroImage*, vol. 39, no. 2, pp. 647–60, 2008.

[6] S. Moeller, E. Yacoub, C. A. Olman, E. Auerbach, J. Strupp, N. Harel, and U. K., "Multiband multislice GE-EPI at 7 tesla, with 16-fold acceleration using partial parallel imaging with application to high spatial and temporal whole-brain fMRI," *Magnetic Resonance in Medicine*, vol. 63(5), pp. 1144–1153, 2010.

[7] D. Purves, A. G. J., F. D., H. W. C., L. A-S., and W. L. E. McNamara J. O., *Neuroscience*. 2008.

[8] D. C. V. Essen and J. L. Gallant, "Neural mechanisms of form and motion processing in the primate visual system," *Neuron*, vol. 13, no. 1, pp. 1 – 10, 1994.

[9] B. A. Wandell, S. O. Dumoulin, and A. A. Brewer, "Visual field maps in human cortex," *Neuron*, vol. 56, no. 2, pp. 366 – 383, 2007.

[10] C. S. Sherrington, "Observations on the scratch-reflex in the spinal dog ," *The Journal of Physiology*, vol. 34, pp. 1–50, 1906.

[11] H. K. Hartline, "The response of single optic nerve fibers of the vertebrate eye to illumination of the retina," *American Journal of Physiology*, vol. 121, pp. 400–415, 1938.

[12] B. A. Wandell and J. Winawer, "Imaging retinotopic maps in the human brain," *Vision Research*, vol. 51, no. 7, pp. 718–737, 2011.

[13] M. W. H. Talbot, S.A, "Physiological Studies on Neural Mechanisms of Visual Localization and Discrimination," *American Journal of Ophthalmology*, vol. 24, pp. 1255–1264, 1941.

[14] S. Zeki, "Representation of central visual fields in prestriate cortex," *Brain Research*, vol. 14, pp. 271–291, 1969.

[15] P. M. Daniel and D. Whiteridge, "Receptive fields of single neurones in the cat's striate cortex," *The Journal of Physiology*, vol. 10(9), p. 203–221, 1987.

[16] B. M. Dow, R. G. Vautin, and R. Bauer, "The Mapping of Visual Space onto Foveal Striate Cortex in the Macaque Monkey," *The Journal of Neuroscience*, vol. 5, p. 890–902, 1985.

[17] D. H. Hubel and T. N. Wiesel, "Receptive fields of single neurones in the cat's striate cortex," *The Journal of Physiology*, vol. 148, p. 574–591, 1959.

[18] S. W. Kuffler, "Discharge Patterns and Functional Organization in Mammalian Retina," *The Journal of Neurophysiology*, vol. 16, p. 37–67, 1953.

[19] M. Glickstein and D. Whitteridge, "Tatsuji Inouye and the mapping of the visual fields on the human cerebral cortex," *Trends in Neurosciences*, vol. 16, p. 350–353, 1953.

[20] P. T. Fox, M. A. Mintun, M. E. Raichle, F. M. Miezin, J. M. Allman, and D. C. Van Essen, "Mapping human visual cortex with positron emission tomography," *Nature*, vol. 323(6091), pp. 806–809, 1986.

[21] P. T. Fox, F. M. Miezin, J. M. Allman, D. C. Van Essen, and M. E. Raichle, "Retinotopic organization of human visual cortex mapped with positron emission tomography," *Journal of Neuroscience*, vol. 7(3), pp. 913–922, 1987.

[22] J. C. Horton and W. F. Hoyt, "The representation of the visual field in human striate cortex," *Archives of Ophthalmology*, vol. 109(6), pp. 816–824, 1991.

[23] I. Alvarez, D. S. Schwarzkopf, G. Rees, B. de Haas, and C. A. Clark, "Comparing different stimulus configurations for population receptive field mapping in human fMRI," *Frontiers in Human Neuroscience*, vol. 9, no. February, pp. 1–16, 2015.

[24] J. A. van Dijk, B. de Haas, C. Moutsiana, and D. S. Schwarzkopf, "Intersession reliability of population receptive field estimates," *NeuroImage*, vol. 143, pp. 293–303, dec 2016.

[25] T. M. Dekker, D. S. Schwarzkopf, B. D. Haas, M. Nardini, and M. I. Sereno, "Population receptive field tuning properties of visual cortex during childhood," *Developmental Cognitive Neuroscience*, no. November 2018, p. 100614, 2019.

[26] A. Hummer, M. Ritter, M. Woletz, A. A. Ledolter, M. Tik, S. O. Dumoulin, G. E. Holder, U. Schmidt-erfurth, and C. Windischberger, "NeuroImage Artificial scotoma estimation based on population receptive fi eld mapping," vol. 169, no. May 2017, pp. 342–351, 2018.

[27] A. Hummer, M. Ritter, M. Tik, A. A. Ledolter, M. Woletz, G. E. Holder, S. O. Dumoulin, U. Schmidt-erfurth, and C. Windischberger, "Eyetracker-based gaze correction for robust mapping of population receptive fields," *NeuroImage*, vol. 142, pp. 211–224, 2016.

[28] M. Castelo-Branco, M. Fatima, J. W. Brascamp, S. O. Dumoulin, and B. M. Harvey, "Radial asymmetries in population receptive field size and cortical magnification factor in early visual cortex," vol. 167, no. September 2016, pp. 41–52, 2018.

[29] S. Schwarzkopf, "Delineating visual ROIs with SamSrf," pp. 1–13.

[30] P. N. Rosa, P. Figueiredo, and C. J. Silvestre, "On the distinguishability of HRF models in fMRI," *Frontiers in Computational Neuroscience*, vol. 9, pp. 1–13, 2015.

[31] N. K. Logothetis and B. A. Wandell, "Interpreting the bold signal," *Annual Review of Physiology*, vol. 66, no. 1, pp. 735–769, 2004. PMID: 14977420.

[32] D. A. Handwerker, O. J. M., and D. M., "Variation of bold hemodynamic responses across subjects and brain regions and their effects on statistical analyses," *NeuroImage*, vol. 21(4), pp. 1639–1651, 2004.

[33] K. J. Friston, F. P., O. Josephs, H. A., R. M.D., and R. Turner, "Event-related fmri: Characterizing differential responses," *NeuroImage*, vol. 7(1), pp. 30–40, 1998.

[34] A. A. Brewer and B. Barton, "Visual cortex in aging and Alzheimer's disease: changes in visual field maps and population receptive fields," *Frontiers in Psychology*, vol. 5, p. 74, 2014.

[35] D. S. Schwarzkopf, E. J. Anderson, B. de Haas, S. J. White, and G. Rees, "Larger extrastriate population receptive fields in autism spectrum disorders," *The Journal of Neuroscience*, vol. 34(7), pp. 2713–2724, 2014.

[36] K. Ahmadi, A. Fracasso, J. A. V. Dijk, and C. Kruijt, "Altered organization of the visual cortex in FHONDA syndrome," *NeuroImage*, vol. 190, no. January 2018, pp. 224–231, 2019.

[37] E. J. Anderson, M. S. Tibber, D. S. Schwarzkopf, S. S. Shergill, E. Fernandez-Egea, G. Rees, and S. C. Dakin, "Visual population receptive fields in people with schizophrenia have reduced inhibitory surrounds," *The Journal of Neuroscience*, vol. 37(6), p. 1546–1556, 2017.

[38] K. Mikellidou, R. Arrighi, G. Aghakhanyan, F. Tinelli, F. Frijia, S. Crespi, and F. D. Masi, "Plasticity of the human visual brain after an early cortical lesion," *Neuropsychologia*, no. October, pp. 0–1, 2017.

[39] P. A., K. G. A., P. T. D., S. Y., K. E., P. E., S. K., B. A., S. U., L. N. K., and S. S. M., "Population receptive field analysis of the primary visual cortex complements perimetry in patients with homonymous visual field defects," *Proceedings of the National Academy of Sciences of the United States of America*, vol. 111(16), no. 5, pp. 1656–1665, 2014.

[40] K. V. Haak, F. W. Cornelissen, and A. B. Morland, "Population receptive field dynamics in human visual cortex," *PLoS ONE*, vol. 7, no. 5, pp. 1–8, 2012.

[41] K. Mikellidou, J. W. Kurzawski, F. Frijia, D. Montanaro, V. Greco, and D. C. Burr, "Area Prostriata in the Human Brain Report Area Prostriata in the Human Brain," *Current Biology*, vol. 27, no. 19, pp. 3056–3060.e3, 2017.

[42] J. Gomez, A. Drain, B. Jeska, V. S. Natu, M. Barnett, and K. Grill-spector, "Development of population receptive fields in the lateral visual stream improves spatial coding amid stable structural-functional coupling," *NeuroImage*, vol. 188, no. November 2018, pp. 59–69, 2019.

[43] T. M. and L. D. A., "Visual Cortex: The Eccentric Area Prostriata in the Human Brain," *Current Biology*, vol. 1, pp. 17–19, 2018.

[44] M. M. Himmelberg and A. R. Wade, "Eccentricity-dependent temporal contrast tuning in human visual cortex measured with fMRI," *NeuroImage*, vol. 184, no. May 2018, pp. 462–474, 2019.

[45] J. A. Brissenden, S. M. Tobyne, D. E. Osher, E. J. Levin, M. A. Halko, D. C. Somers, J. A. Brissenden, S. M. Tobyne, D. E. Osher, E. J. Levin,

M. A. Halko, and D. C. Somers, "Topographic Cortico-cerebellar Networks Revealed by Visual Attention and Working Memory Article Topographic Cortico-cerebellar Networks Revealed by Visual Attention and Working Memory," *Current Biology*, vol. 28, no. 21, pp. 3364–3372.e5, 2018.

[46] B. M. Harvey and S. O. Dumoulin, "Visual motion transforms visual space representations similarly throughout the human visual hierarchy," *NeuroImage*, vol. 127, pp. 173–185, 2016.

[47] D. He, C. Mo, Y. Wang, and F. Fang, "Position shifts of fMRI-based population receptive fields in human visual cortex induced by Ponzo illusion," *Experimental Brain Research*, vol. 233, no. 12, pp. 3535–3541, 2015.

[48] B. P. Klein, A. Fracasso, J. A. V. Dijk, C. L. E. Paffen, F. Susan, and S. O. Dumoulin, "Cortical depth dependent population receptive field attraction by spatial attention in human V1," *NeuroImage*, vol. 176, no. April, pp. 301–312, 2018.

[49] K. N. Kay, K. S. Weiner, and k. Grill-Spector, "Attention reduces spatial uncertainty in human ventral temporal cortex," *Current Biology*, vol. 25, pp. 595–600, 2015.

[50] F. Yildirim, J. Carvalho, and F. W. Cornelissen, "A second-order orientation-contrast stimulus for population- receptive-field-based retinotopic mapping," *NeuroImage*, vol. 164, pp. 183–193, 2018.

[51] M. Reuter, N. J. Schmansky, H. D. Rosas, and B. Fischl, "Within-subject template estimation for unbiased longitudinal image analysis," *NeuroImage*, vol. 61, no. 4, pp. 1402–1418, 2012.

[52] *SPM12 Manual*. 12 Queen Square, London WC1N 3BG, UK: Functional Imaging Laboratory, Wellcome Trust Centre for Neuroimaging, Institute of Neurology, University College London, 2019.

[53] MATLAB, *version 9.3.0.713579 (R2017b)*. Natick, Massachusetts: The MathWorks Inc., 2017.

[54] J. D. Swisher, M. A. Halko, L. B. Merabet, S. A. McMains, and D. C. Somers, "Visual topography of human intraparietal sulcus," *Journal of Neuroscience*, vol. 27, no. 20, pp. 5326–5337, 2007.

[55] B. A. Wandell, A. A. Brewer, and R. F. Dougherty, "Visual field map clusters in human cortex," *Philosophical Transactions of the Royal Society of London, Series B, Biological sciences*, vol. 360(1456), p. 693–707, 2005.

[56] M. W. E., W. J., and C. C. E., "Visual field map clusters in human frontoparietal cortex," *eLife*, vol. 6, 2017.

[57] N. C. Benson, K. W. Jamison, M. J. Arcaro, A. Vu, M. F. Glasser, T. S. Coalson, D. C. Van Essen, E. Yacoub, K. Ugurbil, J. Winawer, and K. Kay, "The hcp 7t retinotopy dataset: Description and prf analysis," *bioRxiv*, 2018.

[58] D. H. Braniard, "The psychophysics toolbox," *Spatial Vision*, vol. 10(4), pp. 433–436, 1997.

[59] S. Clare, *Functional Magnetic Resonance Imaging: Methods and Applications.* PhD thesis, University of Nottingham, 1997.

[60] F. S. Nahm, "Nonparametric statistical tests for the continuous data: the basic concept and the practical use.," *Korean Journal of Anesthesiology*, vol. 69(1), p. 8–14, 2016.

[61] M. A. Addicott, L. L. Yang, A. M. Peiffer, L. R. Burnett, J. H. Burdette, M. Y. Chen, S. Hayasaka, R. A. Kraft, J. A. Maldjian, and P. J. Laurienti, "The effect of daily caffeine use on cerebral blood flow: How much caffeine can we tolerate?," *Human Brain Mapping*, vol. 30, no. 10, pp. 3102–3114.

[62] D. Navon, "Forest before trees: The precedence of global features in visual perception," *Cognitive Psychology*, vol. 9, no. 3, pp. 353 – 383, 1977.

[63] S. Lux, J. Marshall, A. Ritzl, P. Weiss, U. Pietrzyk, N. Shah, K. Zilles, and G. Fink, "A functional magnetic resonance imaging study of local/global processing with stimulus presentation in the peripheral visual hemifields," *Neuroscience*, vol. 124, no. 1, pp. 113 – 120, 2004.

[64] K. Hugdahl, "Visual-spatial information processing in the two hemispheres of the brain is dependent on the feature characteristics of the stimulus," *Frontiers in Neuroscience*, vol. 7, p. 10, 2013.

[65] C. Chiandetti, T. Pecchia, F. Patt, and G. Vallortigara, "Visual hierarchical processing and lateralization of cognitive functions through domestic chicks' eyes," *PLOS ONE*, vol. 9, pp. 1–5, 01 2014.

[66] G. Berlucchi, G. Mangun, and M. Gazzaniga, "Visuospatial attention and the split brain," *Physiology*, vol. 12, no. 5, pp. 226–231, 1997.

[67] S. Pollmann and M. Morrillo, "Left and right occipital cortices differ in their response to spatial cueing," *NeuroImage*, vol. 18, no. 2, pp. 273 – 283, 2003.

[68] E. H. Silson, R. C. Reynolds, D. J. Kravitz, and C. I. Baker, "Differential sampling of visual space in ventral and dorsal early visual cortex," *Journal of Neuroscience*, vol. 38, no. 9, pp. 2294–2303, 2018.

Appendix A

Figures

A.1 Detailed Parameter Tables for fMRI Scans (Test 1, Test 2, Test 3)

SIEMENS MAGNETOM TrioTim syngo MR B17

\\USER\BOYACI Lab\Batuhan\Low-Res Seqs\mbep2d_1.2_MB6 (1.60mm TR 1s)

TA: 3:15   PAT: Off   Voxel size: 1.6×1.6×1.6 mm   Rel. SNR: 1.00   USER: cmrr_mbep2d_bold

Properties

Prio Recon	Off
Before measurement	
After measurement	
Load to viewer	On
Inline movie	Off
Auto store images	On
Load to stamp segments	Off
Load images to graphic segments	Off
Auto open inline display	Off
Start measurement without further preparation	On
Wait for user to start	Off
Start measurements	single

Routine

Slice group 1	
Slices	78
Dist. factor	0 %
Position	L1.8 A21.5 F17.2
Orientation	Transversal
Phase enc. dir.	A >> P
Rotation	0.00 deg
Phase oversampling	0 %
FoV read	192 mm
FoV phase	100.0 %
Slice thickness	1.60 mm
TR	1000 ms
TE	18.0 ms
Multi-band accel. factor	6
Filter	None
Coil elements	BC

Contrast

MTC	Off
Magn. preparation	None
Flip angle	22 deg
Fat suppr.	Fat sat.
Averaging mode	Long term
Reconstruction	Magnitude
Measurements	185
Delay in TR	0 ms
Multiple series	Off

Resolution

Base resolution	120
Phase resolution	100 %
Phase partial Fourier	5/8
Interpolation	Off
PAT mode	None
Matrix Coil Mode	Auto (CP)
Distortion Corr.	Off
Prescan Normalize	Off
Raw filter	On
Elliptical filter	Off
Hamming	Off

Geometry

Multi-slice mode	Interleaved
Series	Interleaved
Special sat.	None

System

Body	On
Positioning mode	FIX
Table position	H
Table position	0 mm
MSMA	S - C - T
Sagittal	R >> L
Coronal	A >> P
Transversal	F >> H
Coil Combine Mode	Sum of Squares
Auto Coil Select	Default
Shim mode	Standard
Adjust with body coil	Off
Confirm freq. adjustment	Off
Assume Silicone	Off
? Ref. amplitude 1H	0.000 V
Adjustment Tolerance	Auto
Adjust volume	
Position	L1.8 A21.5 F17.2
Orientation	Transversal
Rotation	0.00 deg
R >> L	192 mm
A >> P	192 mm
F >> H	125 mm

Physio

1st Signal/Mode	None

BOLD

GLM Statistics	Off
Dynamic t-maps	Off
Starting ignore meas	0
Ignore after transition	0
Model transition states	On
Temp. highpass filter	On
Threshold	4.00
Paradigm size	15
Meas[1]	Baseline
Meas[2]	Baseline
Meas[3]	Baseline
Meas[4]	Baseline
Meas[5]	Baseline
Meas[6]	Baseline
Meas[7]	Baseline
Meas[8]	Baseline
Meas[9]	Baseline
Meas[10]	Baseline
Meas[11]	Active
Meas[12]	Active
Meas[13]	Active
Meas[14]	Active
Meas[15]	Active
Motion correction	On
Interpolation	3D-K-space
Spatial filter	Off

Sequence

Introduction	Off
Contrasts	1
Bandwidth	1666 Hz/Px
Flow comp.	No
Free echo spacing	Off
Echo spacing	0.74 ms
EPI factor	120
Gradient mode	Fast

SIEMENS MAGNETOM TrioTim syngo MR B17

RF spoiling	Off
Excite pulse duration	2740 us
Single-band images	Off
MB LeakBlock kernel	Off
MB dual kernel	Off
MB RF phase scramble	Off
Invert RO/PE polarity	Off
PF omits higher k-space	Off
Force equal slice timing	Off
Online multi-band recon.	Online
FFT scale factor	1.00
Physio recording	Off
Triggering scheme	Standard

SIEMENS MAGNETOM TrioTim syngo MR B17

\\USER\BOYACI Lab\Batuhan\Low-Res Seqs\mbep2d_1.2_MB6 (1.60mm TR 1.5s)				
TA: 4:51	PAT: Off	Voxel size: 1.6×1.6×1.6 mm	Rel. SNR: 1.00	USER: cmrr_mbep2d_bold

Properties

Prio Recon	Off
Before measurement	
After measurement	
Load to viewer	On
Inline movie	Off
Auto store images	On
Load to stamp segments	Off
Load images to graphic segments	Off
Auto open inline display	Off
Start measurement without further preparation	On
Wait for user to start	Off
Start measurements	single

Routine

Slice group 1	
Slices	84
Dist. factor	0 %
Position	L1.8 A21.5 F17.2
Orientation	Transversal
Phase enc. dir.	A >> P
Rotation	0.00 deg
Phase oversampling	0 %
FoV read	192 mm
FoV phase	100.0 %
Slice thickness	1.60 mm
TR	1500 ms
TE	43.0 ms
Multi-band accel. factor	6
Filter	None
Coil elements	BC

Contrast

MTC	Off
Magn. preparation	None
Flip angle	22 deg
Fat suppr.	Fat sat.
Averaging mode	Long term
Reconstruction	Magnitude
Measurements	185
Delay in TR	0 ms
Multiple series	Off

Resolution

Base resolution	120
Phase resolution	100 %
Phase partial Fourier	7/8
Interpolation	Off
PAT mode	None
Matrix Coil Mode	Auto (CP)
Distortion Corr.	Off
Prescan Normalize	Off
Raw filter	On
Elliptical filter	Off
Hamming	Off

Geometry

Multi-slice mode	Interleaved
Series	Interleaved
Special sat.	None

System

Body

Body	On
Positioning mode	FIX
Table position	H
Table position	0 mm
MSMA	S - C - T
Sagittal	R >> L
Coronal	A >> P
Transversal	F >> H
Coil Combine Mode	Sum of Squares
Auto Coil Select	Default
Shim mode	Standard
Adjust with body coil	Off
Confirm freq. adjustment	Off
Assume Silicone	Off
? Ref. amplitude 1H	0.000 V
Adjustment Tolerance	Auto
Adjust volume	
Position	L1.8 A21.5 F17.2
Orientation	Transversal
Rotation	0.00 deg
R >> L	192 mm
A >> P	192 mm
F >> H	135 mm

Physio

1st Signal/Mode	None

BOLD

GLM Statistics	Off
Dynamic t-maps	Off
Starting ignore meas	0
Ignore after transition	0
Model transition states	On
Temp. highpass filter	On
Threshold	4.00
Paradigm size	15
Meas[1]	Baseline
Meas[2]	Baseline
Meas[3]	Baseline
Meas[4]	Baseline
Meas[5]	Baseline
Meas[6]	Baseline
Meas[7]	Baseline
Meas[8]	Baseline
Meas[9]	Baseline
Meas[10]	Baseline
Meas[11]	Active
Meas[12]	Active
Meas[13]	Active
Meas[14]	Active
Meas[15]	Active
Motion correction	On
Interpolation	3D-K-space
Spatial filter	Off

Sequence

Introduction	Off
Contrasts	1
Bandwidth	1544 Hz/Px
Flow comp.	No
Free echo spacing	Off
Echo spacing	0.79 ms
EPI factor	120
Gradient mode	Fast

SIEMENS MAGNETOM TrioTim syngo MR B17

RF spoiling	Off
Excite pulse duration	4920 us
Single-band images	Off
MB LeakBlock kernel	Off
MB dual kernel	Off
MB RF phase scramble	Off
Invert RO/PE polarity	Off
PF omits higher k-space	Off
Force equal slice timing	Off
Online multi-band recon.	Online
FFT scale factor	1.00
Physio recording	Off
Triggering scheme	Standard

\\USER\BOYACI Lab\Batuhan\Low-Res Seqs\mbep2d_1.2_MB6 (1.60mm TR 2s)

TA: 6:26   PAT: Off   Voxel size: 1.6×1.6×1.6 mm   Rel. SNR: 1.00   USER: cmrr_mbep2d_bold

Properties	
Prio Recon	Off
Before measurement	
After measurement	
Load to viewer	On
Inline movie	Off
Auto store images	On
Load to stamp segments	Off
Load images to graphic segments	Off
Auto open inline display	Off
Start measurement without further preparation	On
Wait for user to start	Off
Start measurements	single

Routine	
Slice group 1	
Slices	84
Dist. factor	0 %
Position	L1.8 A21.5 F17.2
Orientation	Transversal
Phase enc. dir.	A >> P
Rotation	0.00 deg
Phase oversampling	0 %
FoV read	192 mm
FoV phase	100.0 %
Slice thickness	1.60 mm
TR	2000 ms
TE	60.0 ms
Multi-band accel. factor	6
Filter	None
Coil elements	BC

Contrast	
MTC	Off
Magn. preparation	None
Flip angle	22 deg
Fat suppr.	Fat sat.
Averaging mode	Long term
Reconstruction	Magnitude
Measurements	185
Delay in TR	0 ms
Multiple series	Off

Resolution	
Base resolution	120
Phase resolution	100 %
Phase partial Fourier	7/8
Interpolation	Off
PAT mode	None
Matrix Coil Mode	Auto (CP)
Distortion Corr.	Off
Prescan Normalize	Off
Raw filter	On
Elliptical filter	Off
Hamming	Off

Geometry	
Multi-slice mode	Interleaved
Series	Interleaved
Special sat.	None

System

Body	On
Positioning mode	FIX
Table position	H
Table position	0 mm
MSMA	S - C - T
Sagittal	R >> L
Coronal	A >> P
Transversal	F >> H
Coil Combine Mode	Sum of Squares
Auto Coil Select	Default
Shim mode	Standard
Adjust with body coil	Off
Confirm freq. adjustment	Off
Assume Silicone	Off
? Ref. amplitude 1H	0.000 V
Adjustment Tolerance	Auto
Adjust volume	
Position	L1.8 A21.5 F17.2
Orientation	Transversal
Rotation	0.00 deg
R >> L	192 mm
A >> P	192 mm
F >> H	135 mm

Physio	
1st Signal/Mode	None

BOLD	
GLM Statistics	Off
Dynamic t-maps	Off
Starting ignore meas	0
Ignore after transition	0
Model transition states	On
Temp. highpass filter	On
Threshold	4.00
Paradigm size	15
Meas[1]	Baseline
Meas[2]	Baseline
Meas[3]	Baseline
Meas[4]	Baseline
Meas[5]	Baseline
Meas[6]	Baseline
Meas[7]	Baseline
Meas[8]	Baseline
Meas[9]	Baseline
Meas[10]	Baseline
Meas[11]	Active
Meas[12]	Active
Meas[13]	Active
Meas[14]	Active
Meas[15]	Active
Motion correction	On
Interpolation	3D-K-space
Spatial filter	Off

Sequence	
Introduction	Off
Contrasts	1
Bandwidth	1042 Hz/Px
Flow comp.	No
Free echo spacing	Off
Echo spacing	1.1 ms
EPI factor	120
Gradient mode	Fast

1/+

SIEMENS MAGNETOM TrioTim syngo MR B17

RF spoiling	Off
Excite pulse duration	4920 us
Single-band images	Off
MB LeakBlock kernel	Off
MB dual kernel	Off
MB RF phase scramble	Off
Invert RO/PE polarity	Off
PF omits higher k-space	Off
Force equal slice timing	Off
Online multi-band recon.	Online
FFT scale factor	1.00
Physio recording	Off
Triggering scheme	Standard

A.2   Supplementary Figures
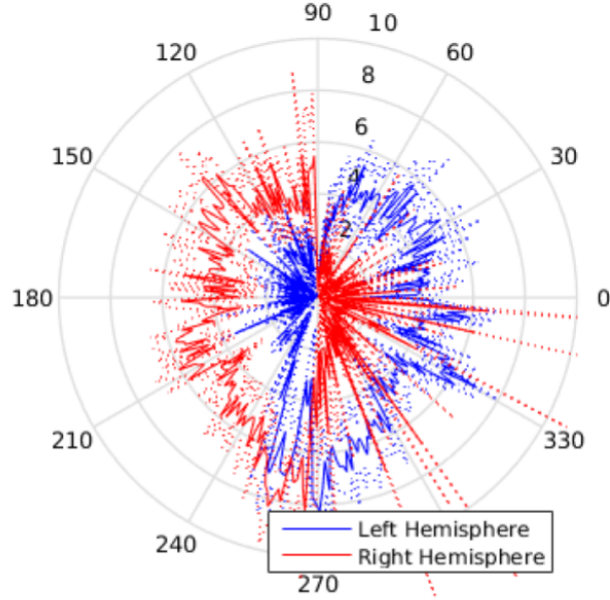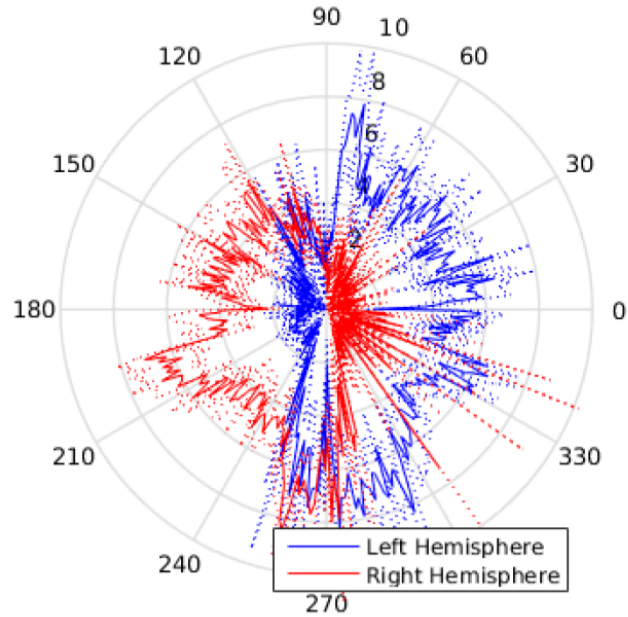
Figure A.1: Mean eccentricity at each polar angle value, estimated from (A) Stimulus 1 and (B) Stimulus 2 experiments that demonstrates the visual field of subject
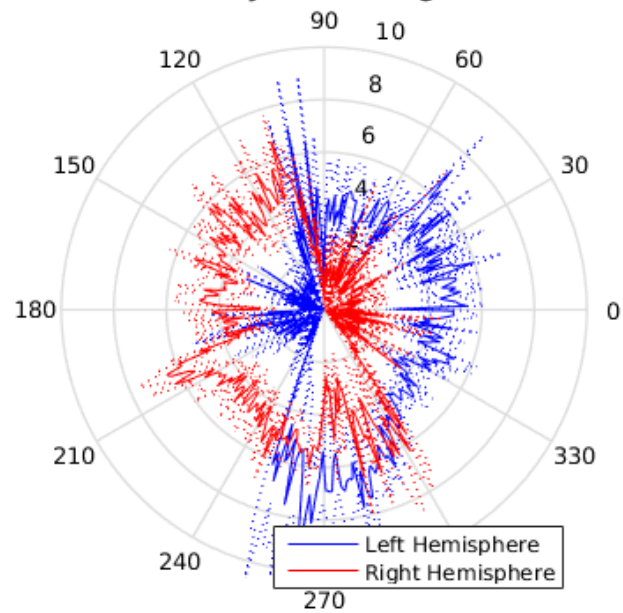
Figure A.2: Mean eccentricity at each polar angle value, estimated from Stimulus 3 experiment that demonstrates the visual field of subject
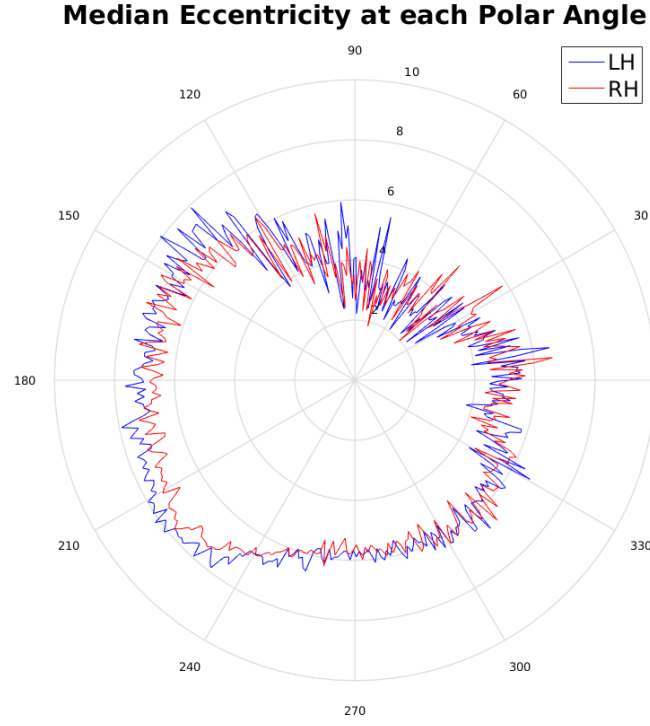
Figure A.3: Median eccentricity values at each polar angle. Here we demonstrate the eccentricity values at each polar angle degree at $R^2 = 0$, with all data from the occipital cortex. It shows that the model is inclined to be biased when there is no restriction for significance threshold. As presented on Figure 1.3 in previous sections, the prediction involves a binary aperture matrix, that is used in generating time-series followed by calculating the correlation between each time-series with vertex data. It is seen on the Figure A.3 that this leads to fitting vertices with predefined model parameters when the correlation between them is non-significant. Thus it is very important analyze pRF map data with correct R^2 threshold. And based on that, our local pRF maps shown on Figure 5.2, 5.3 and 5.4 visualized with $R^2 = 0.3$ may be biased to some extent.

Appendix B

Code

B.1   HRF Estimation Code

```matlab
% HRF Estimation  Procedure
% Batuhan  Erkat
% 7  June  2019
onsets  =  [ ] ;
HRFlength  =  15;
for  i  =  1:150
    if  mod( i , HRFlength )  ==  1
        onsets  =  [ onsets ;  i ] ;
    end
end
TR  =  150;
FIR  =  zeros (TR, HRFlength ) ;
cols  =  1: HRFlength ;
for  jO  =  1:numel( onsets )
    rows  =  onsets (jO ) : onsets (jO)+HRFlength −1;
    for  kR  =  1:numel( rows ) ;
        FIR( rows (kR) , cols (kR) )  =  1;
    end
```

```matlab
end
Train = zeros(TR,1); Train(onsets) = 1;
%%
load('y1248.mat') % GLM output ROIs
y = zscore(y1248);
y = detrend(y);
y = y/max(y);
nVox = size(y,2);
bHats = pinv(FIR'*FIR)*FIR'*y;
Mean = mean(bHats,2);
SEM = std(bHats,0,2)./sqrt(nVox);
CI = tinv([0.025 0.975], nVox-1);
CI2 = bsxfun(@times, SEM, CI95);
%%
h_emp = Mean';
t = 1:HRFlength;
x0 = [6 3 5 0.5 6 8]; % if interpolated with 0.1, change
    last value from 6 to 8.
fun = @(x)sseval(x,t,h_emp);
options = optimset('MaxFunEvals',100000000000, 'MaxIter',
    100000000000 );
[param, fval, exitreason, output] = fminsearch(fun,x0,
    options);
a = param(1); b = param(2); c = param(3); d = param(4); e
    = param(5); f = param(6);
h = a*gampdf(t,b,c) - d*gampdf(t,e,f);
```

B.2   A Guideline for pRF Analysis

In this guideline, I will explain the steps of pRF estimation with annotated code. I have included my personal notes pointing out to the problems I have faced during

implementing this analysis pipeline. Readers should feel free to contribute and further improve this guideline.

To conduct pRF estimation protocol based on this guideline, the reader must have installed Freesurfer v5.3 [51], SPM12 [52], SamSrf 6.05 and MATLAB with a version higher than 2012. Octave is not tested. The readers can follow instructions at Appendix B.4 to install and run the necessary programs. I suggest to use a single computer for the analysis, based on our experience with Freesurfer v5.3, hardware differences can lead to difference in the output. I strongly recommend at least around 32GB of RAM mounted on hardware, in case it is not attainable, you can ask for permission to use servers in you research facility. If that is not possible, there is a set of alternative code we have written for the BOLD averaging, as seen on Figure 2.2, since at that section of the analysis RAM is used extensively and therefore MATLAB may throw a memory error. I strongly recommend the readers to read the SamSrf Cookbook and Delineation documents [29]. By doing that you can get detailed information on the steps of this pipeline. This pipeline consists mainly of code from SamSrf toolbox and custom code written to work along the toolbox.

There are two main MATLAB scripts in this guideline to estimate pRF maps. In Appendix B.3 I share and explain the code PProcSrv1.m and in Appendix B.4 I share and explain the code PProcSrv2.m. The abbreviation PProcSrv1 refers to Preprocessing server 1, is a basic script that finds the motion corrected data in the initialized folder structure (1 T1-weighted and 12 T2-weighted runs, names starting with T1* and MOCO_0001, MOCO_0002 et cetera). The folder names are renamed in line with your experimental protocol and stimulus configurations (Bar, Ridge etc.). Then DICOM import is run to convert IMA files to NIFTI format (.nii) for T1-weigted images. When conversion is done, single T1-weighed image is renamed with subject name defined at the beginning of the script (e.g. BE_T1.nii) and relocated to Freesurfer folder. When the file is relocated, you have to manually start reconstruction on Freesurfer terminal. Further instructions on how to set up Freesurfer and run reconstruction procedure is explained in Appendix B.4

> **An Important Note:**
>
> Before starting the analysis, take all the raw data and store it on drive or a device for safety. Drive is a good option as external drives are vulnerable to unexpected failures. Ask your research facility if there is a GSuite option.

B.3   PProcSrv1.m

In this section, for the code to run without problems, you have to check the 'things to edit' section to set your folder paths, the name of the session, the name of the runs in relation to your stimulus configuration. Then you can run the code. If everything goes well as planned, you should find your NIFTI converted T1-weighted image located in the Freesurfer folder.

```matlab
%% Script to be used BEFORE Freesurfer recon−all
% O. Batuhan Erkat
% Last edit 09/2018
clear all; close all; clc
addpath(genpath('/auto/k1/batuhan/'))
%% Things to edit for your PC
RootFolder = '/auto/data/batuhan/raw'; % where my raw
    dicoms are at
Subject = 'BE'; % subject initials, folder name of raw and
     procd data
FSFolder = '/auto/data/batuhan/output'; % freesurfer path
NoOfRuns = 12; T1NoOfMeas = 176; Runname = 'Ridge'; %
    Ridge1, 2, 3: the functional run folder names
```

Additional notes for help:

- FSFolder is the location that T1 file will be sent for you to conduct recon-all

on Freesurfer.

- When I do an MRI scan, I write the initials of my subject on MRI console as the name of study. Here as subject name I put the same initials, so forth it looks for a folder with the initials of your subject.

- My RootFolder path is where I have my raw data. Inside my raw data folder I only have the folders from MOCO_0001 to MOCO_0012 and T1. If you have other folders, you can edit the code to recognize them, or delete them after backing everything up on drive.

```matlab
%% Initializations that don't require editing, but check
    if correct
RootSubject = [RootFolder filesep Subject];
T1root = [RootSubject filesep 'T1']; % Raw T1 files
T1out = [RootSubject filesep 'T1out']; % Imported T1 as
    single nii
Runnames = {}; Outfolders = {};
Dataloc = [RootFolder filesep Subject '*'];
afolders = [RootFolder filesep]; a = dir(Dataloc);
a = [afolders a(1).name];
b = dir(a); b = b(3:end,:); b = [a filesep b(1).name];
c = dir(b); c = c(3:end,:); d = {};
```

- At the end of above section of the code, there are a, b, c and d variables. These are used for directory listing purposes, and although it may seem unreasonable, a = a(3:end,:), b = b(3:end,:) and c = c(3:end,:) lines are crucial. This is done because dir function refers to "." and ".." as first two elements of a folder on Windows and Ubuntu computers. You can check if it would be the same in Mac computers to make sure there are no unnecessary file names in your cell array. In addition, the output of dir function can be different in different MATLAB versions. Therefore, if you receive an error related with dir function, you can inspect your MATLAB version and

change the code. You can also use a getsubfolders function, but I believe that using dir and inspecting the output can provide more flexibility in your code.

```matlab
%% Initialize Rootfolder (raw data location) and move/
    rename folders.
if ~exist(RootSubject) % Makes the RootSubject folder for
    renaming importing output
    mkdir(RootSubject)
end
for z = 1:NoOfRuns+1
    d{z,1} = [b filesep c(z).name];
end
for i=1:NoOfRuns % Folder name array
    Runnames{i,1} = [Runname num2str(i)];
    Outfolders{i,1} = [RootSubject filesep Runnames{i,1}];
end
Outfolders{end+1,1} = T1root;
for t = 1:length(d)
    movefile(d{t}, Outfolders{t})
end
if ~exist(T1out) % Makes the RootSubject folder for output
    mkdir(T1out)
end
disp('Raw data moved');
%% Initializations for DICOM import only for T1
T1outcell = cellstr(T1out);
r = T1root; r = char(r); r = dir(r); r = r(3:end,:);
T1files = {}; T1paths = {}; T1locs = {};
for n = 1:T1NoOfMeas
    T1files{n} = r(n).name;
    T1paths{n} = T1root;
    T1locs{n,1} = [T1paths{n} filesep T1files{n}];
end
```

- The code above mainly is about initialization of folder structure and data paths. It would be good to run these code section by section to inspect the outputting arrays.

```matlab
%% Import T1
spm('defaults','fmri'); spm_jobman('initcfg');
matlabbatch{1}.spm.util.import.dicom.data = T1locs; %
    where dicom files are for each run
matlabbatch{1}.spm.util.import.dicom.root = 'flat';
matlabbatch{1}.spm.util.import.dicom.outdir = T1outcell; %
    output dir for each run
matlabbatch{1}.spm.util.import.dicom.protfilter = '.*';
matlabbatch{1}.spm.util.import.dicom.convopts.format = '
    nii'; % output format
matlabbatch{1}.spm.util.import.dicom.convopts.icedims = 0;
spm_jobman('run',matlabbatch);
clear matlabbatch
% Here it does the DICOM import for T1 files
disp('DICOM import for T1 is done');
%% Rename the output T1, and relocate it for Freesurfer
    recon-all
e = T1out; e = char(e); e = dir(e); e = e(3:end,:);
e_in = [T1out filesep e(1).name];
T1out_name = [Subject '_T1.nii'];
e_out = [FSFolder filesep T1out_name];
movefile(e_in, e_out); % Renames and moves the file
rmdir(T1out); % delete the empty directory
disp('T1 file is relocated for recon-all on Freesurfer');
```

- This is the DICOM import part for T1-weighted files. DICOM import is a function of SPM12 [52]. I have automatized it on SPM12's [52] scripting

tool from the graphical user interface. After this section of code, you should have the motion corrected runs in your root folder renamed in terms of the Runname variable, and T1-weighted file at the Freesurfer folder ready for the next analysis.

B.4   Freesurfer on Ubuntu or Mac

If your operating system is a version of Ubuntu or Mac, you can read this guideline to download Freesurfer v5.3 and install it on your preferred location: FSv5.3 Download and Install

If you use Ubuntu on Windows 10 (available at Windows store), you have to take slightly different approach in installation and running Freesurfer v5.3. You can read this guideline for Freesurfer installation: Ubuntu on Windows (from Windows Store) Guidelines

It is also possible to use a virtual machine such as Neurodebian on Windows. Although I am not very familiar with this approach, it can be preferred over to Ubuntu on Windows due to the recency.

> **A Note**:
>
> The virtual machine or Ubuntu on Windows (from the Windows store) will use a slightly different directory structure to reach folders and files. For example, instead of typing "C:
> Freesurfer", you may need to type "/mnt/c/FreeSurfer".

After you set Freesurfer at usr/local (or another directory of your preference), you can write bash on your terminal, and write these lines with your own installation paths. I have included $>>$ at the beginning of the lines to specify that you are to writing these lines on the terminal.

```
>> bash
>> export FREESURFER_HOME=/usr/local/freesurfer
```

```
>> source $FREESURFER_HOME/SetUpFreeSurfer.sh
```

After setting the Freesurfer environment, you can export subjects directory. You can as well use the default subjects directory.

```
>> export SUBJECTS_DIR=/home/batu/output
```

> **A Note:**
>
> You can add the export and source lines on the .bashrc file of your system. If you add these lines it will run them automatically whenever you write bash on your terminal. You can edit .bashrc via "nano /.bashrc" or "gedit /.bashrc" command. You can save a copy of .bashrc beforehand. So forth if anything goes wrong, you can revert it by deleting the lines you have added.

If you are at the directory of relocated T1-weighted file (BE_T1.nii), you can type these lines for reconstruction. (You can check your location with typing pwd on terminal.)

```
>> recon-all -i BE_T1.nii -s BE -all
```

If you are not on the directory of relocated T1-weighted file, you can use the full path of the file (BE_T1.nii):

```
>> recon-all -i /home/batu/output/BE_T1.nii -s BE -all
```

> **A Note:**
>
> If you already have started an analysis with the same subject name, or if you have a folder named BE at the directory you are trying to start the analysis, the analysis will not start due to name conflict. You have to erase, rename or relocate the folder with the same subject name and try again.

After the reconstruction procedure is completed, you can see the T1.mgz in the mri folder inside the subject folder. You have to convert it to NIFTI to proceed

with the analysis. If you are at the mri folder (in this example, /home/batu/output/BE/mri/), you can directly use mri_convert function.

```
>> mri_convert T1.mgz T1.nii
```

If you are at a different directory, you have to specify the full path for mri_convert function.

```
>> mri_convert /home/batu/output/BE/mri/T1.mgz T1.nii
```

After you successfully completed these instructions, you can continue on PProcSrv2.m code in Appendix B.5.

B.5   PProcSrv2.m

In this script, initializations are conducted in the beginning. Then the T2-weighted functional images are converted to NIFTI format with DICOM import function. They are then realigned to the first functional image and unwarped to correct for any gradient inhomogenities. After that coregistration is done with the estimate (not reslice) option. The code continues on merging the functional runs into 4D NIFTI files, z-score and detrend the BOLD data due to scanner drift. The odd and even runs are averaged seperately and concatenated to represent a single pRF experiment session. The concatenated BOLD data is projected on the inflated surface mesh retrieved from Freesurfer reconstruction analysis. At the end, the projected data is used to compare predicted BOLD data based on the pRF model and the best representing receptive field profile is assigned to the vertex on the inflated brain surface. The x, y and σ parameters are fine tuned to represent empirical BOLD data at best. Eccentricity and polar angle maps are calculated based on the best fitting x and y parameter values.

In this section, for the code to run without problems, you have to check the 'things to edit' section to set your folder paths, the name of the session, the name of the runs in relation to your stimulus configuration. Then you can run the

code. If everything goes well as planned, after the analysis is completed, you can to go to freesurfer/subject/pRF directory on MATLAB, and inpect the maps with DisplayMaps function of SamSrf toolbox, which will open a graphical user interface, where you can select rh_pRF_Gaussian.mat or lh_pRF_Gaussian.mat which contain the pRF maps.

```matlab
%% AFTER Freesurfer recon-all Script
% O. Batuhan Erkat
% Last edit 09/2018
clear all; close all; clc
addpath(genpath('/auto/k1/batuhan/'))
%% Things to edit for paths and sequence parameters
RootFolder = '/auto/data/batuhan/raw'; % where my dicoms
    are at
FSFolder = '/auto/data/batuhan/output'; % Where my
    freesurfer files are
Subject = 'BE'; % subject initials and/or folder name for
    data
Runname = 'Ridge';% Ridge1, 2, 3 the run folders
TR = 2; Ecc = 13.5; % max ecc screen, 6.7 + 6.7 = 13.5
NoOfRuns = 12; % 12 functional runs
NoOfMeas = 185; % how many image files are there for each
    run
Dummy = 5; % how many empty scans at the beginning of each
    run
Overrun = 0; % how many empty scans at the end of each run
```

- Our screen in the scanner room can represent the center 13.5 visual degree with our current settings. Therefore we signify the eccentricity as 13.5 (Ecc = 13.5). You have to calculate the maximum visual degree possible to scan in your research center.

- NoOfMeas is the number of measurements of a functional scan including

both Dummy and Overrun measurements, which are initial or last measurements where the screen is left blank due to gradient saturation. In our experimental protocol we had 5 dummy measurements and no overrun measurements.

```matlab
%% Initializations that don't require editing, but check
    if correct
FSSubject = [FSFolder filesep Subject];
RootSubject = [RootFolder filesep Subject];
SPMFolder = [FSSubject filesep 'spm' filesep];
mriFolder = [FSSubject filesep 'mri' filesep];
pRFFolder = [FSSubject filesep 'pRF' filesep];
surfFolder = [FSSubject filesep 'surf' filesep];
SPM_T1 = [FSFolder filesep Subject '_T1.nii'];
labelFolder = [FSSubject filesep 'label' filesep];
CoregFS_T1 = [mriFolder 'T1.nii,1'];
Freesurfer_T1 = [mriFolder 'T1'];
% Empty cell arrays
Runnames = cell(NoOfRuns, 1);
IMAfolders = cell(NoOfRuns, 1);
Niifolders = cell(NoOfRuns, 1);
Imagefiles = cell(NoOfMeas, NoOfRuns);
Imagepaths = cell(NoOfMeas, NoOfRuns);
Imagelocs = cell(NoOfMeas, NoOfRuns);
Niifiles = cell(NoOfMeas, NoOfRuns);
Niipaths = cell(NoOfMeas, NoOfRuns);
Niilocations = cell(NoOfMeas, NoOfRuns);
afolders = cell(NoOfMeas, NoOfMeas);
bfolders = cell(NoOfMeas,NoOfMeas);
Allpaths = {}; Allfiles = {}; Finallocs = {}; Deletefiles
    = {};
%% Loops for initialization of folders and paths
if ~exist(SPMFolder); mkdir(SPMFolder); end
if ~exist(pRFFolder); mkdir(pRFFolder); end
```

```matlab
% Folder name array
for i=1:NoOfRuns; Runnames{i,1} = [Runname num2str(i)];
   end
for j = 1:NoOfRuns % Root subject data folder names
    IMAfolders{j,1} = [RootSubject filesep Runnames{j,1}];
    Niifolders{j,1} = [SPMFolder Runnames{j,1}];
end
for m = 1:length(Niifolders) % Makes the functional folder
   names for output
    if ~exist(char(Niifolders(m))); mkdir(char(Niifolders(
       m))); end
end
for k = 1:NoOfRuns % Takes the image file names and
   location, cats it to a fullpath for spm
    for s = 1:NoOfMeas
        afolders(s,k) = IMAfolders(k,1); a = IMAfolders(k
           ,1);
        a = char(a); a = dir(a); a = a(3:end,:);
        Imagefiles{s,k} = a(s).name;
        Imagelocs{s,k} = [afolders{s,k} filesep Imagefiles
           {s,k}];
    end
end
disp('initializations done');
```

- The code above mainly does the initializations for data paths and folders. When it is done, it will display that initializations are done on MATLAB command line.

```matlab
%% Does conversion job
spm('defaults','fmri'); spm_jobman('initcfg');
for h = 1:NoOfRuns
```

```matlab
        matlabbatch{h}.spm.util.import.dicom.data = Imagelocs
            (:,h); % where dicom files are for each run
        matlabbatch{h}.spm.util.import.dicom.root = 'flat';
        matlabbatch{h}.spm.util.import.dicom.outdir =
            Niifolders(h); % output dir for each run
        matlabbatch{h}.spm.util.import.dicom.protfilter = '.*'
            ;
        matlabbatch{h}.spm.util.import.dicom.convopts.format =
            'nii'; % output format
        matlabbatch{h}.spm.util.import.dicom.convopts.icedims
            = 0;
end
spm_jobman('run',matlabbatch);
clear matlabbatch;
for w = 1:NoOfRuns % Takes the output image file names and
    location, cats it to full path
    for t = 1:NoOfMeas % You should substract -Dummy here
        if you already deleted the dummy volumes by hand
            bfolders(t,w) = Niifolders(w,1);
            b = Niifolders(w,1); b = char(b); b = dir(b); b =
                b(3:end,:);
            Niifiles{t,w} = b(t).name;
            Niilocations{t,w} = [bfolders{t,w} filesep
                Niifiles{t,w}];
    end
end
disp('DICOM import done');
%% Erase dummy and overrun volumes
if Dummy
if Overrun
    for y=1:NoOfRuns
        delete(Niilocations{1:Dummy,y});
        delete(Niilocations{(NoOfMeas-Overrun+1):end,y});
```

```matlab
        end
else
        for y=1:NoOfRuns; delete(Niilocations{1:Dummy,y}); end
end
Niilocations((NoOfMeas-Overrun+1):end,:) = [];
    Niilocations(1:Dummy,:) = [];
end
% Add 1 to the end
for e=1:NoOfMeas-Dummy-Overrun
        for o=1:NoOfRuns; Niilocations{e,o} = [Niilocations{e,
            o} ',1']; end
end
disp('Dummy files are deleted');
```

- At the section above, the code converted the functional images to NIFTI format with DICOM import function. The dummy and overrun measurements will be deleted and excluded from the further analysis. From this point it will continue on preprocessing of functional images using functions of SPM12 toolbox [52].

```matlab
%% SPM Preprocessing
% Realign and unwarp
for p=1:NoOfRuns
    matlabbatch{1}.spm.spatial.realignunwarp.data(p).scans
        = Niilocations(:,p);
    matlabbatch{1}.spm.spatial.realignunwarp.data(p).
        pmscan = '';
end
matlabbatch{1}.spm.spatial.realignunwarp.eoptions.quality
    = 0.9;
matlabbatch{1}.spm.spatial.realignunwarp.eoptions.sep = 4;
matlabbatch{1}.spm.spatial.realignunwarp.eoptions.fwhm =
    5;
```

```
matlabbatch{1}.spm.spatial.realignunwarp.eoptions.rtm = 0;
matlabbatch{1}.spm.spatial.realignunwarp.eoptions.einterp
    = 2;
matlabbatch{1}.spm.spatial.realignunwarp.eoptions.ewrap =
    [0 0 0];
matlabbatch{1}.spm.spatial.realignunwarp.eoptions.weight =
     '';
matlabbatch{1}.spm.spatial.realignunwarp.uweoptions.basfcn
     = [12 12];
matlabbatch{1}.spm.spatial.realignunwarp.uweoptions.
    regorder = 1;
matlabbatch{1}.spm.spatial.realignunwarp.uweoptions.lambda
     = 100000;
matlabbatch{1}.spm.spatial.realignunwarp.uweoptions.jm =
    0;
matlabbatch{1}.spm.spatial.realignunwarp.uweoptions.fot =
    [4 5];
matlabbatch{1}.spm.spatial.realignunwarp.uweoptions.sot =
    [];
matlabbatch{1}.spm.spatial.realignunwarp.uweoptions.uwfwhm
     = 4;
matlabbatch{1}.spm.spatial.realignunwarp.uweoptions.rem =
    1;
matlabbatch{1}.spm.spatial.realignunwarp.uweoptions.noi =
    5;
matlabbatch{1}.spm.spatial.realignunwarp.uweoptions.
    expround= 'Average';
matlabbatch{1}.spm.spatial.realignunwarp.uwroptions.
    uwwhich = [2 1];
matlabbatch{1}.spm.spatial.realignunwarp.uwroptions.
    rinterp = 4;
matlabbatch{1}.spm.spatial.realignunwarp.uwroptions.wrap =
     [0 0 0];
```

```matlab
matlabbatch{1}.spm.spatial.realignunwarp.uwroptions.mask =
    1;
matlabbatch{1}.spm.spatial.realignunwarp.uwroptions.prefix
    = 'u';
spm_jobman('run',matlabbatch);
clear matlabbatch
disp('realign and unwarp done');
```

- At the section above, the functional images are realigned to the first image and unwarped to overcome gradient inhomogenities. Realingment and unwarping can take up to 2 hours based on the size of you functional images.

- Following realignment and unwarping, the code will delete and exclude the non-realigned images. This approach is taken since there will be many preprocessed files created and could stress your system's disk space. If you inspect after the procedure you can see around 360 files, the originals and the preprocessed functional images in each run folder. As the motion corrected raw IMA files are preserved, we can confidently delete files that are unnecessary for the following steps.

```matlab
%% Delete the old ones that start with f, mean (m) and r,
    leaves the u ones.
for w = 1:NoOfRuns % Takes the output image file names and
    location, cats it to full path
    c = Niifolders(w,1);
    c = char(c); c = dir(c); c = c(3:end,:);
    nooffiles = length({c.name});
    for t = 1:nooffiles
        cfolders(t,w)= Niifolders(w,1); Allfiles{t,w} = c(
            t).name;
        Finallocs{t,w} = [cfolders{t,w} filesep Allfiles{t
            ,w}];
        if regexp(Allfiles{t,w}, '^f\w*')
```

```matlab
                Deletefiles{end+1,1} = Finallocs{t,w};
                    Finallocs{t,w} = [];
            elseif regexp(Allfiles{t,w}, '^m\w*')
                Deletefiles{end+1,1} = Finallocs{t,w};
                    Finallocs{t,w} = [];
            elseif regexp(Allfiles{t,w}, '^r\w*')
                Deletefiles{end+1,1} = Finallocs{t,w};
                    Finallocs{t,w} = [];
            end
        end
end
Finallocs = Finallocs(:); Finallocs(all(cellfun(@isempty,
    Finallocs),2), :) = [];
for e=1:length(Finallocs); Finallocs{e} = [Finallocs{e} '
    ,1']; end % Add 1 to the end
delete(Deletefiles{:,1}); % delete them
disp('old files are deleted');
```

- In the section below, the code coregisters the first functional image to the Freesurfer reconstructed T1-weighted image, which was previously converted to NIFTI format manually using mri_convert function on Freesurfer. The transformation matrix produced by aligning anatomical and functional images will be applied to all other functional slices in this step.

```matlab
%% Coregistration: Estimate
matlabbatch{1}.spm.spatial.coreg.estimate.ref = {
    CoregFS_T1};
matlabbatch{1}.spm.spatial.coreg.estimate.source =
    Finallocs(1);
matlabbatch{1}.spm.spatial.coreg.estimate.other =
    Finallocs(2:end);
matlabbatch{1}.spm.spatial.coreg.estimate.eoptions.
    cost_fun = 'nmi';
```

```
matlabbatch {1}.spm.spatial.coreg.estimate.eoptions.sep =
    [4  2];
matlabbatch {1}.spm.spatial.coreg.estimate.eoptions.tol =
    [0.02  0.02  0.02  0.001  0.001  0.001  0.01  0.01  0.01  0.001
    0.001  0.001];
matlabbatch {1}.spm.spatial.coreg.estimate.eoptions.fwhm =
    [7  7];
spm_jobman ('run', matlabbatch); disp ('coregistration:
    estimate done');
clear matlabbatch
```

- In the following section, preprocessing for the pRF estimation procedure will be conducted. In the merging part, all of the functional data from 12 runs (each consists of 180 images that represent the signal intensities in each voxel at the time of measurement) will be merged into a single NIFTI file.

- At the step of averaging the preprocessed functional images will be averaged to represent a pRF session. If you receive a memory error at this step, you can change the AverageRidge() to AverageRidge_Batu() which would not throw out of memory error. Your computer may crush due to memory usage, therefore I recommend you limit MATLAB's use of RAM from the preferences.

> **A Note**:
>
> In the first part of Section 4.2 of this study we have used a combined wedge and ring stimulus as seen on the Figure 4.1. For the averaging of that stimulus our protocol was demonstrated in the Figure 2.2. For the local pRF estimation experiment, as seen on the Figure 5.1 averaging method we employed was slightly different. To average pRF sessions utilizing bar stimulus, we have separated the BOLD data from forward and reversed blocks and averaged them within the forward or reversed conditions. Therefore, at the end of averaging step, we had an average of 28 measurements representing the forward condition and another 28 for reversed condition. After that we have concatenated the average data from two conditions to represent a pRF session. Since number of measurements is in the bar stimulation is low and RAM problem is less likely to occur, it is possible to use AverageRidgeSingleDirection function, which is a modified version of AverageRidge that allows to average each block with each other to represent a pRF session.

- At the projecting part, the code uses samsrf_vol2srf function to match the BOLD data from each voxel of functional images to the outputting surface file from the Freesurfer analysis. Based on the rule you select, the code takes the mean, maximum, minimum or geometric mean of the voxels to assign to the corresponding vertex. The default method is mean, which we have selected to use in this study.

```
%% Preprocessing of BOLD for pRF model fitting
RunTypes={'Ridge','T1','FastT1','Prev'};
NoOfRuns = 12; % How many would you like to analyse? If
    less then
FolderVector={}; %there are only main runs, no hrf or
    another folder
Merging=1; Averaging=1; Projecting=1; Hemis = {'lh', 'rh'
    }; %Hemis = {'rh'}; % you can do prf on one hemisphere
```

```matlab
spm_jobman('initcfg');
disp('merging niis into run-wise 4D files');
if Merging; MergeData(SPMFolder, pRFFolder, NoOfRuns,
    FolderVector); end
disp('averaging odd and even runs');
if Averaging; AverageRidge(pRFFolder, NoOfRuns); end
disp('projecting data onto reconstructed surface');
if Projecting; ProjectData(pRFFolder, surfFolder,
    Freesurfer_T1, Hemis); end
```

- In the code below, pRF estimation is conducted. SamSrf functions need the surface files in a cell array to continue the estimation procedure, therefore they are initialized at the beginning. Then the pRF_DoSubject function is run that collects necessary files from the folders and starts the analysis.

```matlab
%% pRF model fitting
SrfFullPaths={}; Filenames = dir(char(pRFFolder));
    Filenames = Filenames(3:end,:);
for t = 1:length(Filenames)
    if regexp(Filenames(t).name, '^lh\w*')
        SrfFullPaths{end+1,1} = [pRFFolder Filenames(t).
            name];
    elseif regexp(Filenames(t).name, '^rh\w*')
        SrfFullPaths{end+1,1} = [pRFFolder Filenames(t).
            name];
    end
end
SrfFiles = {};
for a = 1:length(SrfFullPaths)
    [pth SrfFiles{a,1}] = fileparts(char(SrfFullPaths{a
        ,1}));
end
[z ~] = size(SrfFiles);
```

```matlab
SrfFiles = reshape(SrfFiles, z/2, 2); % As there are two
    hemis, we can do it like this to feed by columns
StartTime=tic; disp('fitting pRF model...');
Rois = {'lh_occ' 'rh_occ'}; % Hemis = {'lh', 'rh'};
pRF_DoSubject(pRFFolder, FSFolder, surfFolder, SrfFiles,
    Rois);
```

- pRF_DoSubject makes occipital ROIs with MakeOccRoi(), and retrieves your aperture matrix from Freesurfer folder (or any other folder you want to put your aperture matrix). Your aperture matrix is a binary matrix consisting of 0s and 1s, shows the mask of your stimulus over time.

```matlab
function pRF_DoSubject(pRFFolder, FSFolder, surfFolder,
    SrfFiles, Rois)
cd (pRFFolder);
MakeOccRoi(surfFolder); % creates occipital label to
    restrict analysis
%% Check that everything is there
if ~exist(fullfile(cd, 'src_pRF.mat'), 'file')
    disp('Search space doesn''t exist.');
end
if ~exist(fullfile(cd, 'aps_Ridge_mirror.mat'), 'file')
    disp('Aps file doesn''t exist.');
    copyfile([FSFolder filesep 'aps_Ridge_mirror.mat'], ...
        [pRFFolder 'aps_Ridge_mirror.mat']);
    disp('Copied aps file from freesurfer directory');
end
%% Fit model for each hemisphere
for iHemi = 1:2
    PerceptualLearning_2D_Gaussian_Prf(SrfFiles(:,iHemi),
        pRFFolder, Rois{iHemi})
end
end
```

- We have renamed the Standard_2D_Gaussian_Prf function as Perceptual-Learning_2D_Gaussian_Prf for the purpose of another study. It is possible to utilize different pRF models and to add new parameters to for the search grid. samsrf_fit_prf is the function that does the parameter fitting to find the best fitting values. In PerceptualLearning_2D_Gaussian_Prf function initializations for samsrf_fit_prf function are carried. Post-processings are conducted after the fit for eccentricity and polar angle maps and smoothing for visualization purposes.

> **A Note:**
>
> The post-processing functions do conduct smoothing on raw pRF maps, so forth when pRF data is plotted it is not affected.

```matlab
function PerceptualLearning_2D_Gaussian_Prf(SrfFiles,
   pRFFolder, Roi)


%% 2D Gaussian pRF
Model.Prf_Function = @(P,ApWidth) prf_gaussian_rf(P(1), P
   (2), P(3), ApWidth); % Which pRF model function?
Model.Name = 'pRF_Gaussian'; % File name to indicate type
   of pRF model
Model.Param_Names = {'x0'; 'y0'; 'Sigma'}; % Names of
   parameters to be fitted
Model.Scaled_Param = [1 1 1]; % Which of these parameters
   are scaled
Model.Only_Positive = [0 0 1]; % Which parameters must be
   positive?
Model.Scaling_Factor = 13.5; % Scaling factor of the
   stimulus space (e.g. eccentricity)
Model.TR = 2; % Repetition time (TR) of pulse sequence
Model.Hrf = []; % HRF file or vector to use (empty =
   canonical)
```

```matlab
Model.Aperture_File = [pRFFolder 'aps_Ridge_mirror']; %
    Aperture file
Model.Replace_Bad_Fits = false; % (Optional) If true, uses
    coarse fit for bad slow fits
Model.Smoothed_Coarse_Fit = 0; % (Optional) If > 0,
    smoothes data for coarse fit
Model.Coarse_Fit_Only = false; % (Optional) If true, only
    runs the coarse fit

% Search grid for coarse fit
Model.Param1 = -1.05 : 0.15 : 1.05; % X0 search grid
Model.Param2 = -1.05 : 0.15 : 1.05; % Y0 search grid
Model.Param3 = 2 .^ (-5.6 : 0.2 : 1); % Sigma search grid
Model.Param4 = 0; % Unused
Model.Param5 = 0; % Unused

%% Open dialogs if needed
HomePath = pwd;
% Choose data files
if nargin == 0
    [SrfFiles, PathName] = uigetfile('*h_*.mat', 'Choose
        SamSrf files', 'MultiSelect', 'on');
    if SrfFiles ~= 0
        cd(PathName);
    else
        error('No data files selected!');
    end
end
% Choose ROI label
if nargin <= 1
    [Roi, RoiPath] = uigetfile('*.label', 'Choose ROI
        label');
    if Roi ~= 0
```

```matlab
            Roi = [RoiPath Roi(1:end-6)];
        else
            Roi = '';
        end
end

%% Fit pRF model
MapFile = samsrf_fit_prf(Model, SrfFiles, pRFFolder, Roi);

%% Post-processing
load(MapFile);

% Field sign, CMF & smooth
R2_Threshold = 0.05; % R^2 threshold for surface
    calculations
Eccentricity_Range = [1 Model.Scaling_Factor]; %
    Eccentricity range for surface calculations
Smoothing_Kernels = [10 3]; % First kernel for field sign
    & second kernel for everything else.
Srf = samsrf_surfcalcs(Srf, Roi, R2_Threshold,
    Eccentricity_Range, 'S', Smoothing_Kernels, false); %
    dijkstra method as it is best

%% Save again
save(MapFile, 'Srf', 'Model', '-v7.3');

%% Return home
cd(HomePath);
```

- The function samsrf_fit_prf predicts time series based on the pRF model and provided aperture file. Then the predicted time-series are convolved with SPM12's [52] default HRF as can be seen on the Figure 1.3. Then it is

continued on correlating the predicted and convolved time-series data with the empirical BOLD data on the brain surface. The comparisons result in coarse fit pRF maps. Then the best correlated receptive field profiles are taken and the parameter values are further optimized with fminsearch function. After the optimization fine fit pRF maps are generated, and can be inspected with DisplayMaps function.